FINAL REPORT

(NASA-CR-149992) RESEARCH STUDY ON IPS DIGITAL CONTROLLER DESIGN Final Report (Systems Research Lab., Champaign, Ill.) 120 p HC $5.50 CSCL 22A

N76-32214

Unclas
G3/13 03490

RESEARCH STUDY ON STABILIZATION AND CONTROL:

MODERN SAMPLED-DATA CONTROL THEORY

SYSTEMS RESEARCH LABORATORY

P.O. BOX 2277, STATION A
3206 VALLEY BROOK DRIVE
CHAMPAIGN, ILLINOIS 61820

PREPARED FOR GEORGE C. MARSHALL SPACE FLIGHT CENTER,
HUNTSVILLE, ALABAMA

FINAL REPORT

RESEARCH STUDY ON IPS DIGITAL CONTROLLER DESIGN

B. C. KUO
C. FOLKERTS

September 1, 1976

Prepared for:

NATIONAL AERONAUTICS AND SPACE ADMINISTRATION
GEORGE C. MARSHALL SPACE FLIGHT CENTER

Under Contract NAS8-31570
DCN 1-6-ED-02909(IF)

Systems Research Laboratory
P. O. Box 2277, Station A
Champaign, Illinois 61820

TABLE OF CONTENTS

1. Analysis of the Continuous-Data Instrument Pointing System

The objective of this chapter is to investigate the performance of the simplified continuous-data model of the Instrument Pointing System (IPS). Although the ultimate objective is to study the digital model of the system, knowledge on the performance of the continuous-data model is important in the sense that the characteristics of the digital system should approach those of the continuous-data system as the sampling period approaches zero.

The planar equations which describe the motion of the Spacelab using Inside-Out Gimbal (IOG) for the pointing base are differential equations of the fourteenth order.[1] A total of seven degrees of freedom are represented by these equations. Three of these degrees of freedom (X_s, Z_s, Φ) belong to the orbitor, and three degrees of freedom (X_m, Z_m, Ψ) are for the mount, and the scientific instrument (SI) has one degree of freedom in ε.

A simplified model of the IPS model is obtained by assuming that all but motion about two of the seven degrees of freedom axes are negligible. The simplified IPS model consists of only the motion about the scientific instrument axis, ε, and the mount rotation Ψ. The block diagram of the simplified linear IPS control system is shown in Figure 1-1.

In this chapter we shall investigate only the performance of the continuous-data IPS control system. The signal flow graph of the continuous-data IPS control system in Figure 1-1 is shown in Figure 1-2.

The characteristic equation of the continuous-data IPS is obtained from Figure 1-2.

$$\Delta = (1 - K_4K_6)s^5 + (K_2 + K_1K_7 - K_1K_4K_7)s^4 + (K_3 - K_0K_4K_7 + K_0K_7 + K_1K_2K_7)s^3$$

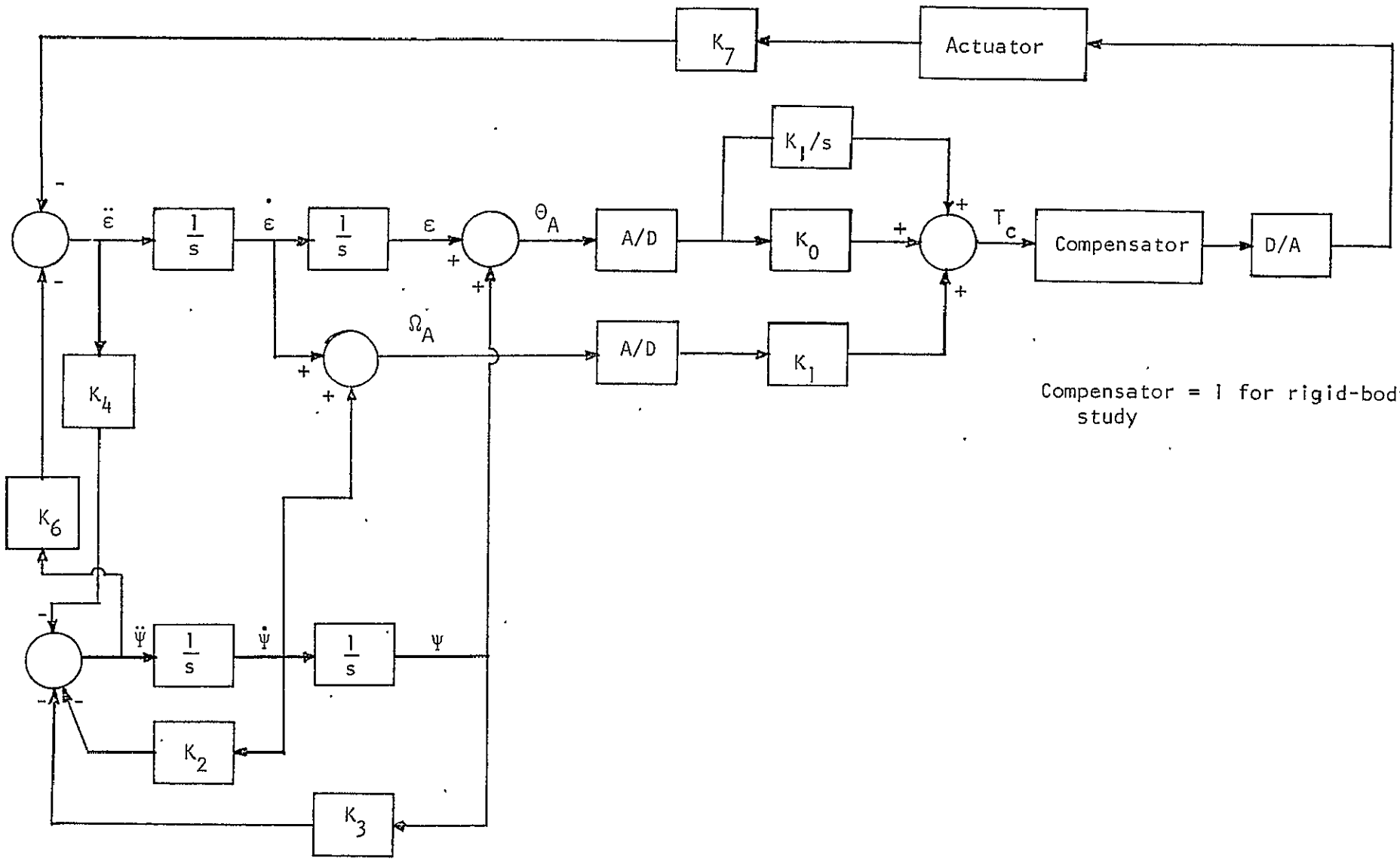

Figure I-1. Block diagram of simplified linear IPS control system.

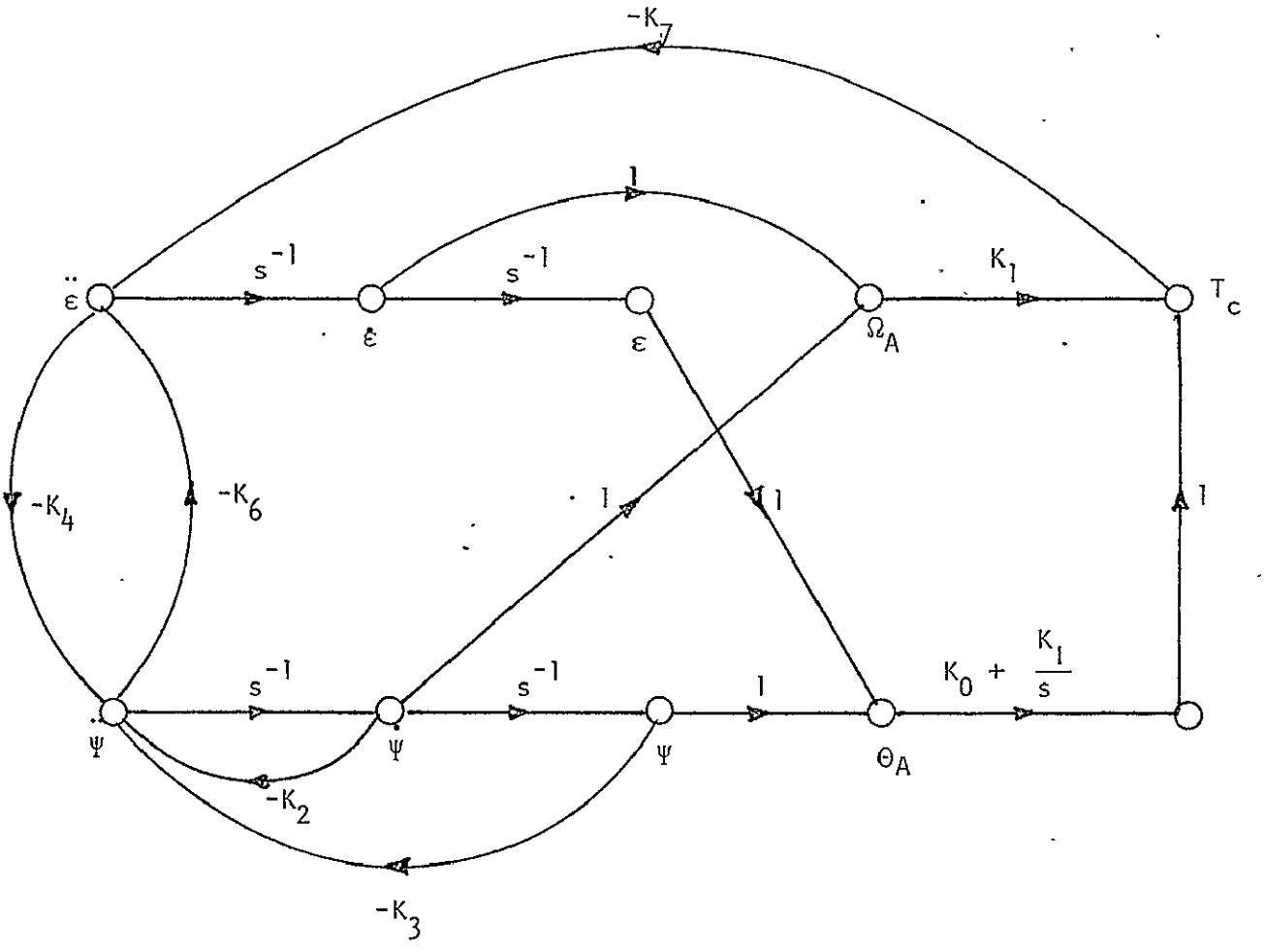

Figure 1-2. Signal flow graph of the simplified linear continuous-data IPS control system.

$$+ (K_1K_7 - K_1K_4K_7 + K_1K_3K_7 + K_0K_2K_7)s^2 + (K_1K_2K_7 + K_0K_3K_7)s + K_1K_3K_7 = 0 \quad (1\text{-}1)$$

The system parameters are:

$K_0 = 8 \times 10^5$ n-m

$K_1 = 6 \times 10^4$ n-m/sec

$K_2 = 0.0012528$

$K_3 = 0.0036846$

$K_1 =$ variable

$K_4 = 0.80059$

$K_5 = 10798.49$

$K_6 = 1.1661$

$K_7 = 0.0000926$

Equation (1-1) is simplified to

$$s^5 + 16.704s^4 + 222.63s^3 + (1.706 + 27.816\ 10^{-5}K_1)s^2 + (4.11 + 174.7\ 10^{-8}K_1)s + 513.855\ 10^{-8}K_1 = 0 \quad (1\text{-}2)$$

The root locus plot of Eq. (1-2) when K_1 varies is shown in Figure 1-3. It is of interest to notice that two of the root loci of the fifth-order IPS control system are very close to the origin in the left-half of the s-plane, and these two loci are very insensitive to the variation of K_1.

The characteristic equation roots for various values of K_1 are tabulated in the following:

K_1	ROOTS		
0	0,	-0.00314±j0.13587,	-8.3488±j12.3614
10^4	-0.0125	-0.00313984±j0.135873,	-8.34260±j12.3571
10^5	-0.1262	-0.0031342±j0.135879,	-8.28577±j12.3192
10^6	-1.38146	-0.0031398±j0.135882,	-7.65813±j11.9457

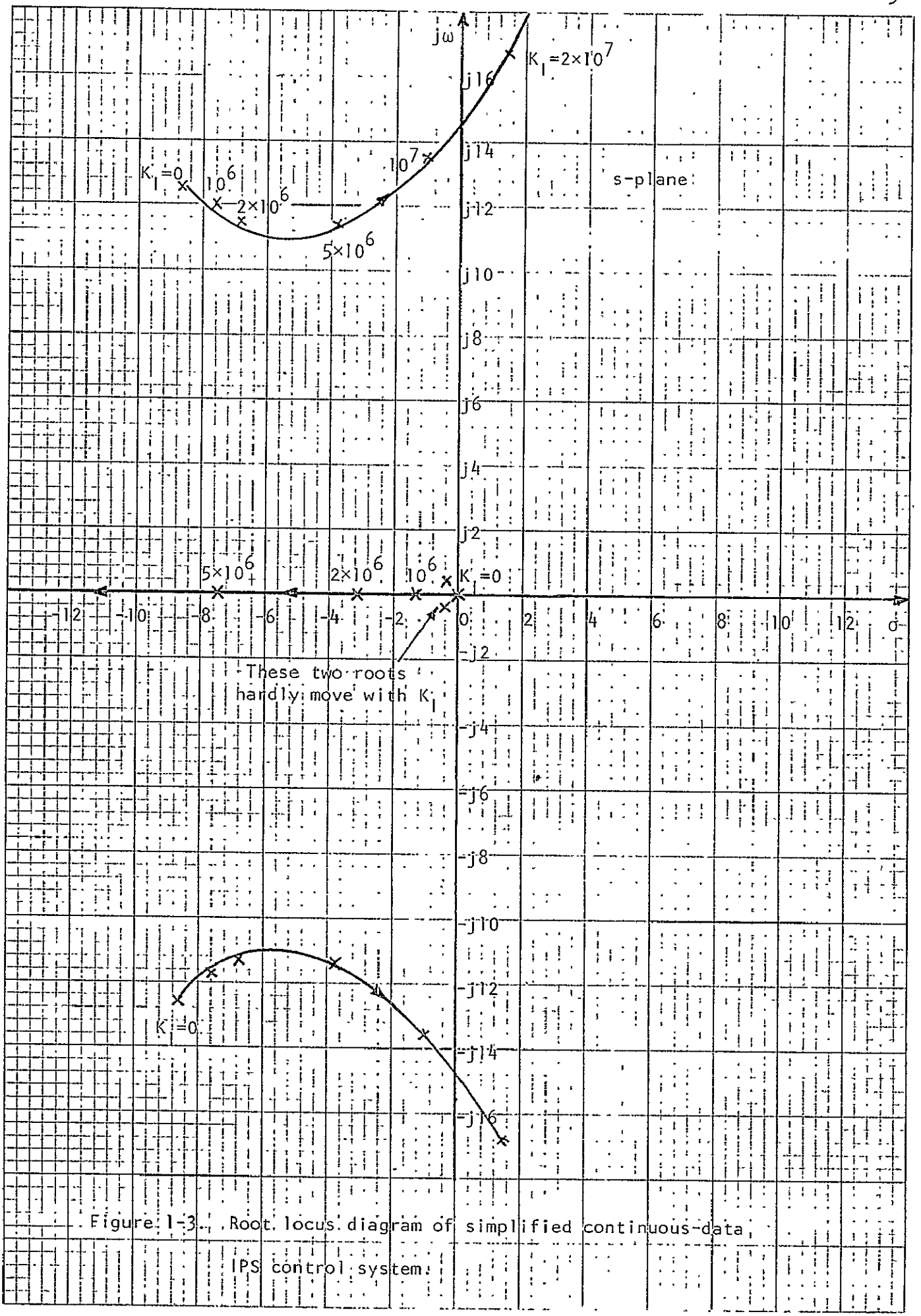

Figure 1-3. Root locus diagram of simplified continuous-data IPS control system.

K_I	ROOTS		
2×10^6	-3.08107,	$-0.00313629\pm j0.135883$,	$-6.80833\pm j11.5845$
5×10^6	-9.07092,	$-0.00314011\pm j0.135881$,	$-3.81340\pm j11.7806$
2×10^7	-19.7201,	$-0.00314025\pm j0.135880$,	$-1.51118\pm j16.7280$
10^7	-14.5468,	$-0.00314020\pm j0.135881$,	$-1.07547\pm j13.7862$
5×10^7	-27.2547,	$-0.00314063\pm j0.135889$,	$5.27850\pm j21.963$
10^8	-34.-97,	$-0.00314035\pm j0.135882$,	$8.69964\pm j27.2045$

The continuous-data IPS control system is asymptotically stable for K_I less than 1.5×10^7.

It is of interest to investigate the response of the IPS control system due to its own initial condition. The transfer function between and its initial condition ε_o for $K_I = 5\times10^6$ is

$$\frac{\varepsilon(s)}{\varepsilon_o(s)} = \frac{s^2(s^3 + 16.7s^2 - 893s - 5581.77)}{s^5 + 16.7s^4 + 222.63s^3 + 1392.5s^2 + 12.845s + 25.693} \qquad (1\text{-}3)$$

where we have considered that $\varepsilon(0) = \varepsilon_o$ is a unit-step function input applied at $t = 0$; i.e., $\varepsilon_o(s) = 1/s$.

It is interesting to note that the response of ε due to its own initial condition is overwhelmingly governed by the poles near the origin. In this case, the transfer function has zeros at $s = 80.5$, $-12.375\pm j23.75$. The zero at $s=80.5$ causes the response of ε to go negative first before eventually reaching zero in the steady-state, as shown in Figure 1-4. The first overshoot is due to the complex poles at $s = -3.8134\pm j11.7806$. Therefore, the eigenvalues of the closed-loop system at $s = -3.8134\pm j11.7806$ controls only the transient response of $\varepsilon(t)$ near $t = 0$, and the time response of $\varepsilon(t)$ has a long

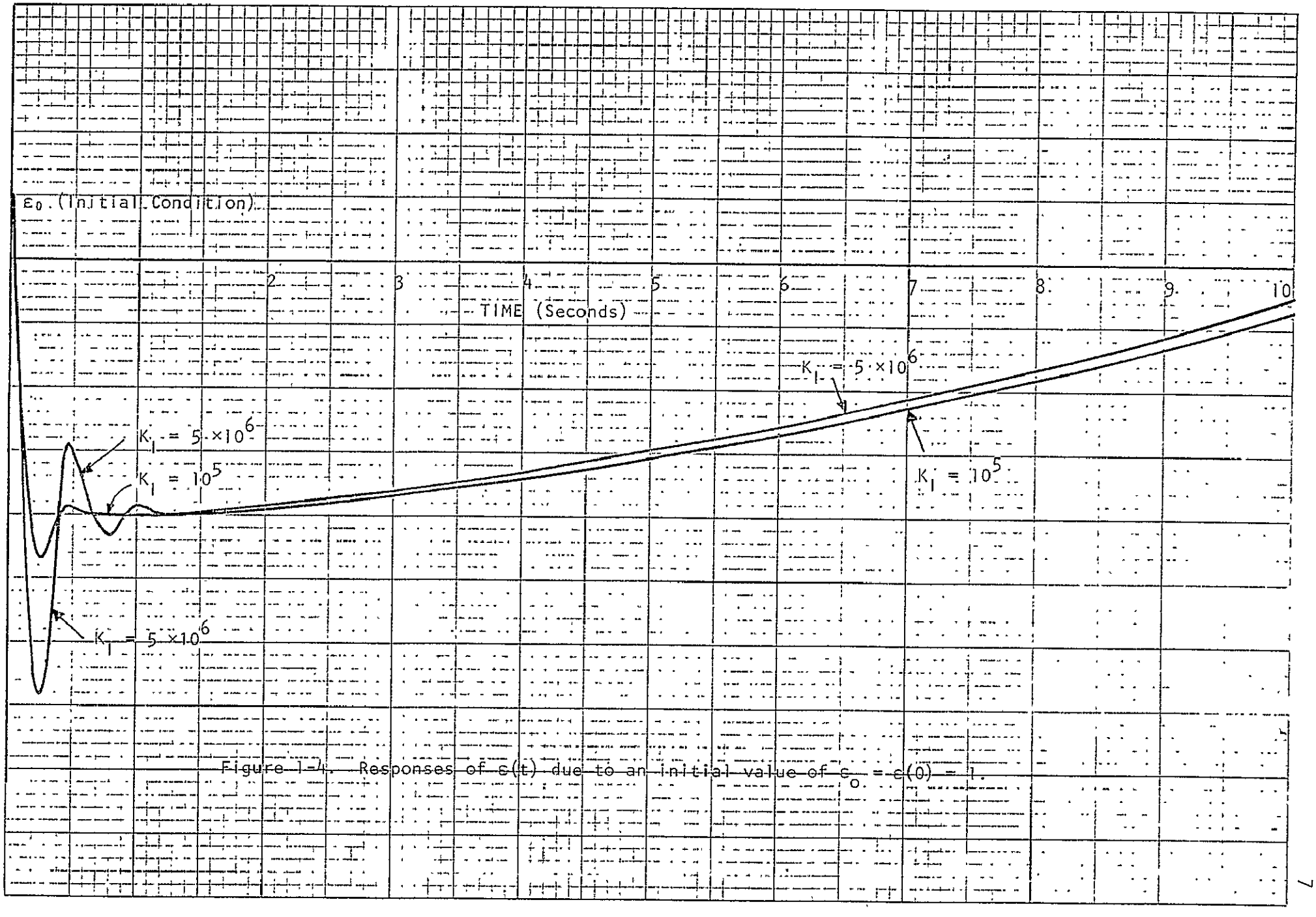

Figure 1-4. Responses of $\varepsilon(t)$ due to an initial value of $\varepsilon_o = \varepsilon(0) = 1$.

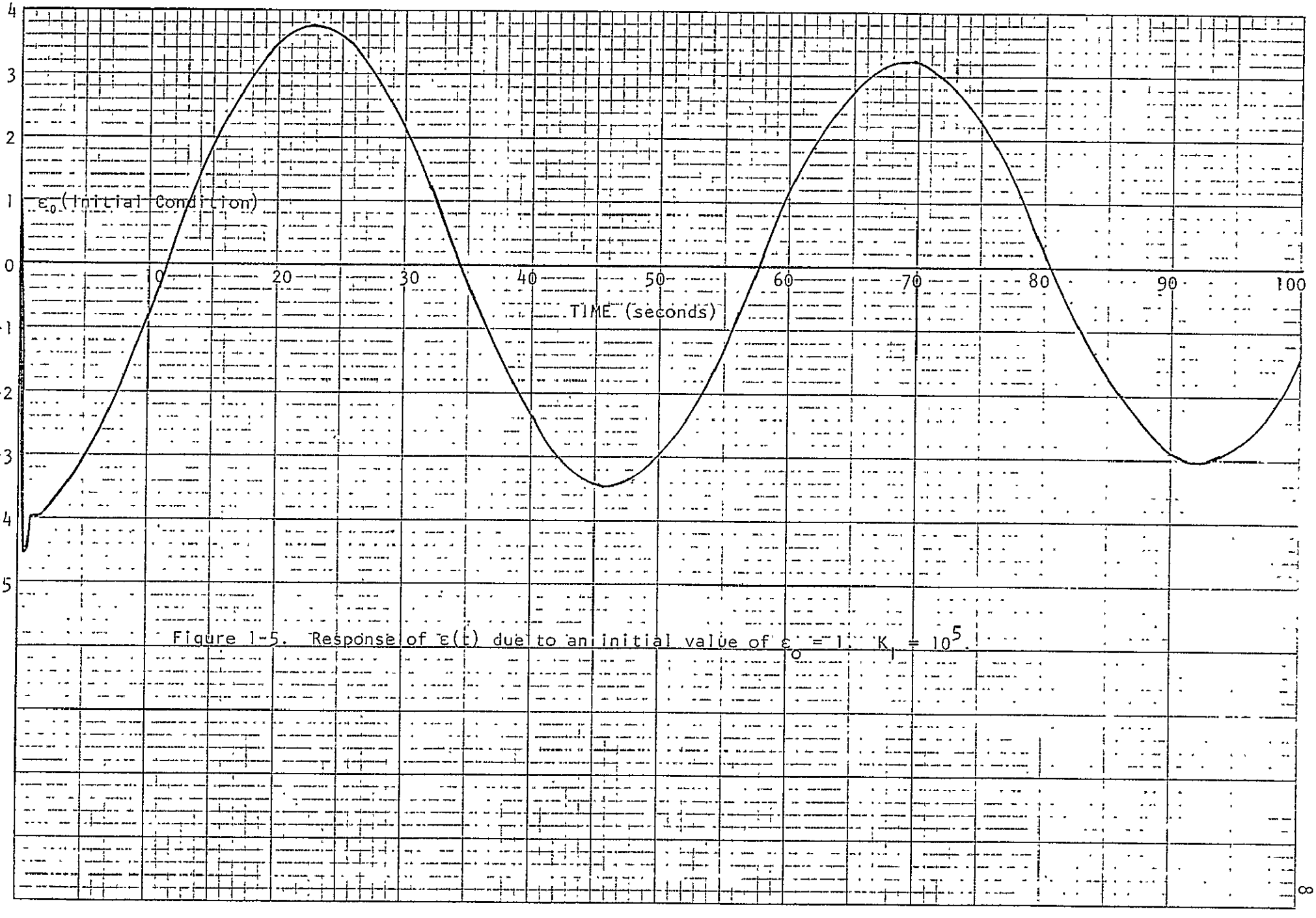

Figure 1-5. Response of $\varepsilon(t)$ due to an initial value of $\varepsilon_o = 1$. $K_1 = 10^5$.

period of oscillation. The eigenvalues at $s = -0.00313 \pm j0.1358$ due to the isolator dynamics give rise to an oscillation which takes several minutes to damp out. The conditional frequency is 0.1358 rad/sec, so the period of oscillation is approximately 46 seconds. Figure 1-5 shows the response of $\varepsilon(t)$ for $\varepsilon_o = 1$ rad on a different time scale over 100 seconds. Although the initial condition of 1 radian far exceeds the limitation under which the linear approximation of the system model is valid, however, for linear analysis, the response will have exactly the same characteristics but with proportionally smaller amplitude if the value of ε_o is reduced.

Since the transient response of the system is dominated by the isolator dynamics with eigenvalues very close to the origin, changing the value of K_1 within the stability bounds would only affect the time response for the first second as shown in Figure 1-4, the oscillatory and slow decay characteristics of the response would not be affected in any significant way.

2. The Simplified Linear Digital IPS Control System

In this chapter the model of the simplified digital IPS control system will be described, and the dynamic performance of the system will be analyzed.

The block diagram of the digital IPS is shown in Figure 2-1, where the element S/H represents sample-and-hold. The system parameters are identical to those defined in Chapter 1. An equivalent signal flow graph of the block diagram in Figure 2-1 is drawn as shown in Figure 2-2.

Applying Mason's gain formula to Figure 2-2 with $\Theta_A(s)$ and $\Omega_A(s)$ as outputs, $\Theta_A^*(s)$ and $\Omega_A^*(s)$ as inputs, we have

$$\Omega_A(s) = -K_1K_7\frac{G_h(s)}{\Delta s}(\Delta_1 - K_4)\Omega_A^*(s) - (K_0 + \frac{K_1T}{z-1})K_7\frac{G_h(s)}{\Delta s}(\Delta_1 - K_4)\Theta_A^*(s) \quad (2\text{-}1)$$

$$\Theta_A(s) = -K_1K_7\frac{G_h(s)}{\Delta s^2}(\Delta_1 - K_4)\Omega_A^*(s) - (K_0 + \frac{K_1T}{z-1})K_7\frac{G_h(s)}{\Delta s^2}(\Delta_1 - K_4)\Theta_A^*(s) \quad (2\text{-}2)$$

where

$$\Delta_1 = 1 + K_2s^{-1} + K_3s^{-2} \quad (2\text{-}3)$$

$$\Delta = 1 - K_4K_6 + K_2s^{-1} + K_3s^{-2} \quad (2\text{-}4)$$

$$G_h(s) = \frac{1 - e^{-Ts}}{s} \quad (2\text{-}5)$$

Letting

$$G_1(s) = K_7\frac{G_h(s)}{\Delta s}(\Delta_1 - K_4) = \frac{K_7(1 - e^{-Ts})\left((1 - K_4)s^2 + K_2s + K_3\right)}{s^2\left((1 - K_4K_6)s^2 + K_2s + K_3\right)} \quad (2\text{-}6)$$

$$G_2(s) = K_7\frac{G_h(s)}{\Delta s^2}(\Delta_1 - K_4) = \frac{G_1(s)}{s} \quad (2\text{-}7)$$

and taking the z-transform on both sides of Eqs.(2-1) and (2-2), we have

$$\Omega_A(z) = -K_1G_1(z)\Omega_A(z) - (K_0 + \frac{K_1T}{z-1})G_1(z)\Theta_A(z) \quad (2\text{-}8)$$

$$\Theta_A(z) = -K_1G_2(z)\Omega_A(z) - (K_0 + \frac{K_1T}{z-1})G_2(z)\Theta_A(z) \quad (2\text{-}9)$$

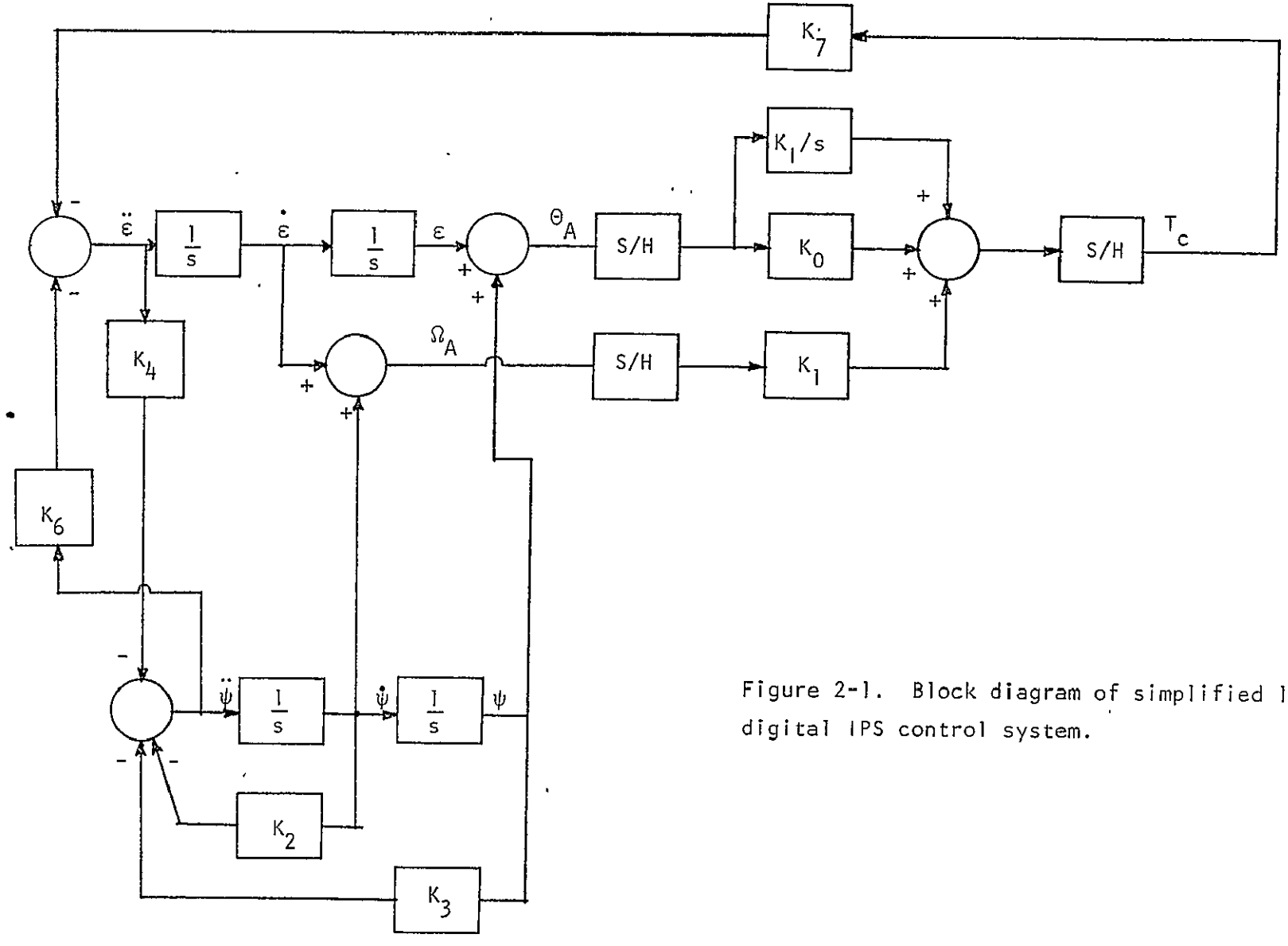

Figure 2-1. Block diagram of simplified linear digital IPS control system.

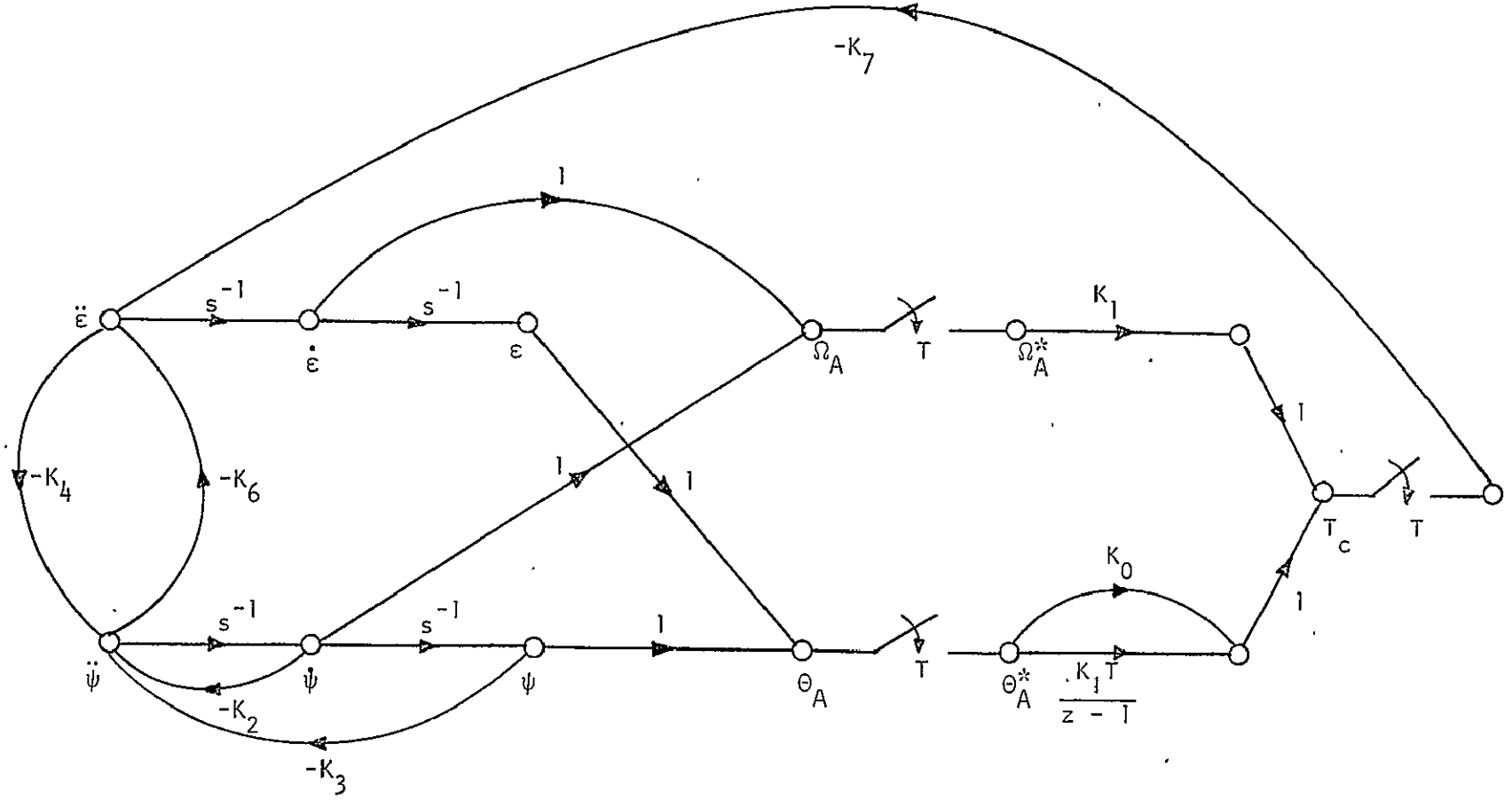

Figure 2-2. Signal flow graph of the simplified linear digital IPS control system.

From these two equations the characteristic equation of the digital system is found to be

$$\Delta(z) = 1 + K_1 G_1(z) + \left(K_0 + \frac{K_1 T}{z - 1}\right) G_2(z) = 0 \qquad (2\text{-}10)$$

where

$$G_1(z) = \mathcal{Z}[G_1(s)] = K_7(1 - z^{-1})\mathcal{Z}\left[\frac{(1 - K_4)s^2 + K_2 s + K_3}{s^2[(1 - K_4K_6)s^2 + K_2 s + K_3]}\right] \qquad (2\text{-}11)$$

$$G_2(z) = \mathcal{Z}[G_1(s)/s] \qquad (2\text{-}12)$$

The characteristic equation of the digital IPS control system is of the fifth order. However, the values of the system parameters are such that two of the characteristic equation roots are very close to the $z = 1$ point in the z-plane. These two roots are inside the unit circle and they are relatively insensitive to the values of K_1 and T, so long as T is not very large. The sampling period appears in terms such as $e^{-0.0094T}$ which is approximately one unless T is very large.

Since the values of K_2 and K_3 are relatively small,

$$G_1(z) \simeq K_7(1 - z^{-1})\mathcal{Z}\left[\frac{1 - K_4}{(1 - K_4K_6)s^2}\right] = \frac{K_7(1 - K_4)}{1 - K_4K_6}\frac{T}{z - 1}$$

$$= 2.79\times10^{-4}\frac{T}{z - 1} \qquad (2\text{-}13)$$

$$G_2(z) \simeq \frac{K_7(1 - K_4)}{1 - K_4K_6}(1 - z^{-1})\mathcal{Z}\left[\frac{1}{s^3}\right] = 2.79\times10^{-4}\ \frac{T^2(z + 1)}{2(z - 1)^2} \qquad (2\text{-}14)$$

Substituting $G_1(z)$ and $G_2(z)$ into Eq. (2-10), the characteristic equation of the digital IPS is approximated by the following third-order equation:

$$z^3 + \left(\frac{K_0K_pT^2}{2} + K_1K_pT - 3\right)z^2 + \left(\frac{K_pK_1T^3}{2} - 2K_1K_pT + 3\right)z$$

$$+ \left(\frac{K_pK_1T^3}{2} + K_1K_pT - 1 - \frac{K_0K_pT^2}{2}\right) = 0 \qquad (2\text{-}15)$$

where $K_p = 2.79\times10^{-4}$, and it is understood that two other characteristic equation roots are at $z = 1^-$. It can be shown that in the limit as T approaches zero, the three roots of Eq. (2-15) approaches to the roots of the characteristic equation of the continuous-data IPS control system, and the two roots near $z = 1$ also approach to near $s = 0$, as shown by the root locus diagram in Figure 1-3.

Substituting the values of the system parameters into Eq. (2-15), we have

$$\Delta(z) = z^3 + (111.6T^2 + 16.74T - 3)z^2 + (3 - 33.48T + 1.395\times10^{-4}K_I T^3)z + (1.395\times10^{-4}K_I T^3 + 16.74T - 111.6T^2 - 1) = 0 \qquad (2\text{-}16)$$

Applying Jury's test on stability to the last equation, we have

(1) $\Delta(1) > 0$ or $K_p K_I T^3 > 0$ (2-17)

Thus, $K_I > 0$, since $T > 0$.

(2) $\Delta(-1) < 0$ or $-8 + 66.96T < 0$ (2-18)

Thus, $T < 0.12$ sec. (2-19)

(3) Also, $|a_0| < a_3$, or

$$|1.395\times10^{-4}K_I T^3 + 16.74T - 111.6T^2 - 1| < 1 \qquad (2\text{-}20)$$

The relation between T and K_I for the satisfaction of Eq. (2-20) is plotted as shown in Fig. 2-3.

(4) The last criterion that must be met for stability is

$$|b_0| > b_2 \qquad (2\text{-}21)$$

where

$$b_0 = a_0^2 - a_3^2$$

$$b_2 = a_0 a_2 - a_1 a_3$$

$$a_0 = 1.395\times10^{-4}K_I T^3 + 16.74T - 111.6T^2 - 1$$

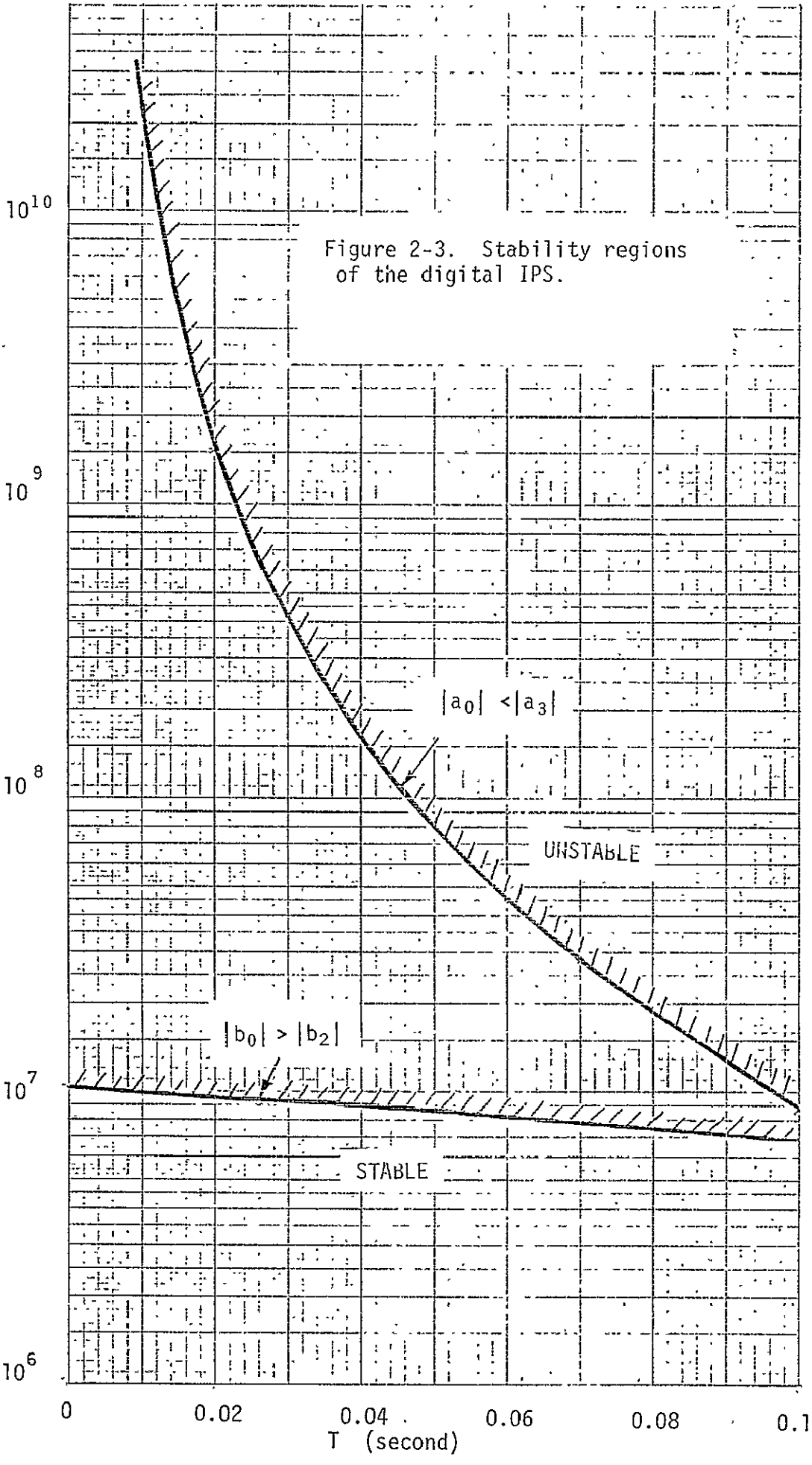

Figure 2-3. Stability regions of the digital IPS.

$$a_1 = 3 - 33.48T + 1.395\times10^{-4}K_1T^3$$

$$a_2 = 111.6T^2 + 16.74T - 3$$

$$a_3 = 1$$

The relation between T and K_1 for the satisfaction of Eq. (2-21) is plotted as shown in Figure 2-3. It turns out that the inequality condition of Eq. (2-21) is the more stringent one for stability. Notice also that as the sampling period T approaches zero, the maximum value of K_1 for stability is slightly over 10^7, as indicated by the root locus plot of the continuous-data IPS.

For quick reference, the maximum values of K_1 for stability corresponding to various T are tabulated as follows:

T	Max. K_1
0.01	10^7
0.08	7.5×10^6
0.1	6.9×10^6

When T = 0.05 sec, the characteristic equation is factored as

$$(z - 1)(z^2 - 0.884z + 0.442 - 0.1744\times10^{-7}K_1) = 0 \qquad (2\text{-}22)$$

Thus, there is always a root at a = 1 for all values of K_1, and the system is not asymptotically stable.

The root locus plot for T = 0.01, 0.08, and 0.1 second when K_1 varies are shown in Figures 2-4, 2-5, and 2-6, respectively. The two roots which are near z = 1 and are not sensitive to the values of T and K_1 are also included in these plots. The root locations on the root loci are tabulated as follows:

T = 0.01 sec

K_I		ROOTS
0	1.00000	0.91072 ± j0.119788
10^6	0.9864	0.917509 ± j0.115822
5×10^6	0.907357	0.957041 ± j0.114946
10^7	0.853393	0.984024 ± j0.137023
5×10^7	0.734201	1.04362 ± j0.224901
10^8	0.672306	1.07457 ± j0.282100

T = 0.08

K_I		ROOTS
0	0.999972	-0.0267061 ± j0.611798
10^6	0.888688	0.0289362 ± j0.583743
5×10^6	0.0273573	0.459601 ± j0.665086
7.5×10^6	-0.156092	0.551326 ± j0.851724
10^7	-0.253228	0.599894 ± j0.989842
10^8	-0.770222	0.858391 ± j2.83716

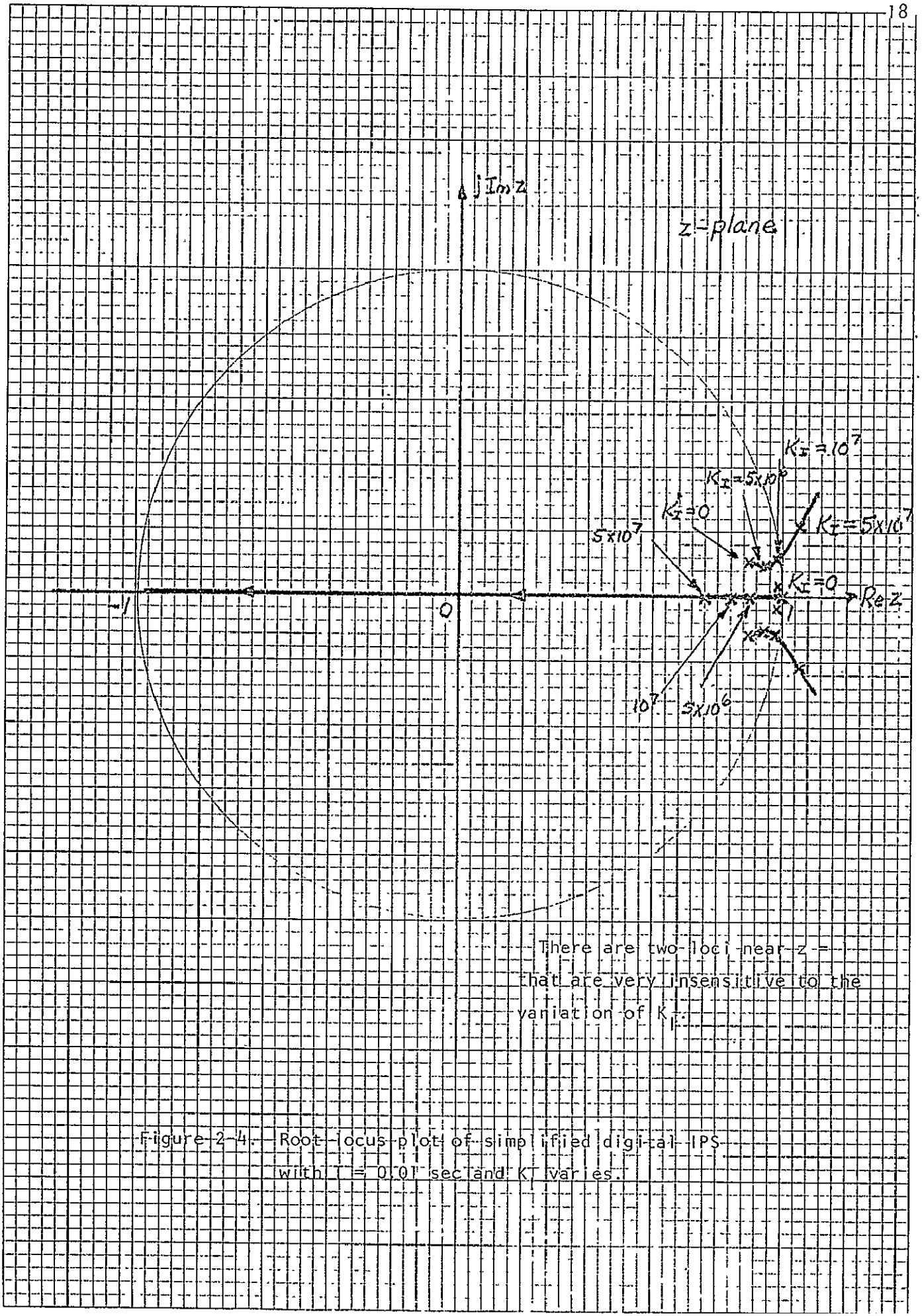

There are two loci near z = 1 that are very insensitive to the variation of K_I.

Figure 2-4. Root locus plot of simplified digital IPS with T = 0.01 sec and K_I varies.

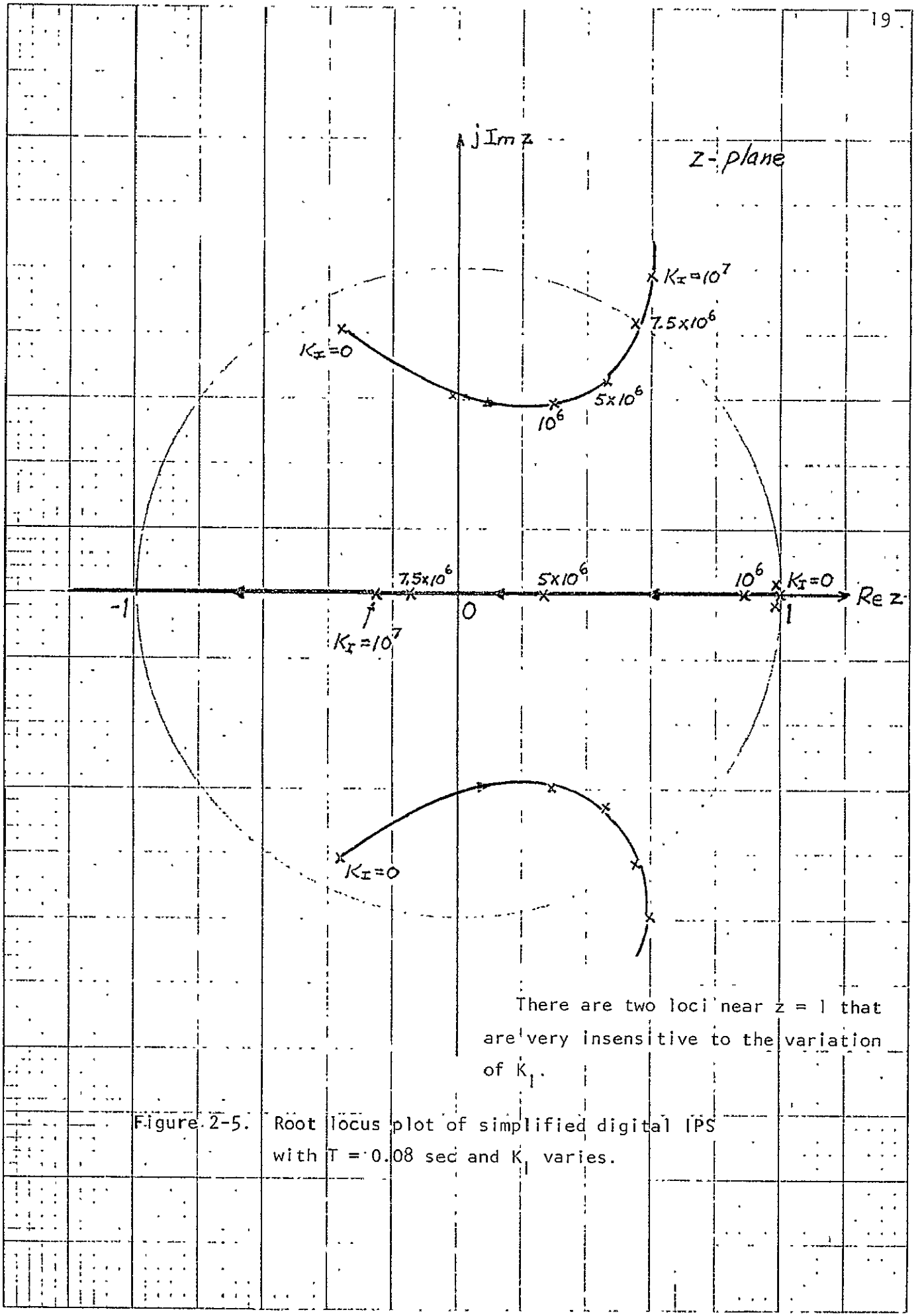

There are two loci near z = 1 that are very insensitive to the variation of K_1.

Figure 2-5. Root locus plot of simplified digital IPS with T = 0.08 sec and K_1 varies.

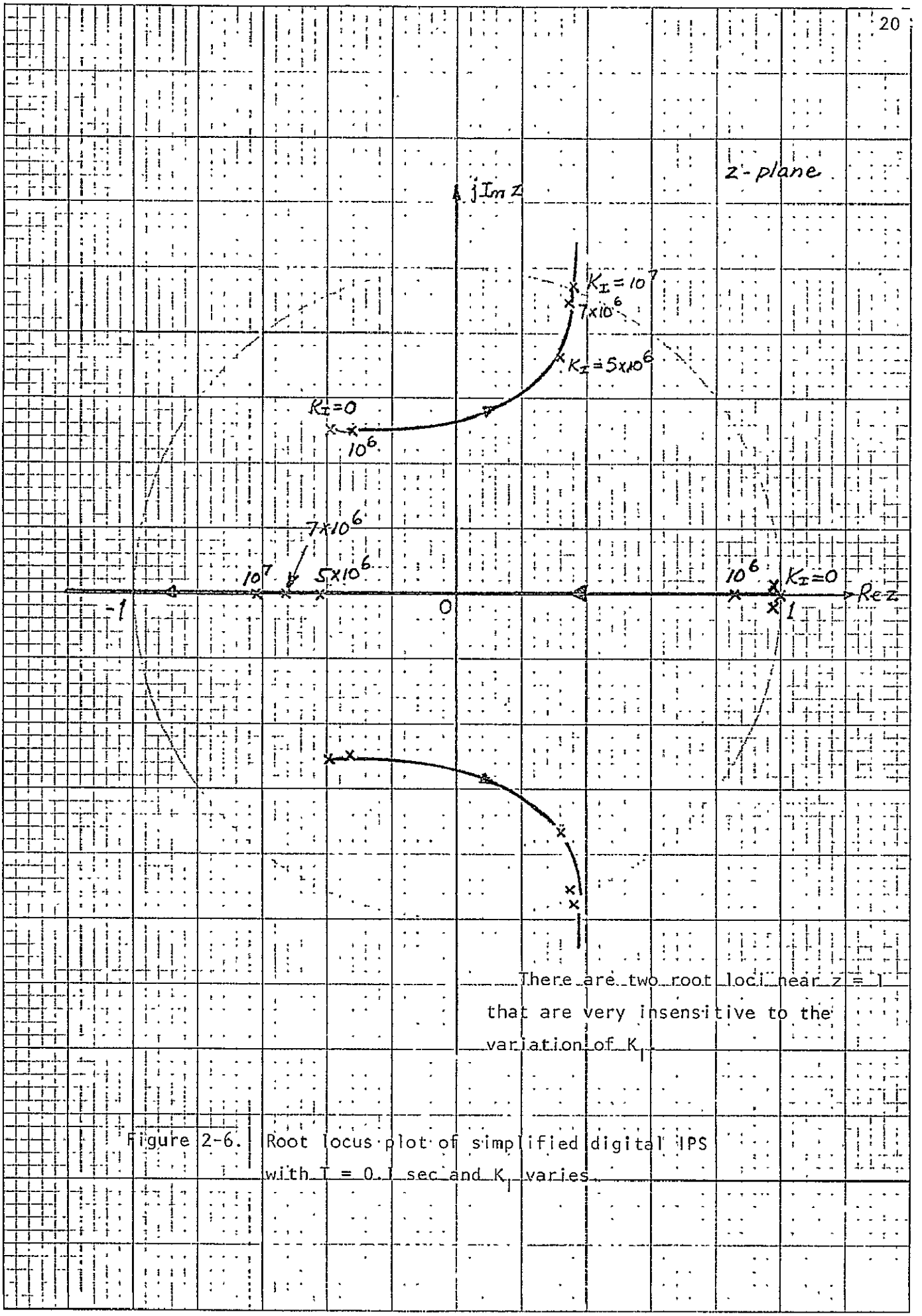

There are two root loci near z = 1 that are very insensitive to the variation of K_I.

Figure 2-6. Root locus plot of simplified digital IPS with T = 0.1 sec and K_I varies.

T = 0.1

K_I	ROOTS	
0	0.990937	$-0.390469 \pm j0.522871$
10^6	0.860648	$-0.325324 \pm j0.495624$
5×10^6	-0.417697	$0.313849 \pm j0.716370$
7×10^6	-0.526164	$0.368082 \pm j0.938274$
10^7	-0.613794	$0.411897 \pm j1.17600$
10^8	-0.922282	$0.566141 \pm j3.78494$

The linear digital IPS control system shown by the block diagram of Figure 2-1, with the system parameters specified in Chapter 1, was simulated on a digital computer. The time response of $\varepsilon(t)$ when the initial value of $\varepsilon(t)$, ε_o is one, is obtained. Figure 2-7 illustrates the responses of $\varepsilon(t)$ for T = 0.01, $K_I = 5\times10^6$, and T = 0.1, $K_I = 10^5$ and $K_I = 10^6$. Similar to the continuous-data IPS control system analyzed in Chapter 1, the time response of the digital IPS is controlled by the closed-loop poles which are very near the z = 1 point in the z-plane. Therefore, when the sampling period T and the value of K_I change within the stable limits, the system response will again be characterized by the long time in reaching zero as time approaches infinity.

The results show that as far at the linear simplified model is concerned, the sampling period can be as large as 0.1 second, and the digital IPS system is still stable for K_I less than 10^7.

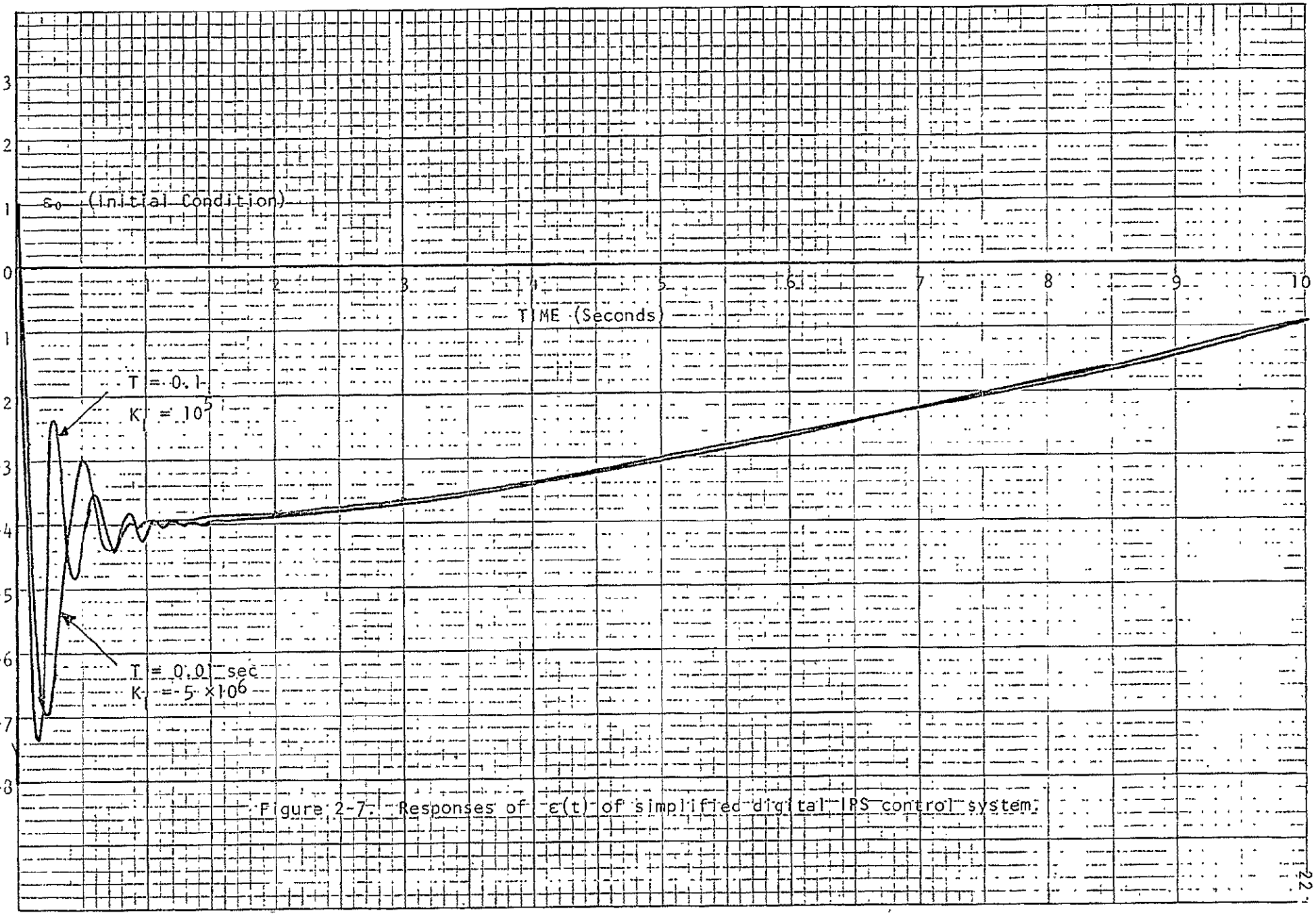

Figure 2-7. Responses of $\varepsilon(t)$ of simplified digital IRS control system.

3. Analysis of Continuous-Data IPS Control System With Wire Cable Torque Nonlinearity

In this chapter we will conduct a stability analysis of the simplified IPS control system with the nonlinear characteristics of the torques caused by the combined effect of the flex pivot of the gimbal and by wire cables, for transmitting power, etc., across the gimbal to the experiment, as shown in Figure 3-1.

The flex pivot torque disturbance has been modeled[2] as a linear spring with slope K_{FP}, as shown in Figure 3-2. The wire torque disturbance is modeled as a nonlinear spring, with a slope of K_{WT}, as shown in Figure 3-3. The total torque disturbance associated with the flex pivot and wire cables is summed up as shown in Figure 3-4. The continuous-data IPS control system with the nonlinear torque characteristics is shown in Figure 3-5.

The objective of the analysis in this chapter is to study the condition of sustained oscillation of the nonlinear IPS control system shown in Figure 3-5.

The Describing Function of the Wire-Cable Nonlinearity

It was pointed out in the above discussion that the wire cable nonlinearity can be modeled by either the arrangement shown in Figure 3-4(a) or Figure 3-4(b). For the model of Figure 3-4(a), a relay characteristic is present between $\dot{\varepsilon}$ and T_c, and, in addition, a linear gain of $K_{WT} + K_{FP}$ exists between ε and T_c, where K_{FP}denotes the gain constant due to the flex pivot torque, Using this model, one can conduct a describing function analysis with the relay nonlinearity, but the linear system model is altered by the addition of the branch with the gain of $K_{WT} + K_{FP}$. However, careful examination of the block diagram of Figure 3-5 reveals that the branch with

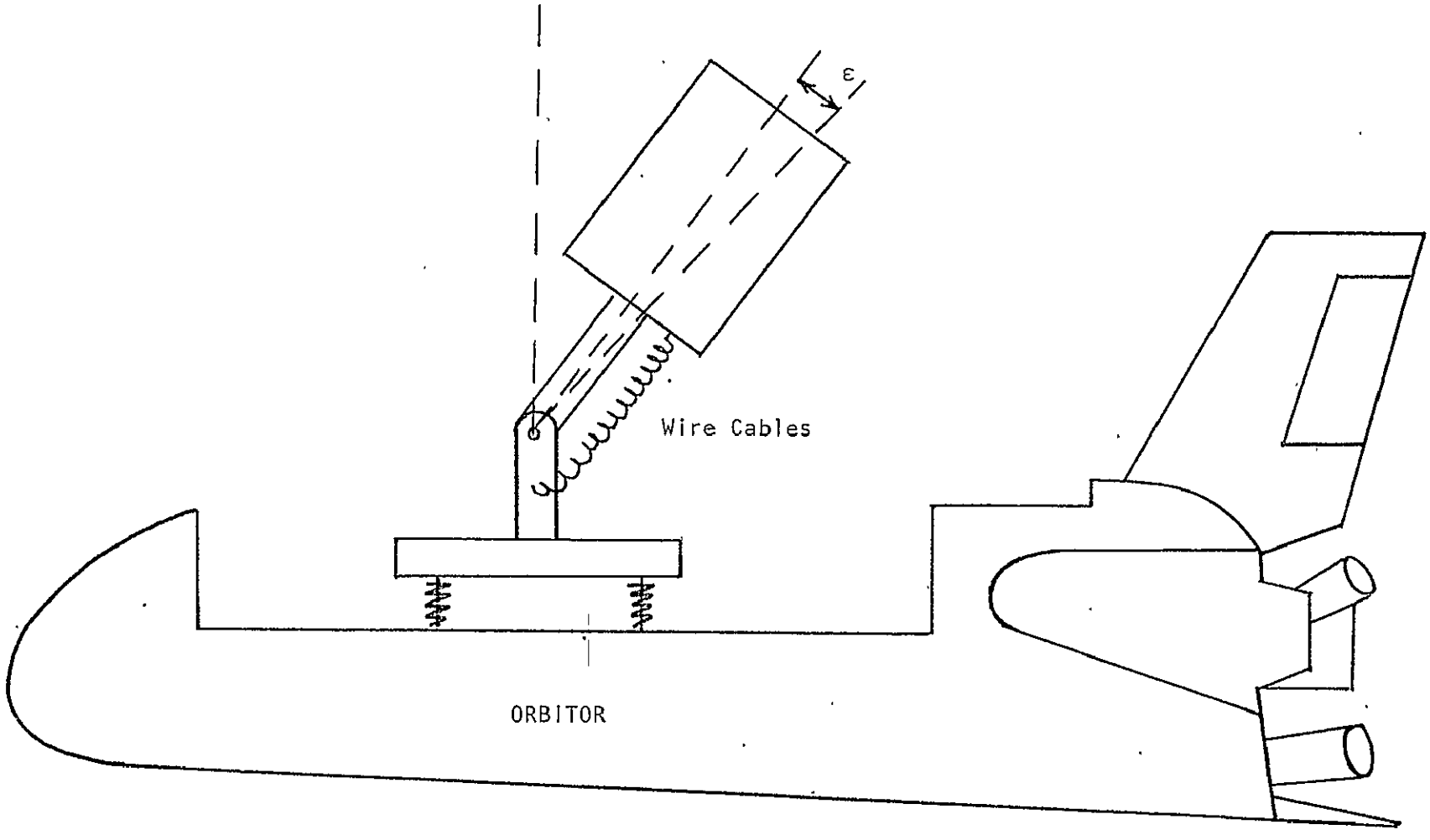

Figure 3-1. Experiment with wire cables

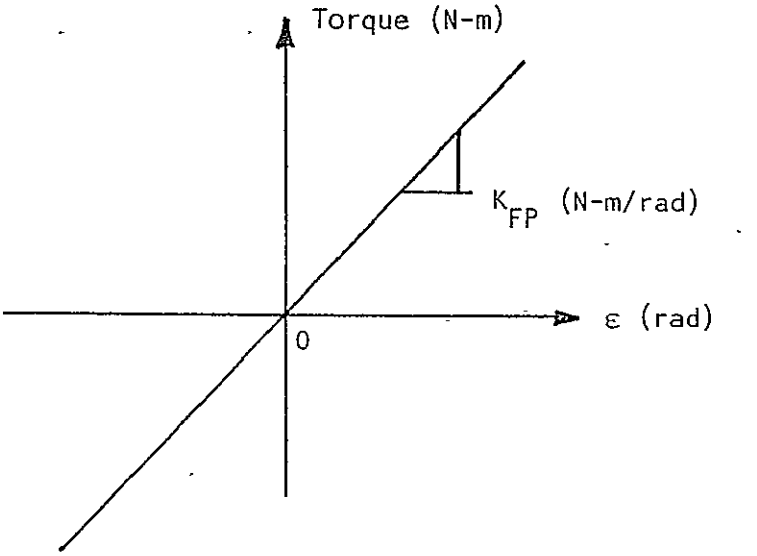

Figure 3-2. Flex-pivot torque characteristic.

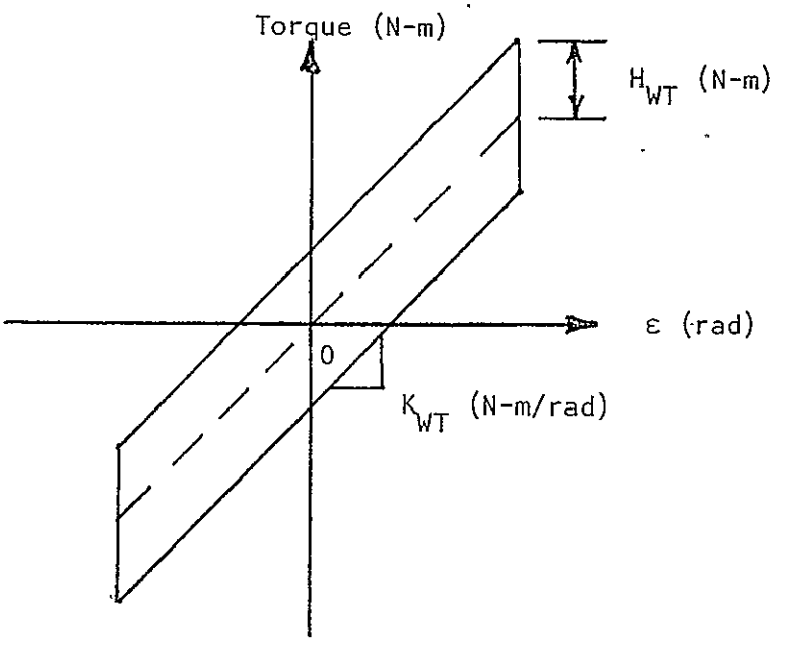

Figure 3-3. Wire cable torque characteric.

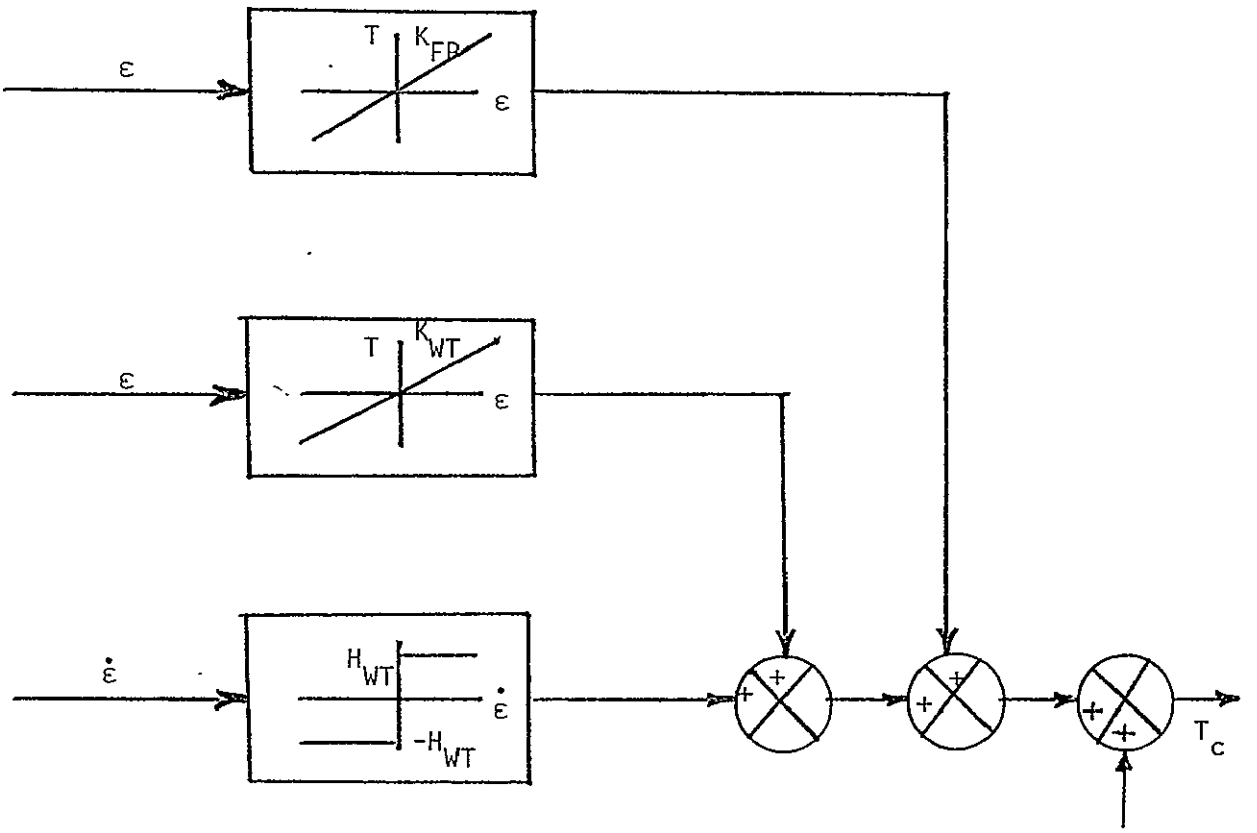

(a)

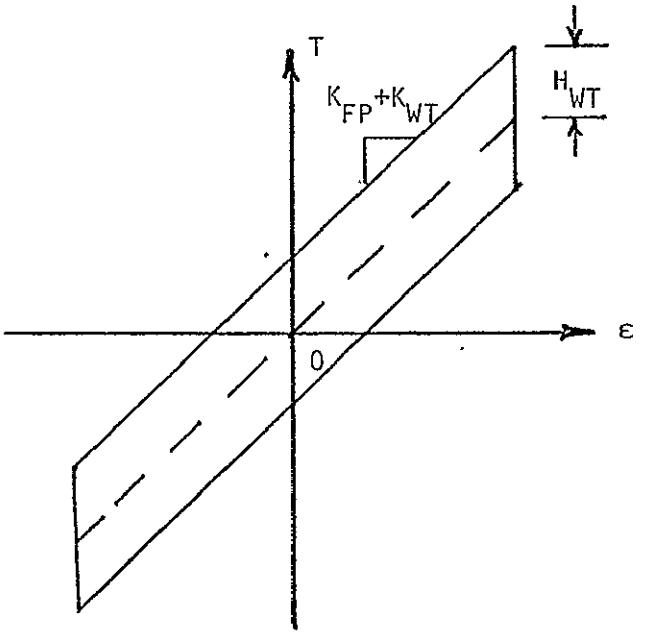

(b)

Figure 3-4. Combined flex pivot and wire cables torque characteristics.

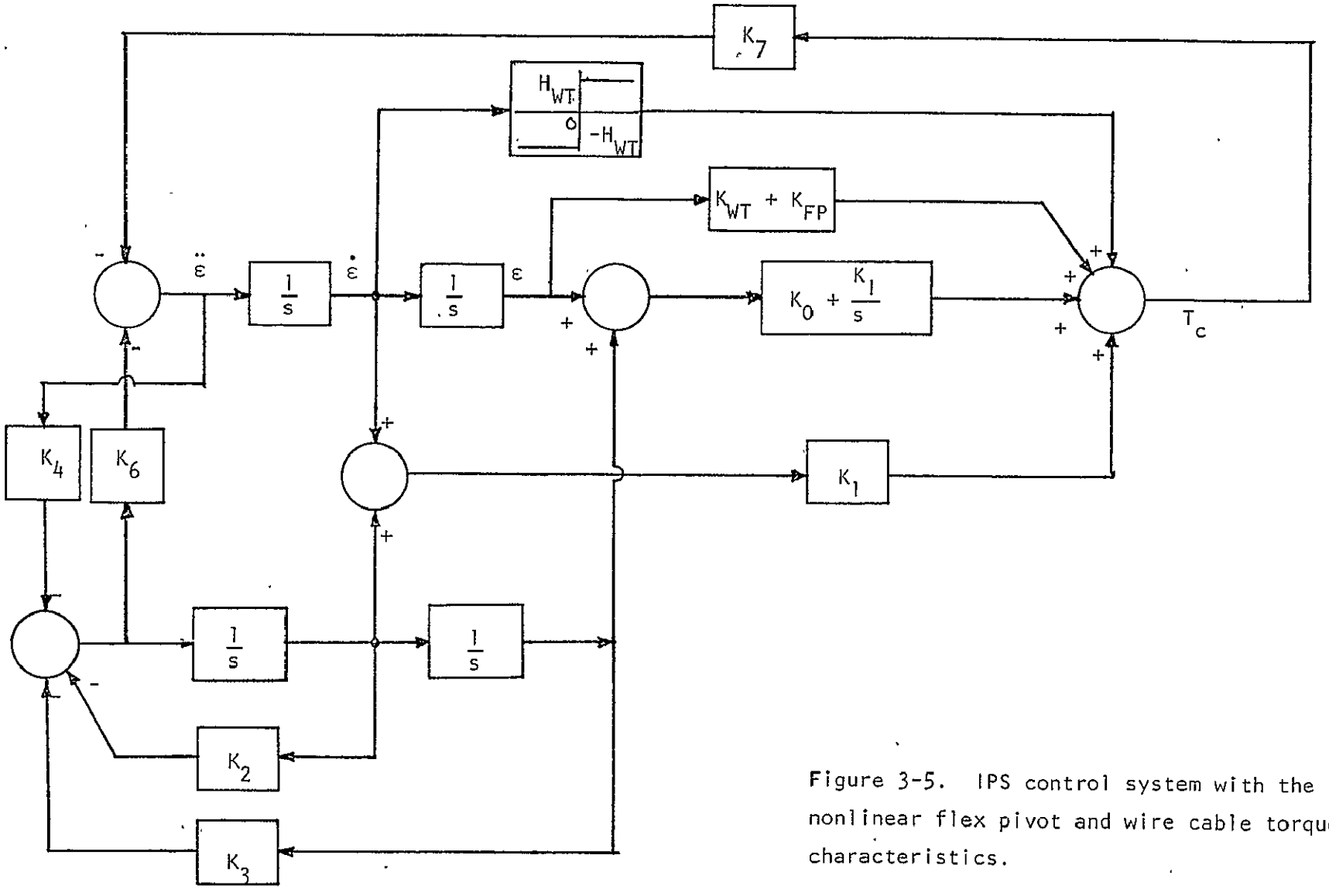

Figure 3-5. IPS control system with the nonlinear flex pivot and wire cable torque characteristics.

the gain of $K_{WT} + K_{FP}$ is parallel to the branch with the gain K_0 which has a magnitude of 8×10^5 N-m/rad. Since the value of K_{WT} lies between 0.25 and 25 N-m/rad, and the maximum value of K_{FP} is in the order of several hundred, it is apparent that the value of K_0 will be predominant on the system performance. This means that the linear transfer function will not change appreciably by the variation of the values of K_{WT} and K_{FP}.

Prediction of Self-Sustained Oscillations With the Describing Function Method

From Figure 3-5 the equivalent characteristic equation of the nonlinear system is written as

$$1 + N(\dot{\varepsilon})G_{eq}(s) = 0 \tag{3-1}$$

where $N(\dot{\varepsilon})$ is the describing function of the relay characteristic shown in Figure 3-4(a), and is given by

$$N(\dot{\varepsilon}) = 4H_{WT}/\pi\dot{\varepsilon} \tag{3-2}$$

The transfer function $G_{eq}(s)$ is derived from Figure 3-5,

$$G_{eq}(s) = \frac{0.0013946(s^4 + 0.0012528s^3 + 0.0036846s^2)}{\Delta(s)} \tag{3-3}$$

where

$$\Delta(s) = s^5 + 16.704s^4 + 222.6s^3 + (2.781\times10^{-4}K_I + 1.706)s^2 + (4.11 + 1.747\times10^{-6}K_I)s + 513.855\times10^{-8}K_I \tag{3-4}$$

A necessary condition of self-sustained oscillation is

$$G_{eq}(s) = -1/N(\dot{\varepsilon}) \tag{3-5}$$

Figure 3-6 shows the frequency response plots of $G_{eq}(s)$ for $K_I = 10^5$, 10^6, and 10^7, as a function of ω, and the trajectory of $-1/N(\dot{\varepsilon}) = -\pi\dot{\varepsilon}/4H_{WT}$;

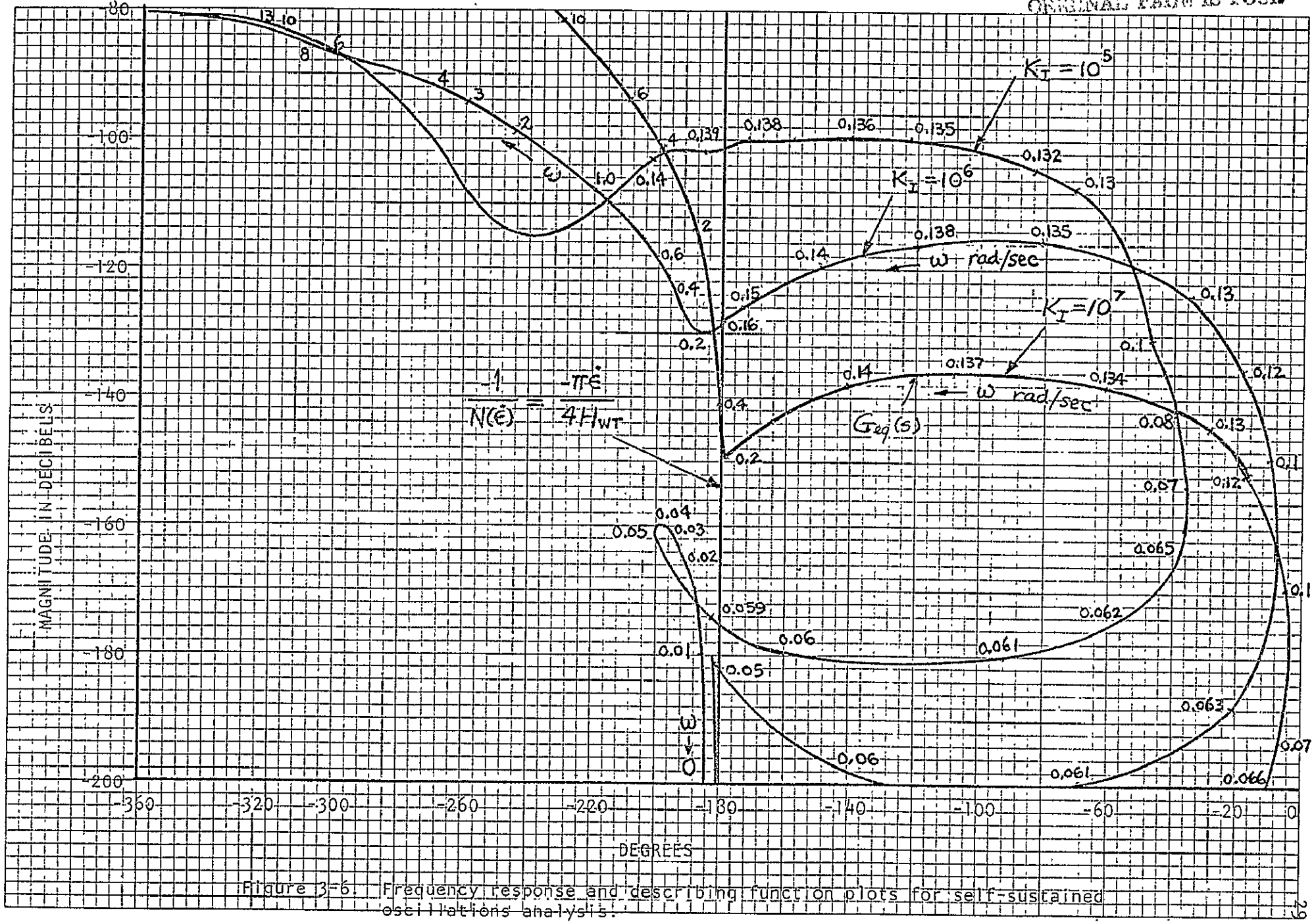

Figure 3-6. Frequency response and describing function plots for self-sustained oscillations analysis.

the latter lies on the -180° axis for all combinations of magnitudes of $\dot{\varepsilon}$ and H_{WT}. Figure 3-6 shows that for each value of K_I there are two equilibrium points, one stable and the other unstable. For instance, for $K_I = 10^6$, the $G_{eq}(s)$ curve intersects the -180° axis at $\omega = 0.16$ rad/sec and $\omega = 0.05$ rad/sec. The equilibrium point that corresponds to $\omega = 0.16$ rad/sec is a stable equilibrium point, whereas $\omega = 0.05$ rad/sec represents an unstable equilibrium point. The stable solutions of the sustained oscillations for $K_I = 10^5$, 10^6, and 10^7 are tabulated below:

K_I	$\dot{\varepsilon}/H_{WT}$ (rad/sec)	ε/H_{WT} (rad)	(arc-sec)	ω(rad/sec)	T_c (sec)
10^7	7.2×10^{-8}	2.39×10^{-7}	0.05	0.3	21
10^6	5.07×10^{-7}	3.17×10^{-6}	0.65	0.16	39
10^5	1.13×10^{-5}	8.19×10^{-5}	16.9	0.14	45

The conclusion is that self-sustained oscillations may exist in the nonlinear continuous-data control system.

Since the value of K_o is very large, the effect of using various values of K_{WT} and K_{FP} within their normal ranges would not be noticeable. Changing the value of H_{WT} has a one-to-one effect on the amplitudes of oscillations of ε and $\dot{\varepsilon}$.

Digital Computer Simulation of the Continuous-Data Nonlinear IPS Control System

Since the transient time duration of the IPS control system is exceedingly long, it is extremely time consuming and expensive to verify the self-sustained oscillation by digital computer simulation. Several digital computer simulation runs indicated that the transient response of the IPS system does not die out after many minutes of real time simulation. It should be pointed out that the

describing function solution simply gives a sufficient condition for self-sustained oscillations to occur. The solutions imply that there is a certain set of initial conditions which will induce the indicated self-sustained oscillations. However, in general, it may be impractical to look for this set of initial conditions, especially if the set is very small. It is entirely possible that a large number of simulation runs will result in a totally stable situations.

Figure 3-7 illustrates a section of the time response of $\varepsilon(t)$ from t = 612 sec to 692 sec. The initial conditions are $\varepsilon(0) = 10^{-4}$ and $\dot{\varepsilon}(0) = 10^{-5}$, and all other initial conditions are set to zero; $K_I = 10^5$, $H_{WT} = 1$, and $K_{WT} + K_{FP} = 100$. It was mentioned earlier that the system is not sensitive to the values of K_{WT} and K_{FP}. From Figure 3-7 it is seen that the period of the oscillation is 48 seconds, or 0.13 rad/sec, which is very close to the predicted value.

Time (sec)	ε(t)
6.1200E 02	-4.7627E-05
6.1400E 02	-2.6500E-05
6.1600E 02	-2.3637E-06
6.1800E 02	1.6859E-05
6.2000E 02	2.3915E-05
6.2200E 02	3.8527E-05
6.2400E 02	4.9397E-05
6.2600E 02	6.1609E-05
6.2800E 02	7.0494E-05
6.3000E 02	6.9333E-05
6.3200E 02	5.8036E-05
6.3400E 02	4.1319E-05
6.3600E 02	2.6582E-05
6.3800E 02	2.0783E-05
6.4000E 02	-4.5983E-06
6.4200E 02	-2.0842E-05
6.4400E 02	-3.4681E-05
6.4600E 02	-5.1003E-05
6.4800E 02	-6.1067E-05
6.5000E 02	-6.1478E-05
6.5200E 02	-5.6092E-05
6.5400E 02	-5.1468E-05
6.5600E 02	-5.3848E-05
6.5800E 02	-4.2871E-05
6.6000E 02	-2.9645E-05
6.6200E 02	-9.3290E-06
6.6400E 02	1.2747E-05
6.6600E 02	2.8828E-05
6.6800E 02	3.1904E-05
6.7000E 02	4.1998E-05
6.7200E 02	4.8158E-05
6.7400E 02	5.5803E-05
6.7600E 02	6.0603E-05
6.7800E 02	5.6122E-05
6.8000E 02	4.2512E-05
6.8200E 02	2.4641E-05
6.8400E 02	9.9768E-06
6.8600E 02	5.4668E-06
6.8800E 02	-8.7772E-06
6.9000E 02	-2.1456E-05
6.9200E 02	-3.7501E-05

Figure 3-7. A section of the response of ε(t). $K_I = 10^5$.

4. Analysis of the Digital IPS Control System With Wire Cable Torque Nonlinearity

In this chapter we will conduct a stability analysis of the simplified digital IPS control system with nonlinear characteristics of the torques caused by the combined effect of the flex pivot of the gimbal and wire cables.

The analysis used here is the discrete describing function which will give sufficient conditions on self-sustained oscillations in nonlinear digital systems. The block diagram of the nonlinear digital IPS system is shown in Figure 4-1. For mathematical convenience, a sample-and-hold is inserted at the input of the nonlinear element.

A signal flow graph of the system in Figure 4-1 is drawn in Figure 4-2. The z-transforms of the variables in Figure 4-2 are written,

$$\Theta_A(z) = -G_2(z)T_c(z) \tag{4-1}$$

$$\Omega_A(z) = -G_1(z)T_c(z) \tag{4-2}$$

$$\dot{\varepsilon}(z) = -G_4(z)T_c(z) \tag{4-3}$$

$$T_c(z) = K_1\Omega_A(z) + \left(K_o + \frac{K_1 T}{z-1}\right)\Theta_A(z) - (K_{WT} + K_{FP})G_3(z)T_c(z) + N(z)\dot{\varepsilon}(z) \tag{4-4}$$

where

$$G_1(z) = \mathcal{Z}\left[K_7 \frac{G_h(s)}{\Delta s}(\Delta_1 - K_4)\right]$$

$$G_2(z) = \mathcal{Z}\left[K_7 \frac{G_h(s)}{\Delta s^2}(\Delta_1 - K_4)\right]$$

$$G_3(z) = \mathcal{Z}\left[K_7 \frac{G_h(s)}{\Delta s^2}\Delta_1\right]$$

$$G_4(z) = \mathcal{Z}\left[K_7 \frac{G_h(s)}{\Delta s}\Delta_1\right]$$

$$G_h(s) = \frac{1 - e^{-Ts}}{s}$$

$$\Delta_1 = 1 + K_2 s^{-1} + K_3 s^{-2}$$

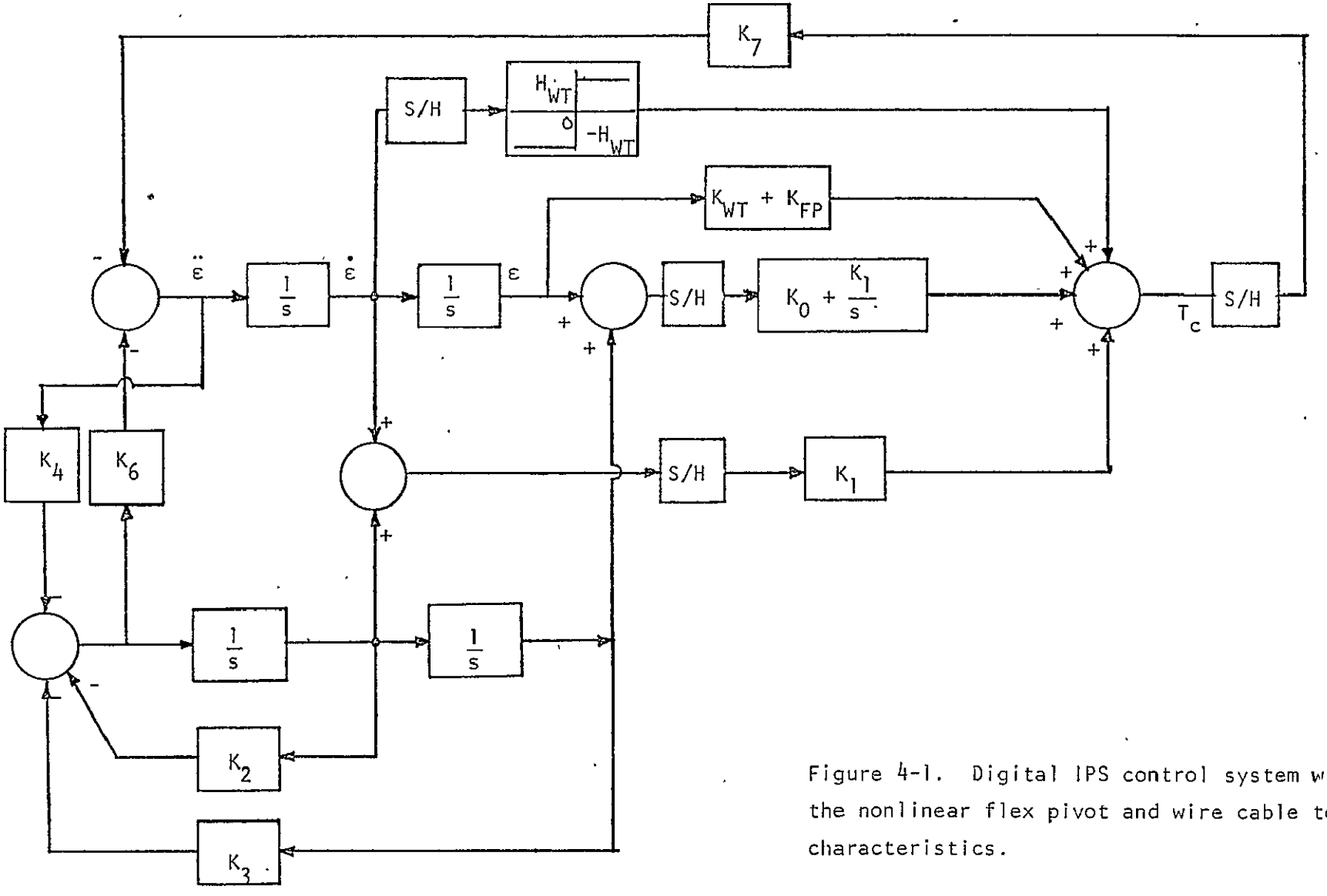

Figure 4-1. Digital IPS control system with the nonlinear flex pivot and wire cable torque characteristics.

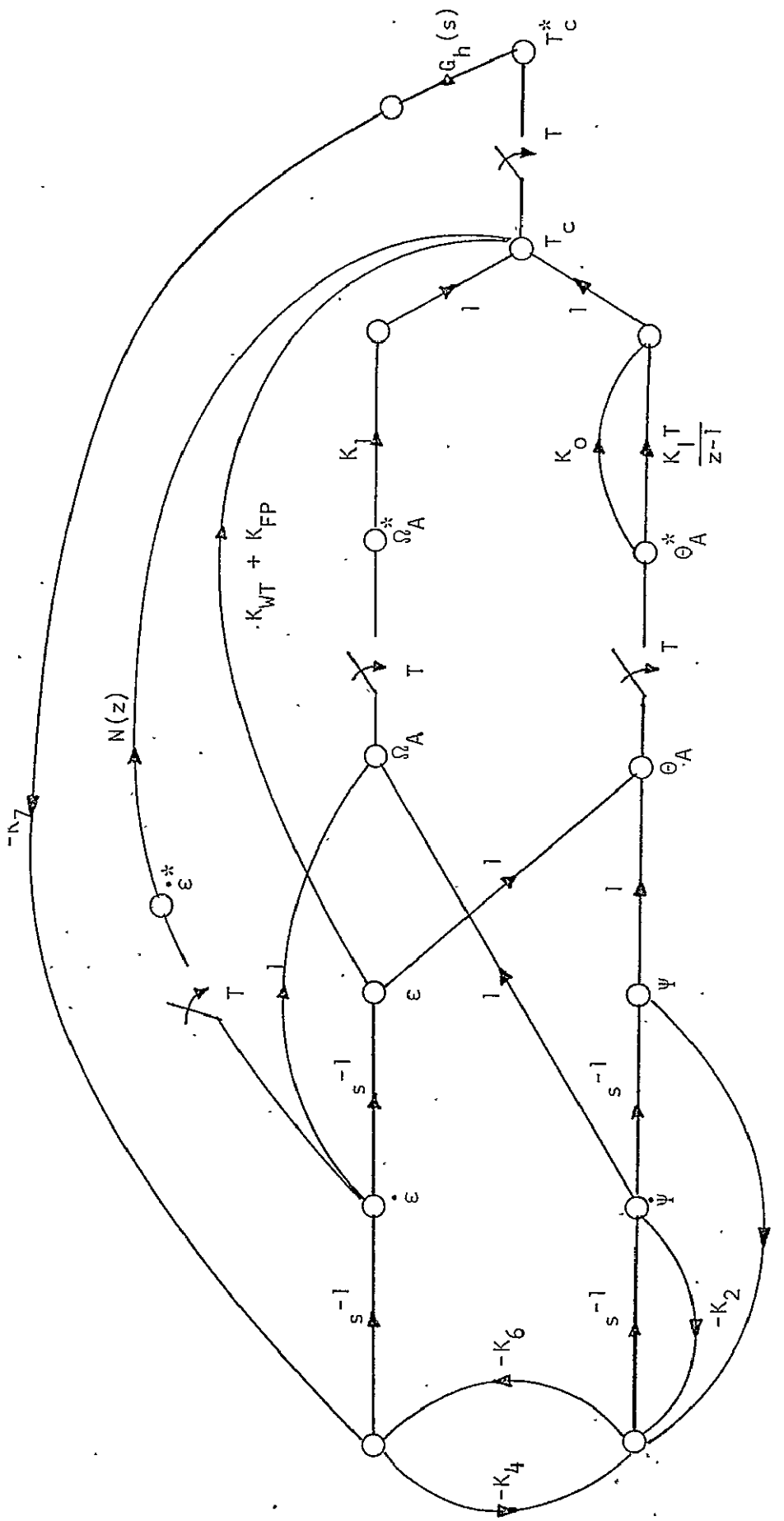

Figure 4-2. Signal flow graph of the digital IPS control system.

$$\Delta = (1 - K_4K_6) + K_2s^{-1} + K_3s^{-2}$$

$N(z)$ = discrete describing function of ideal relay $(+H_{WT}, 0, -H_{WT})$

Since K_2 and K_3 are very small, approximations lead to

$$G_1(z) \simeq \frac{2.79\ 10^{-4}T}{z - 1}$$

$$G_2(z) \simeq \frac{2.79\ 10^{-4}T^2(z + 1)}{2(z - 1)^2}$$

$$G_3(z) \simeq \frac{0.000697T^2(z + 1)}{2(z - 1)^2}$$

$$G_4(z) \simeq \frac{0.0001394T}{z - 1}$$

Equations (4-1) through (4-4) lead to the sampled flow graph of Figure 4-3, from which we have the characteristic equation,

$$\Delta(z) = 1 + K_1G_1(z) + \left(K_o + \frac{K_1T}{z-1}\right)G_2(z) + (K_{WT} + K_{FP})G_3(z) + G_4(z)N(z) \quad (4-5)$$

Equating $\Delta(z)$ to zero, the equivalent transfer fucntion $G_{eq}(z)$ is obtained,

$$G_{eq}(z) = \frac{G_4(z)}{1 + K_1G_1(z) + \left(K_o + \frac{K_1T}{z-1}\right)G_2(z) + (K_{WT} + K_{FP})G_3(z)} \quad (4-6)$$

The intersect between $G_{eq}(z)$ and $-1/N(z)$ gives the condition of self-sustained oscillations in the digital IPS control system.

Figure 4-4 shows the $G_{eq}(z)$ plots for various values of $N > 2$ for $K_1 = 10^5$. In this case, it has been assumed that the periods of oscillations are integral multiples of the sampling period T. Therefore, if T_c denotes the period of oscillation, $T_c = NT$, where N is a positive integer ≥ 2.

From Figure 4-4 it is seen that when N is very large and T is very small, $G_{eq}(z)$ approaches $G_{eq}(s)$. However, for relatively large sampling periods,

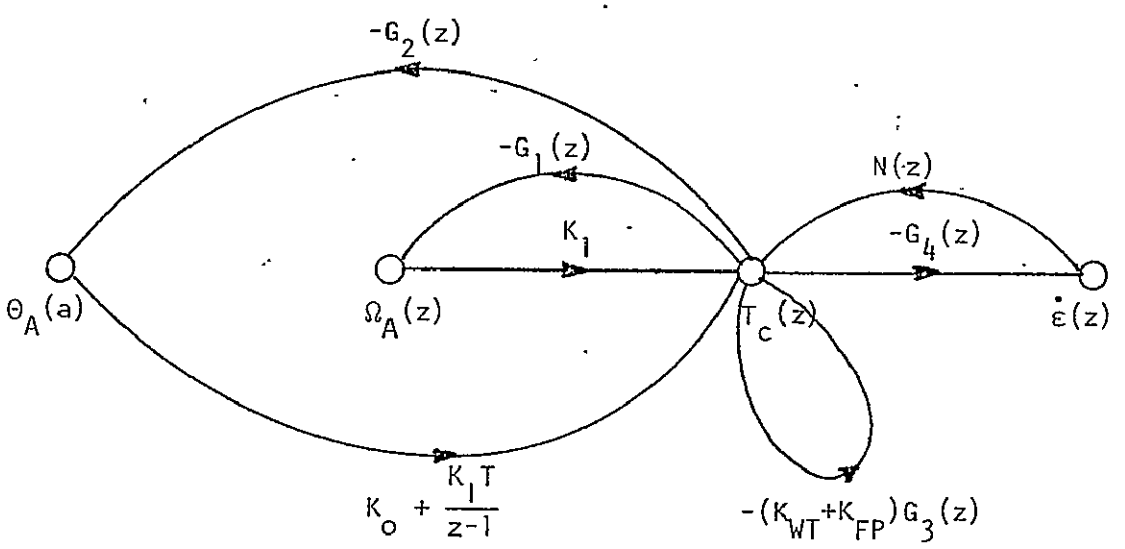

Figure 4-3. Sampled signal flow graph of the digital IPS control system.

$G_{eq}(z)$ does not approach to $G_{eq}(s)$ even for very large N. This indicates the fact that digital simulation of the continuous-data IPS can only be carried out accurately by using extremely small sampling periods.

The critical regions for $-1/N(z)$ of an ideal relay are a family of cylinders in the gain-phase coordinates, as shown in Figure 4-5. These regions extend from $-\infty$ db to $+\infty$ db, since the dead zone of the ideal relay is zero. For N = 2, the critical region is a straight line which lies on the -180° axis. The widest region is for N = 4, which extends from -225° to -135°. Therefore, any portions of the $G_{eq}(z)$ loci which do not lie in the critical regions will correspond to stable operations.

It is interesting to note from Figure 4-4 that the digital IPS system has the tendency to oscillate at very low and very high sampling periods, but there is a range of sampling periods for which self-sustained oscillations can be completely avoided.

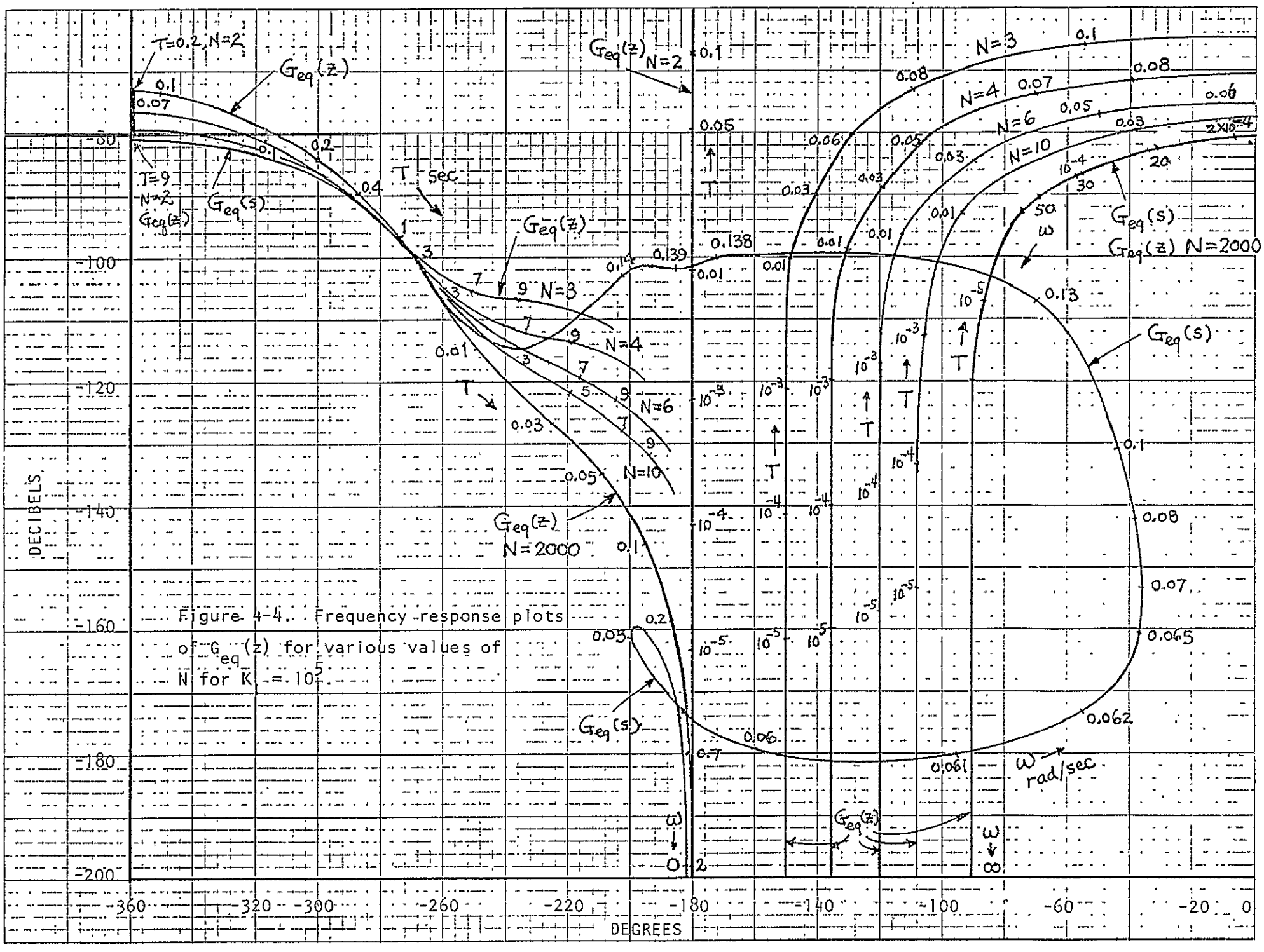

Figure 4-4. Frequency-response plots of $G_{eq}(z)$ for various values of N for $K = 10^5$.

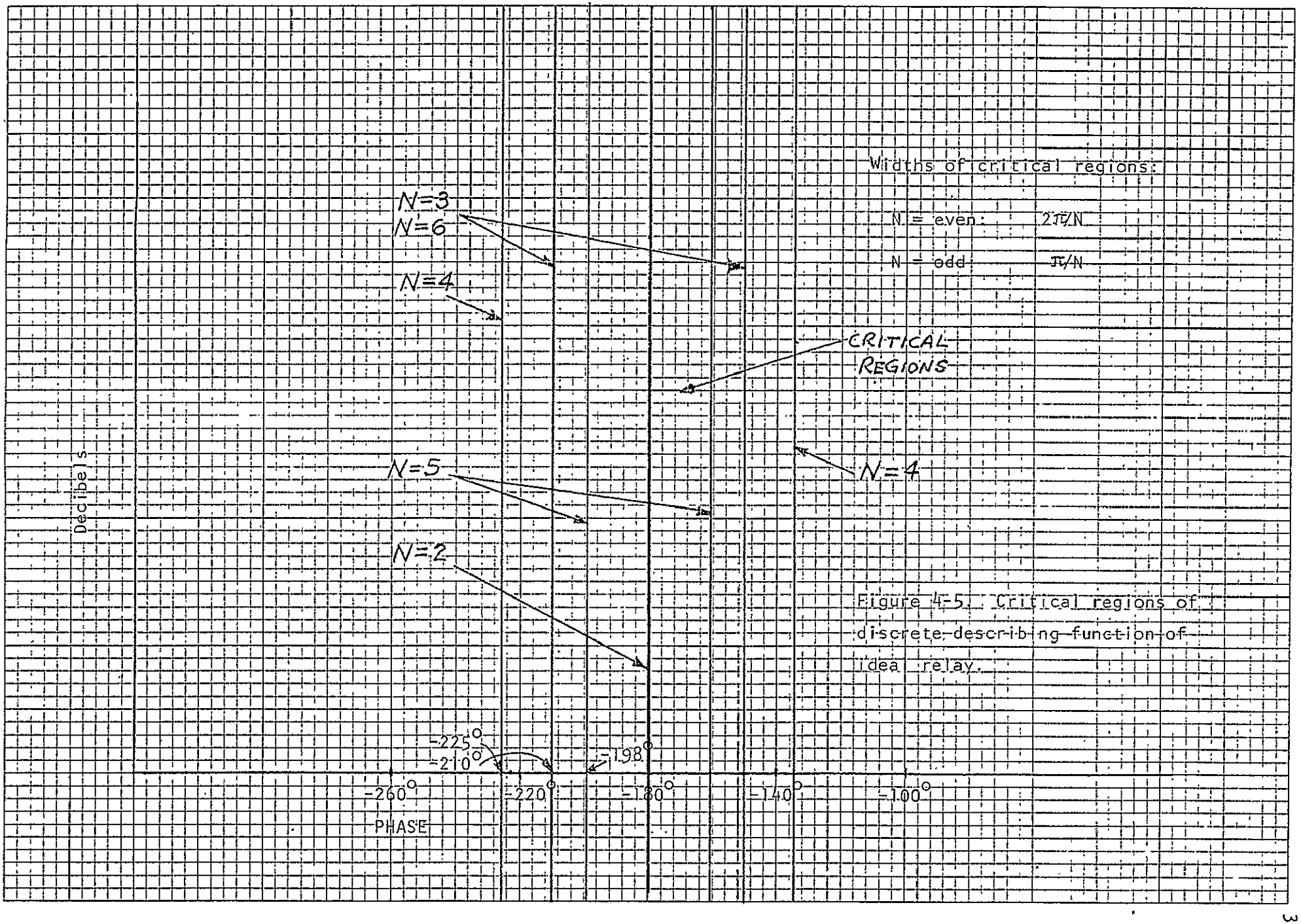

Figure 4-5. Critical regions of discrete-describing function of ideal relay.

Referring to Figure 4-4 it is noticed that when the sampling period T is very small, ($T \leq 10^{-2}$ sec approximately), the loci of $G_{eq}(z)$ for N = 2, 3, and 4 lie in their respective critical regions, and self-sustained oscillations characterized by these modes are possible. However, since the actual period of these oscillations are so small, being 2, 3, or 4 times the sampling period which is itself less than 0.01 sec, the steady-state oscillations are practically impossible to observe on a digital computer simulation unless the print-out interval is made very small. This may explain why it was difficult to pick up a self-sustained oscillation in the digital computer simulation of the continuous-data IPS system, since a digital computer simulation is essentially a sampled-data analysis.

When the sampling period is large ($T \geq 9$ sec approximately), the digital IPS system may again exhibit self-sustained oscillations, as shown by the $G_{eq}(z)$ loci converging toward the -180° axis as T increases. However, the $G_{eq}(z)$ loci of Figure 4-4 show that there is a midrange of T for which the digital system is stable. The $G_{eq}(z)$ locus for N = 2000 actually represents the locus for all large N. Therefore, for T = 0.1, the $G_{eq}(z)$ locus point will be outside of the critical regions, since as N increases, the widths of the critical regions decrease according to

N = even width of critical region = $2\pi/N$

N = odd width of critical region + π/N

Therefore, from the standpoint of avoiding self-sustained oscillations in the simplified digital IPS control system model, the sampling period may be chosen to lie approximately in the range of 0.01 to 1 second.

Digital Computer Simulation of the Digital Nonlinear IPS Control System

The digital IPS control system with wire-cable nonlinearity, as shown by the block diagram of Figure 4-1, has similar characteristics as the continuous-data system, especially when the sampling period is small. The digital IPS control system of Fig. 4-1, without the sample-and-hold in front of the nonlinear element, was simulated on the IBM 360/75 digital computer. With initial conditions set for ε and $\dot{\varepsilon}$, typical responses showed that the nonlinear digital IPS system exhibited a long oscillatory transient period. Figure 4-6 shows the beginning portion of the response of $\varepsilon(t)$ for $\varepsilon(0) = 10^{-3}$, $\dot{\varepsilon}(0) = 10^{-4}$, $K_I = 10^5$, $T = 0.1$ sec, $H_{WT} = 1$, $K_{WT} + K_{FP} = 100$. Figure 4-7 shows the same response over the period of 765 sec to 1015 seconds. Figure 4-8 gives the response of $\varepsilon(t)$ for the time duration of 1530 sec to 1725 sec, and it shows that the response eventually settles to nonoscillatory and finally should be stable.

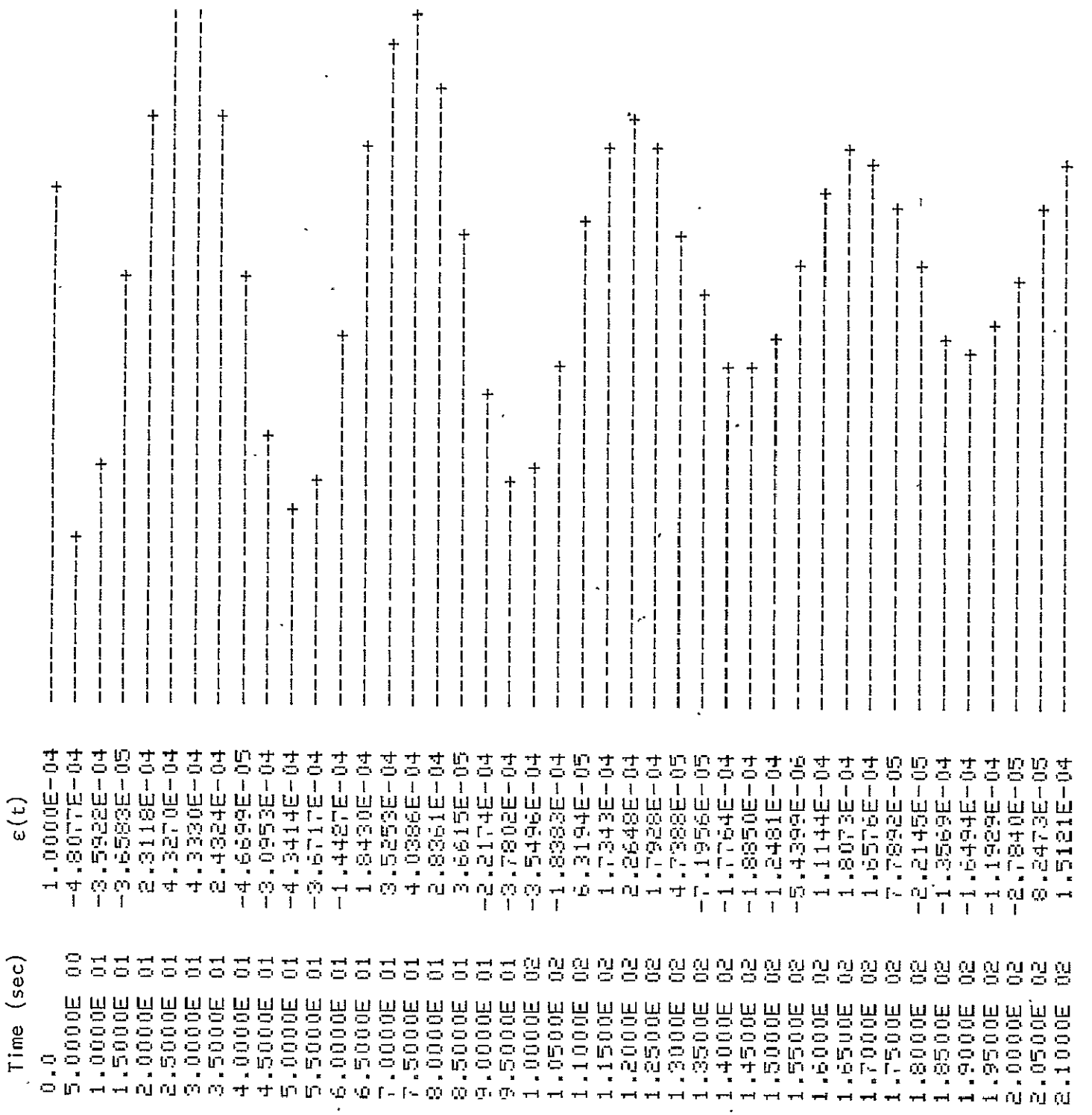

Figure 4-6. Beginning portion of $\varepsilon(t)$ of digital IPS system.

$T = 0.1$ sec, $H_{WT} = 1$, $K_I = 10^5$, $K_{WT} + K_{FP} = 100$.

Time (sec)	ε(t)
7.6500E 02	4.8449E-05
7.7000E 02	4.6277E-05
7.7500E 02	2.5693E-05
7.8000E 02	-3.7121E-06
7.8500E 02	-2.8820E-05
7.9000E 02	-3.8807E-05
7.9500E 02	-2.9759E-05
8.0000E 02	-6.2116E-06
8.0500E 02	2.1103E-05
8.1000E 02	4.0124E-05
8.1500E 02	4.2779E-05
8.2000E 02	2.8384E-05
8.2500E 02	3.7490E-06
8.3000E 02	-2.0021E-05
8.3500E 02	-3.2554E-05
8.4000E 02	-2.8711E-05
8.4500E 02	-1.0671E-05
8.5000E 02	1.3233E-05
8.5500E 02	3.2381E-05
8.6000E 02	3.8522E-05
8.6500E 02	2.9366E-05
8.7000E 02	9.3945E-06
8.7500E 02	-1.2310E-05
8.8000E 02	-2.6196E-05
8.8500E 02	-2.6411E-05
8.9000E 02	-1.3313E-05
8.9500E 02	6.9699E-06
9.0000E 02	2.5337E-05
9.0500E 02	3.3819E-05
9.1000E 02	2.8995E-05
9.1500E 02	1.3396E-05
9.2000E 02	-5.8441E-06
9.2500E 02	-2.0198E-05
9.3000E 02	-2.3537E-05
9.3500E 02	-1.4725E-05
9.4000E 02	2.0082E-06
9.4500E 02	1.9081E-05
9.5000E 02	2.9036E-05
9.5500E 02	2.7771E-05
9.6000E 02	1.6172E-05
9.6500E 02	-3.9172E-07
9.7000E 02	-1.4506E-05
9.7500E 02	-2.0075E-05
9.8000E 02	-1.4941E-05
9.8500E 02	-1.6809E-06
9.9000E 02	1.3672E-05
9.9500E 02	2.4329E-05
1.0000E 03	2.5769E-05
1.0050E 03	1.7654E-05
1.0100E 03	3.8166E-06
1.0150E 03	-9.4976E-06

Figure 4-7. Response of ε(t) of digital IPS control system. T = 0.1 sec, H_{WT} = 1, $K_I = 10^5$, $K_{WT} + K_{FP} = 100$.

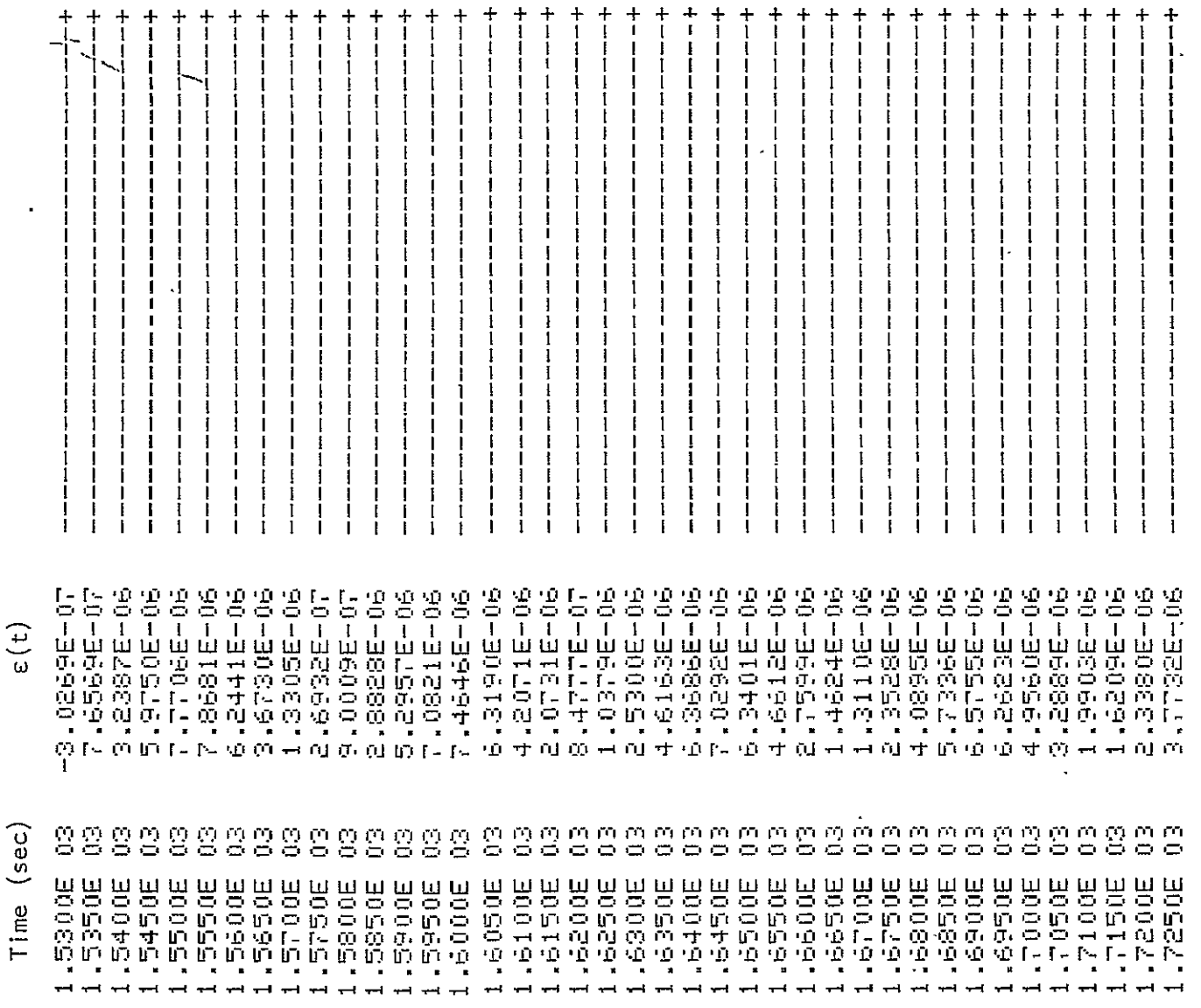

Figure 4-8. Response of $\varepsilon(t)$ of digital IPS control system.

$T = 0.1$ sec, $H_{WT} = 1$, $K_I = 10^5$, $K_{WT} + K_{FP} = 100$.

5. Gross Quantization Error Study of the Digital IPS Control System

This chapter is devoted to the study of the effect of gross quantization in the linear digital IPS control system. The nonlinear characteristics of the torques caused by the combined effect of the flex pivot of the gimbal and wire cables are neglected.

Since the quantization error has a maximum bound of $\pm h/2$, with h as the quantization level, the "worst" error due to quantization in a digital system can be studied by replacing the quantizers in the system by an external noise source with a signal magnitude of $\pm h/2$.

Figure 5-1 shows the simplified digital IPS control system with the quantizers shown to be associated with the sample-and-hold operations. The quantizers in the displacement Θ_A, rate Ω_A, and torque T_c, channels are denoted by Q_o, Q_1, and Q_T, respectively. The quantization levels are represented by h_o, h_1, and h_T, respectively.

Figure 5-2 shows the signal flow graph of the digital IPS system with the quantizers represented as operators on digital signals. Treating the quantizers as noise sources with constant amplitudes of $\pm h_o/2$, $\pm h_1/2$, and $\pm h_T/2$, we can predict the maximum errors in the system due to the effect of quantization. The following equations are written from Figure 5-2. Since the noise signals are constants, the z-transform relations include the factor $z/(z-1)$.

$$T_c(z) = K_1\Omega_A(z) + K_1\left(\pm\frac{h_1}{2}\frac{z}{z-1}\right) + \left(K_o + \frac{K_1T}{z-1}\right)\left(\pm\frac{h_o}{2}\frac{z}{z-1} + \Theta_A(z)\right) \quad (5\text{-}1)$$

$$\Omega_A(z) = \mathcal{Z}\left[\frac{-K_7G_h(s)\Delta_1(s)}{s\Delta(s)} + \frac{K_4K_7G_h(s)}{s\Delta(s)}\right]\left(T_c(z) \pm \frac{h_T}{2}\frac{z}{z-1}\right) \quad (5\text{-}2)$$

$$\Theta_A(z) = \mathcal{Z}\left[\frac{-K_7G_h(s)\Delta_1(s)}{s^2\Delta(s)} + \frac{K_4K_7G_h(s)}{s^2\Delta(s)}\right]\left(T_c(z) \pm \frac{h_T}{2}\frac{z}{z-1}\right) \quad (5\text{-}3)$$

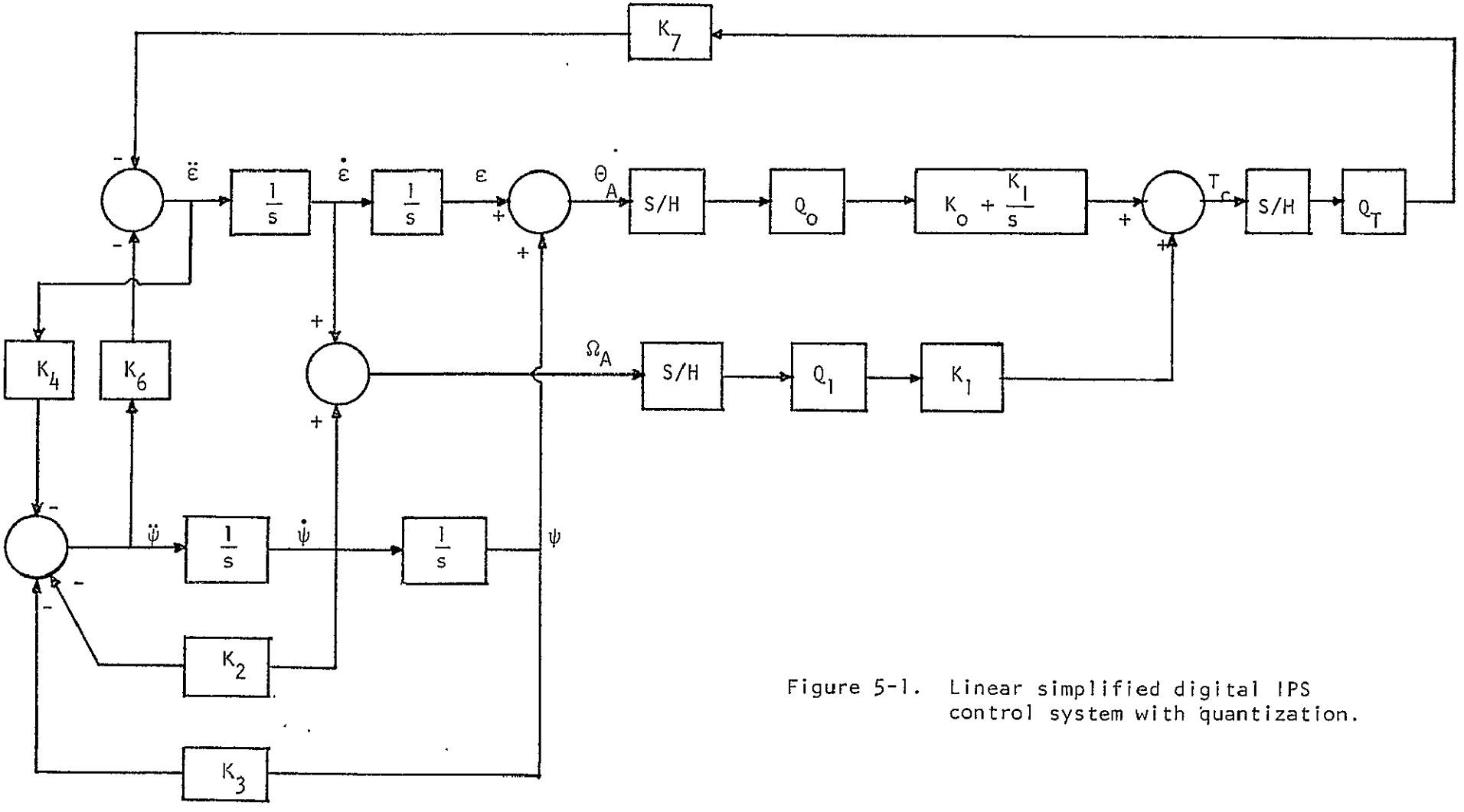

Figure 5-1. Linear simplified digital IPS control system with quantization.

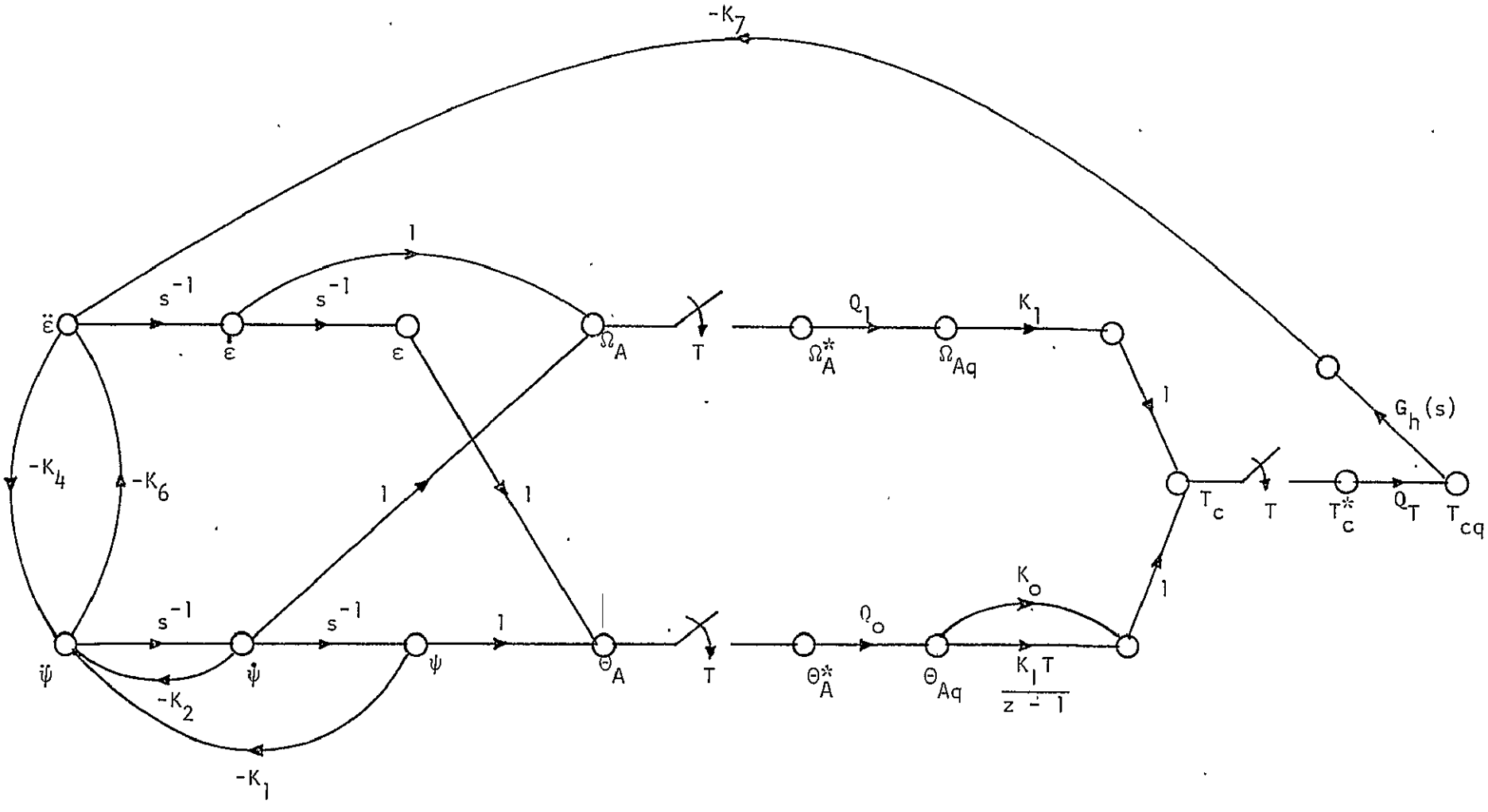

Figure 5-2. Signal flow graph of simplified digital IPS system with quantization.

The last two equations are written as

$$\Omega_A(z) = G_1(z)\left[T_c(z) \pm \frac{h_T}{2}\frac{z}{z-1}\right] \tag{5-4}$$

$$\Theta_A(z) = G_2(z)\left[T_c(z) \pm \frac{h_T}{2}\frac{z}{z-1}\right] \tag{5-5}$$

where

$$\Delta_1(s) = 1 + K_2 s^{-1} + K_2 s^{-2} \tag{5-6}$$

$$\Delta(s) = 1 - K_4 K_6 + K_2 s^{-1} + K_3 s^{-2} \tag{5-7}$$

$$G_1(z) = \frac{2.78\times10^{-4}T}{z-1} \tag{5-8}$$

$$G_2(z) = \frac{2.78\times10^{-4}T^2(z+1)}{2(z-1)^2} \tag{5-9}$$

Figure 5-3 gives the digital signal flow graph representation of Eqs. (5-1), (5-4), and (5-5). Using Figure 5-3 we can analyze the worst-case errors due to quantization in the steady state at any point of the IPS system.

As derived in previous chapters, the transfer functions $G_1(z)$ and $G_2(z)$ are given in Eqs. (5-8) and (5-9). The characteristic equation of the system is obtained from Figure 5-3.

$$\Delta(z) = 1 + K_1 G_1(z) + \left(K_o + \frac{K_1 T}{z-1}\right)G_2(z) \tag{5-10}$$

We shall now evaluate the maximum steady-state quantization errors for Θ_A, Ω_A, and T_c in terms of the quantization levels h_o, h_1, and h_T.

From Figure 5-3, $T_c(z)$ is written

$$T_c(z) = \frac{1}{\Delta}\left\{\pm\frac{h_o}{2}\left(K_o + \frac{K_1 T}{z-1}\right) \pm \frac{h_1}{2}K_1 \mp \frac{h_T}{2}\left(K_o + \frac{K_1 T}{z-1}\right)G_2(z)\right\}\frac{z}{z-1} \tag{5-11}$$

The steady-state value of $T_c(kT)$ is given by the final-value theorem,

$$\lim_{k\to\infty} T_c(kT) = \lim_{z\to 1}(1 - z^{-1})T_c(z) \tag{5-12}$$

Substitution of Eq. (5-11) into Eq. (5-12), we have

$$\lim_{k\to\infty} T_c(kT) = \mp \frac{h_T}{2} \tag{5-13}$$

Similarly,

$$\Theta_A(z) = \frac{1}{\Delta}\left\{\mp \frac{h_o}{2}\left(K_o + \frac{K_1 T}{z-1}\right) \mp \frac{h_1}{2} K_1 \mp \frac{h_T}{2}\right\} G_2(z)\, \frac{z}{z-1} \tag{5-14}$$

Then,

$$\lim_{k\to\infty} \Theta_A(kT) = \lim_{z\to 1} (1 - z^{-1})\Theta_A(z) = \mp \frac{h_o}{2} \tag{5-15}$$

$$\Omega_A(z) = \frac{1}{\Delta}\left\{\mp \frac{h_o}{2}\left(K_o + \frac{K_1 T}{z-1}\right) \mp \frac{h_1}{2} K_1 \mp \frac{h_T}{2}\right\} G_1(z)\, \frac{z}{z-1} \tag{5-16}$$

$$\lim_{k\to\infty} \Omega_A(kT) = \lim_{z\to 1} (1 - z^{-1})\Omega_A(z) = 0 \tag{5-17}$$

Therefore, we conclude that the maximum error in T_c due to quantization is $\mp h_T/2$ and is not affected by the other two quantizers. The quantizer in the Θ_A channel affects only $\Theta_A(z)$ in a one-to-one relation. The quantizer in the Ω_A path does not affect either Θ_A, Ω_A, or T_c.

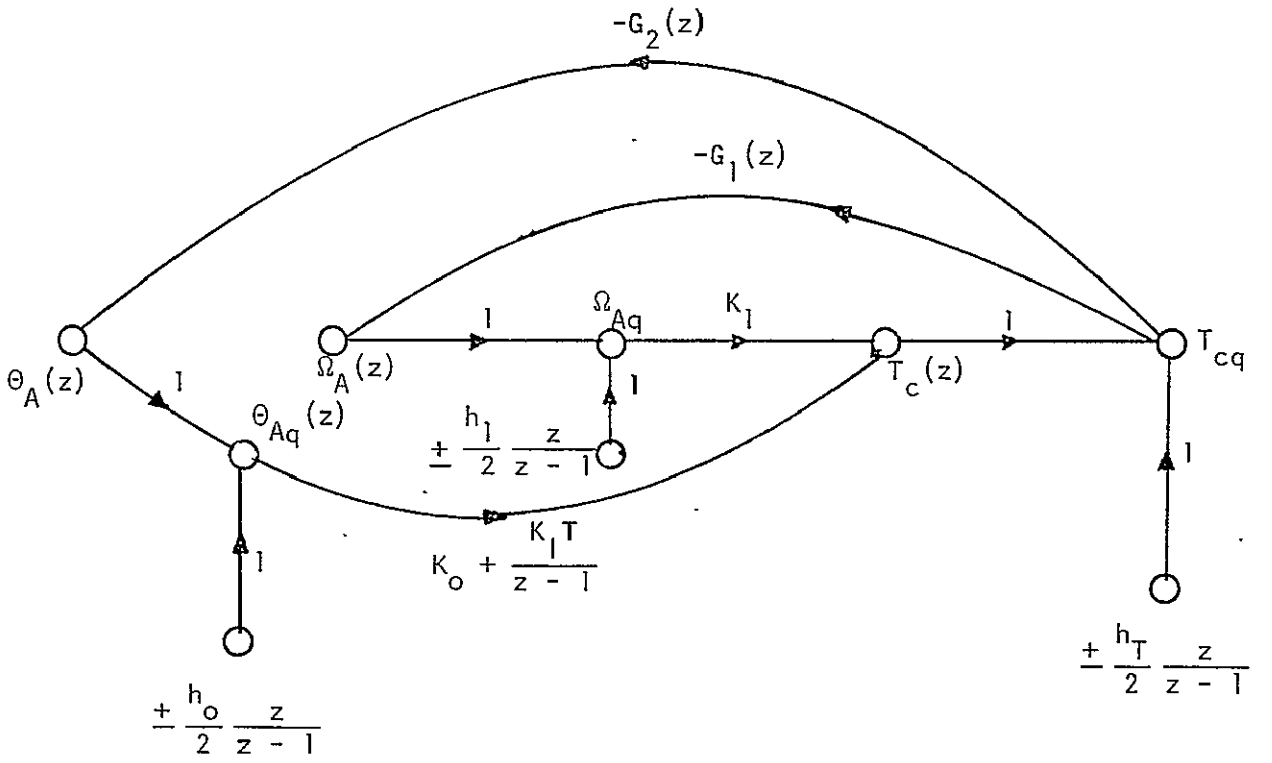

Figure 5-3. Digital signal flow graph of the simplified digital IPS with quantization.

6. Describing Function Analysis of the Quantization Effects of the Digital IPS Control System

In this section the effects of quantization in the digital IPS control system are investigated with respect to self-sustained oscillations.

Since the quantizers represent nonlinear characteristics, it is natural to expect that the level of quantization together with the selection of the sampling period may cause the system to enter into undesirable self-sustained oscillations.

The digital IPS control system with quantizers located in the Θ_A, Ω_A, and T_c channels is shown in Figure 5-1. We shall consider the effects of only one quantizer at a time, since the discrete describing function method is used.

With reference to the signal flow graph of Figure 5-2, which contains all the quantizers, we can find the equivalent characteristic equation of the system when each quantizer is operating alone. Then, the equivalent linear transfer function that each quantizer sees is derived for use in the discrete describing function analysis.

Quantizer in the Θ_A Channel

Let the quantizer in the Θ_A channel be denoted by Q_o, as shown in Figure 5-2, and neglect the effects of the other quantizers. Let the discrete describing function of Q_o be denoted by $Q_o(z)$. From Figure 5-2 the following equations are written:

$$T_c(z) = \left(K_o + \frac{K_1 T}{z - 1}\right) Q_o(z)\Theta_A(z) + K_1\Omega_A(z) \tag{6-1}$$

$$\Theta_A(z) = \mathcal{Z}\left\{\frac{-K_7 G_h(s)\Delta_1(s)}{s^2\Delta} + \frac{K_4 K_7 G_h(s)}{s^2\Delta}\right\} T_c(z)$$

$$= -G_2(z)T_c(z) \tag{6-2}$$

$$\Omega_A(z) = \left[\frac{-K_7 G_h(s)\Delta_1(s)}{s\,\Delta} + \frac{K_4 K_7 G_h(s)}{s\Delta}\right] T_c(z)$$

$$= -G_1(z)T_c(z) \qquad (6\text{-}3)$$

where

$$\Delta_1(s) = 1 + K_2 s^{-1} + K_3 s^{-2} \qquad (6\text{-}4)$$

$$\Delta(s) = 1 - K_4 K_6 + K_2 s^{-1} + K_3 s^{-2} \qquad (6\text{-}5)$$

$$G_1(z) = \frac{2.78\times10^{-4}T}{z - 1} \qquad (6\text{-}6)$$

$$G_2(z) = \frac{2.78\times10^{-4}T^2(z + 1)}{2(z - 1)^2} \qquad (6\text{-}7)$$

A digital signal flow graph portraying Eqs. (6-1), (6-2), and (6-3) is shown in Figure 6-1. The characteristic equation of the system is written directly from Figure 6-1.

$$\Delta(z) = 1 + G_2(z)\left[K_o + \frac{K_1 T}{z - 1}\right]Q_o(z) + K_1 G_1(z) = 0 \qquad (6\text{-}8)$$

To obtain the equivalent transfer function that $Q_o(z)$ sees, we divide both sides of Eq. (6-8) by the terms that do not contain $Q_o(z)$. We have

$$1 + \frac{G_2(z)\left[K_o + \frac{K_1 T}{z - 1}\right]}{1 + K_1 G_1(z)} Q_o(z) = 0 \qquad (6\text{-}9)$$

Thus,

$$G_{eqo}(z) = \frac{G_2(z)\left[K_o + \frac{K_1 T}{z - 1}\right]}{1 + K_1 G_1(z)} \qquad (6\text{-}10)$$

Quantizer in the Ω_A Channel

Using the same method as described in the last section, let $Q_1(z)$ denote the discrete describing function of the quantizer Q_1. When only Q_1 is considered effective, the following equations are written directly from Figure 5-2.

$$\Theta_A(z) = -G_2(z)T_c(z) \qquad (6\text{-}11)$$

$$\Omega_A(z) = -G_1(z)T_c(z) \qquad (6\text{-}12)$$

$$T_c(z) = \left[K_o + \frac{K_1 T}{z - 1}\right] Q_A(z) + K_1 Q_1(z)_{A}(z) \qquad (6\text{-}13)$$

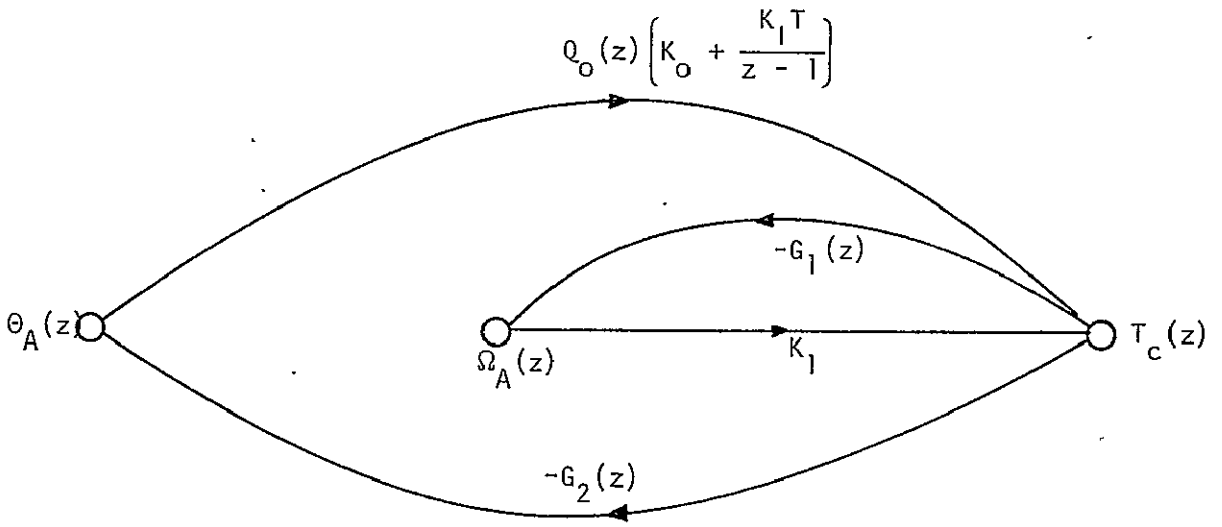

Figure 6-1. Digital signal flow graph of IPS when Q_o is in effect.

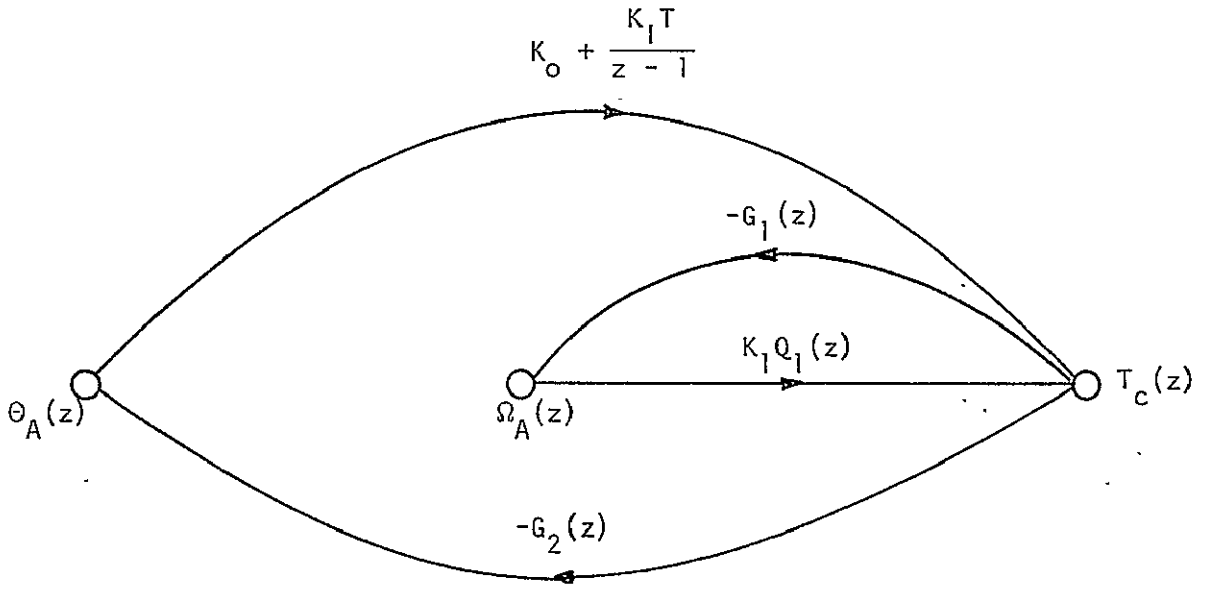

Figure 6-2. Digital signal flow graph of IPS with Q_1 if effect.

The digital signal flow graph for these equations is drawn as shown in Figure 6-2. The characteristic equation of the system is

$$\Delta(z) = 1 + K_1 G_1(z) Q_1(z) + G_2(z)\left(K_o + \frac{K_1 T}{z - 1}\right) = 0 \qquad (6\text{-}14)$$

Thus, the linear transfer function Q(z) sees is

$$G_{eq1}(z) = \frac{K_1 G_1(z)}{1 + G_2(z)\left(K_o + \frac{K_1 T}{z - 1}\right)} \qquad (6\text{-}15)$$

Quantizer in the T_c Channel

If Q_T is the only quantizer in effect, the following equations are written from Figure 5-2.

$$\Theta_A(z) = -G_2(z) Q_T(z) T_c(z) \qquad (6\text{-}16)$$

$$\Omega_A(z) = -G_1(z) Q_T(z) T_c(z) \qquad (6\text{-}17)$$

$$T_c(z) = \left(K_o + \frac{K_1 T}{z - 1}\right)\Theta_A(z) + K_1 \Omega_A(z) \qquad (6\text{-}18)$$

The digital signal flow graph for these equations is drawn in Figure 6-3. The characteristic equation of the system is

$$\Delta(z) = 1 + K_1 G_1(z) Q_T(z) + G_2(z) Q_T(z)\left(K_o + \frac{K_1 T}{z - 1}\right) = 0 \qquad (6\text{-}19)$$

The linear transfer function seen by $Q_T(z)$ is

$$G_{eqT}(z) = K_1 G_1(z) + G_2(z)\left(K_o + \frac{K_1 T}{z - 1}\right) \qquad (6\text{-}20)$$

The discrete describing function of quantizers has been derived in a previous report[3]. By investigating the trajectories of the linear equivalent transfer function of Eqs. (6-10), (6-15), and (6-20) against the critical regions of the discrete describing function of the quantizer, the possibility of self-sustained oscillations due to quantization in the digital IPS system may be determined.

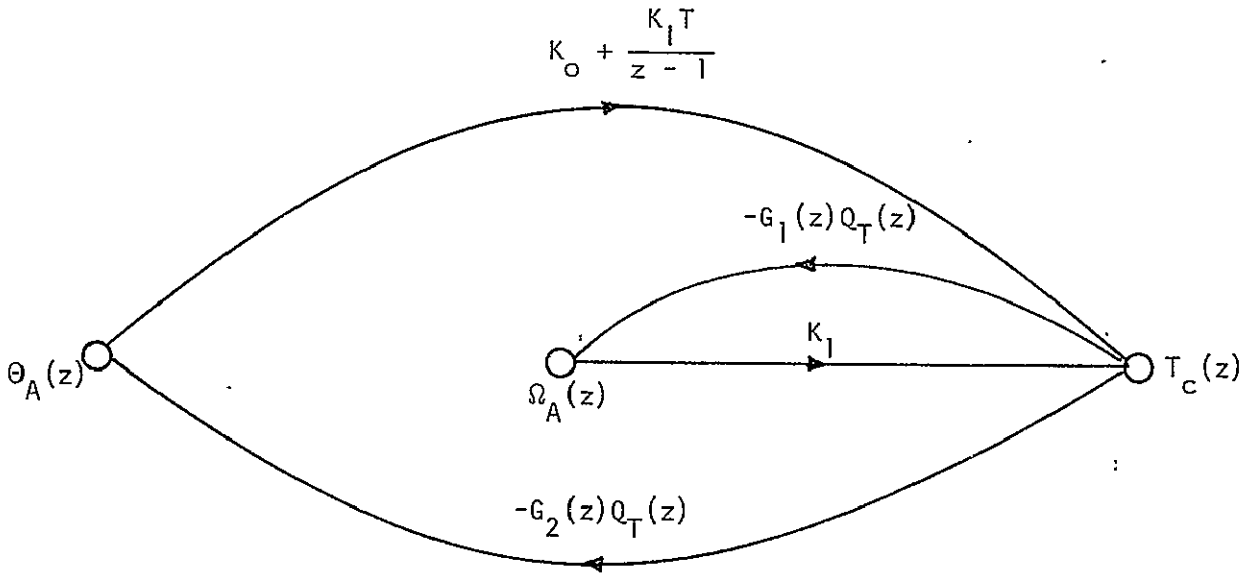

Figure 6-3. Digital signal flow graph of IPS with Q_T in effect.

Let T_c denote the period of the self-sustained oscillation, and

$$T_c = NT$$

where N is a positive integer ≥ 2. T represents the sampling period in seconds.

When N = 2, the periodic output of the quantizer can have an amplitude of kh, where k is a positive integer and h is the quantization level. The critical region of the quantizer for N = 2 is shown in Figure 6-4. For N = 3, the periodic output of the quantizer is a pulse train which can be described by the mode (k_o, k_1, k_2), where $k_o h$, $k_1 h$, and $k_2 h$ are the magnitudes of the output pulses during one period. Similarly, for N = 4, the modes are described by (k_o, k_1). The critical regions of the quantizer for N = 3 and N = 4 are shown in Figures 6-5 and 6-6, respectively. Figure 6-7 illustrates the frequency loci of $G_{eqo}(z)$, $G_{eq1}(z)$, and $G_{eqT}(z)$ of Eqs. (6-10), (6-15), and (6-20), respectively, together with the corresponding critical region of the quantizer. The value of K_1 is equal to 10^5 in this case. It so happens that the frequency loci of these transfer functions are almost identical. Notice that the frequency loci for the range of $0.06 \leq T \leq 0.18$ sec overlap with the critical region. Therefore,

self-sustained oscillations of the mode N = 2 are possible for the sampling period range of $0.06 \leq T \leq 0.18$ sec. It turns out that the frequency loci for N = 2 are not sensitive to the value of K_1 so that the same plots of Figure 6-7 and the same conclusions apply to $K_1 = 10^6$ and $K_1 = 10^7$.

Figures 6-8, 6-9, and 6-10 illustrate the frequency loci of $G_{eqo}(z)$, $G_{eq1}(z)$ and $G_{eqT}(z)$ for N = 3 and for $K_1 = 10^5$, 10^6, and 10^7, respectively. From Figure 6-8 we notice that for $K_1 = 10^5$ the frequency loci do not intersect with the critical region for any sampling period. Thus, for $K_1 = 10^5$ the N = 3 mode of oscillations cannot occur.

For $K_1 = 10^6$, Figure 6-9 shows that sustained oscillations for N = 3 would not occur for $T < 0.075$ sec and large values of T. For $K_1 = 10^7$, Figure 6-10 shows that the critical value of T is increased to approximately 0.085 sec.

For N = 4, Figures 6-11, 6-12, and 6-13 illustrate the critical region and the frequency loci for $K_1 = 10^5$, 10^6, and 10^7, respectively. In this case, self-sustained oscillations are absent for $K_1 = 10^5$ for any sampling period. For $K_1 = 10^6$, the critical sampling period is approximately 0.048 sec for quantizers Q_1 and Q_T, whereas for Q_o the critical T is 0.07 sec. The stability condition is improved when K_1 is increased to 10^7, for Q_1 and Q_T, the critical values of T are 0.05 sec and 0.055 sec, respectively; for Q_o it is 0.09 sec.

As N increases, the critical regions shrinks toward the negative real axis of the complex plane, and at the same time the frequency loci move away from the negative real axis. Thus, the N = 2, 3, and 4 cases represent the worst possible conditions of self-sustained oscillations in the system.

The conclusion of this analysis is that the sampling period of the IPS system should be less than 0.048 second, in order to avoid self-sustained

oscillations excited by the quantizer nonlinearities described in these sections.

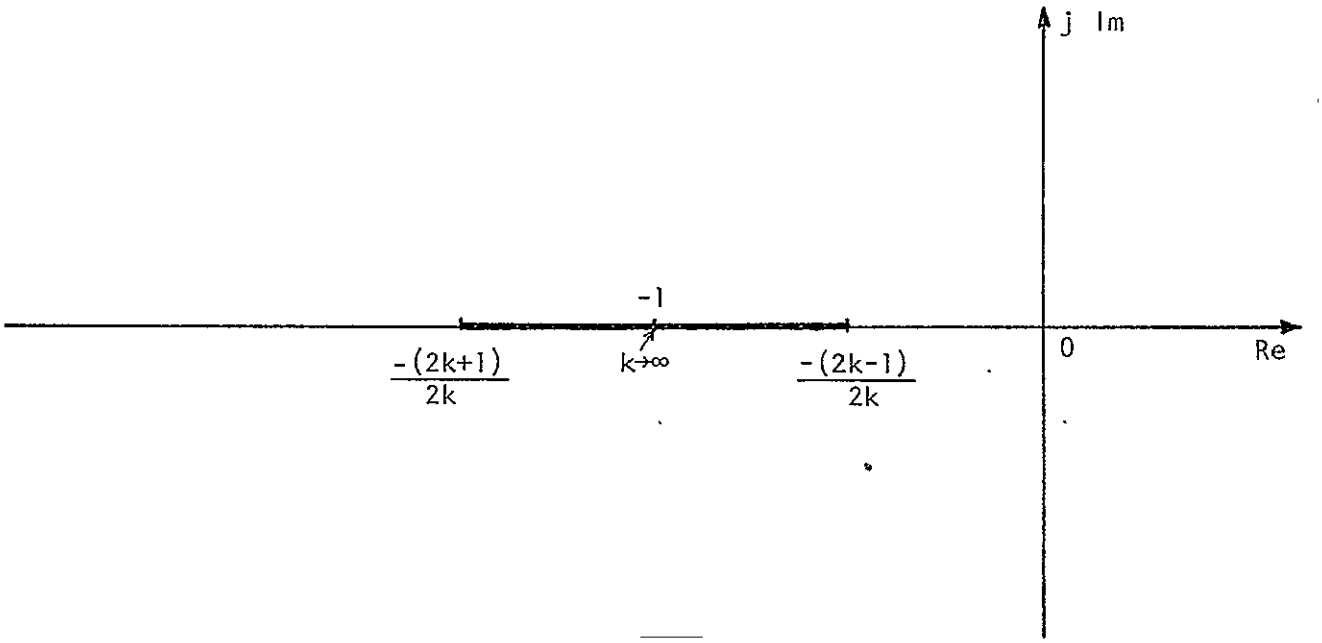

Figure 6-4. Critical region of $-1/Q(z)$ of quantizer for $N = 2$.

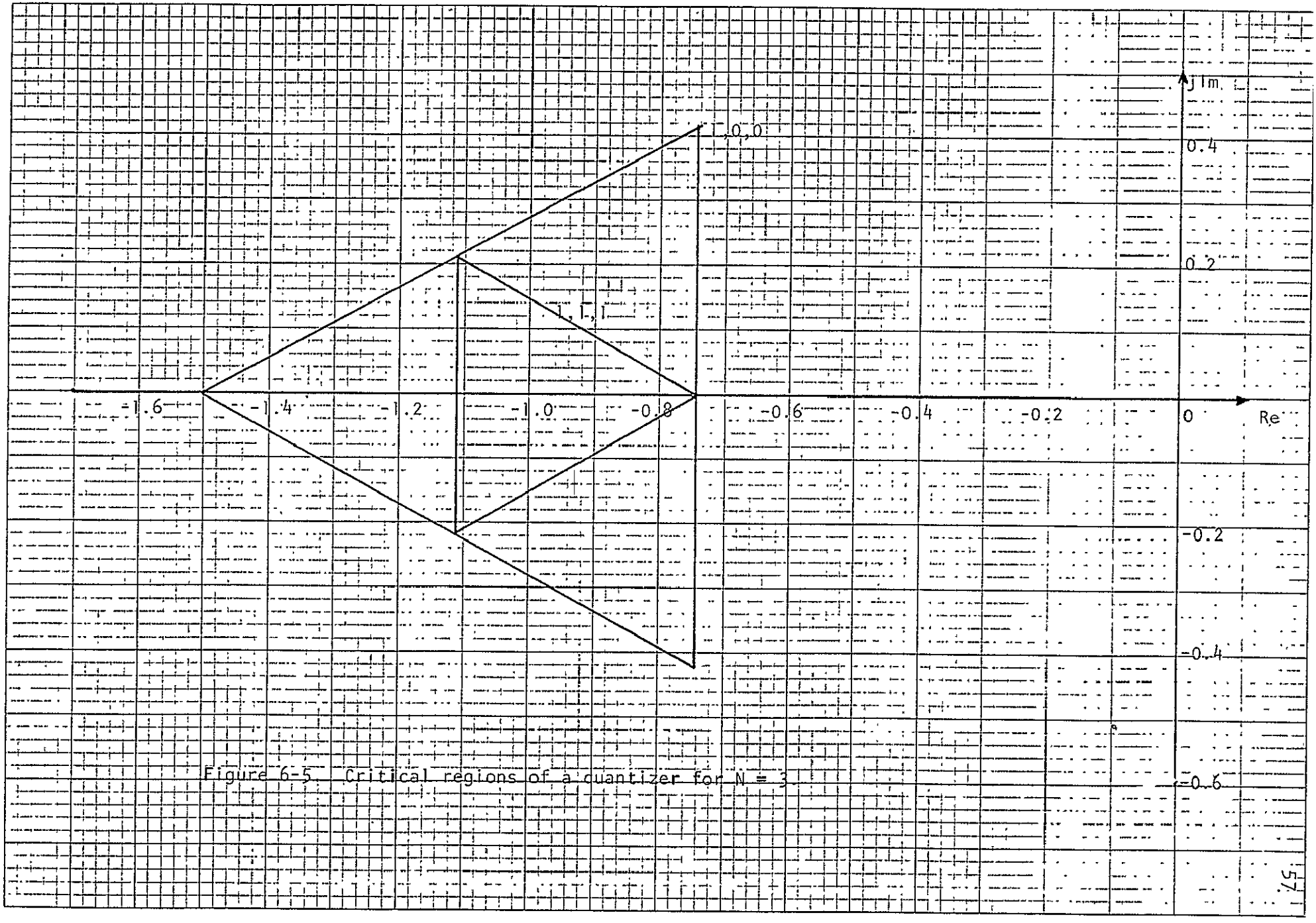

Figure 6-5. Critical regions of a quantizer for N = 3

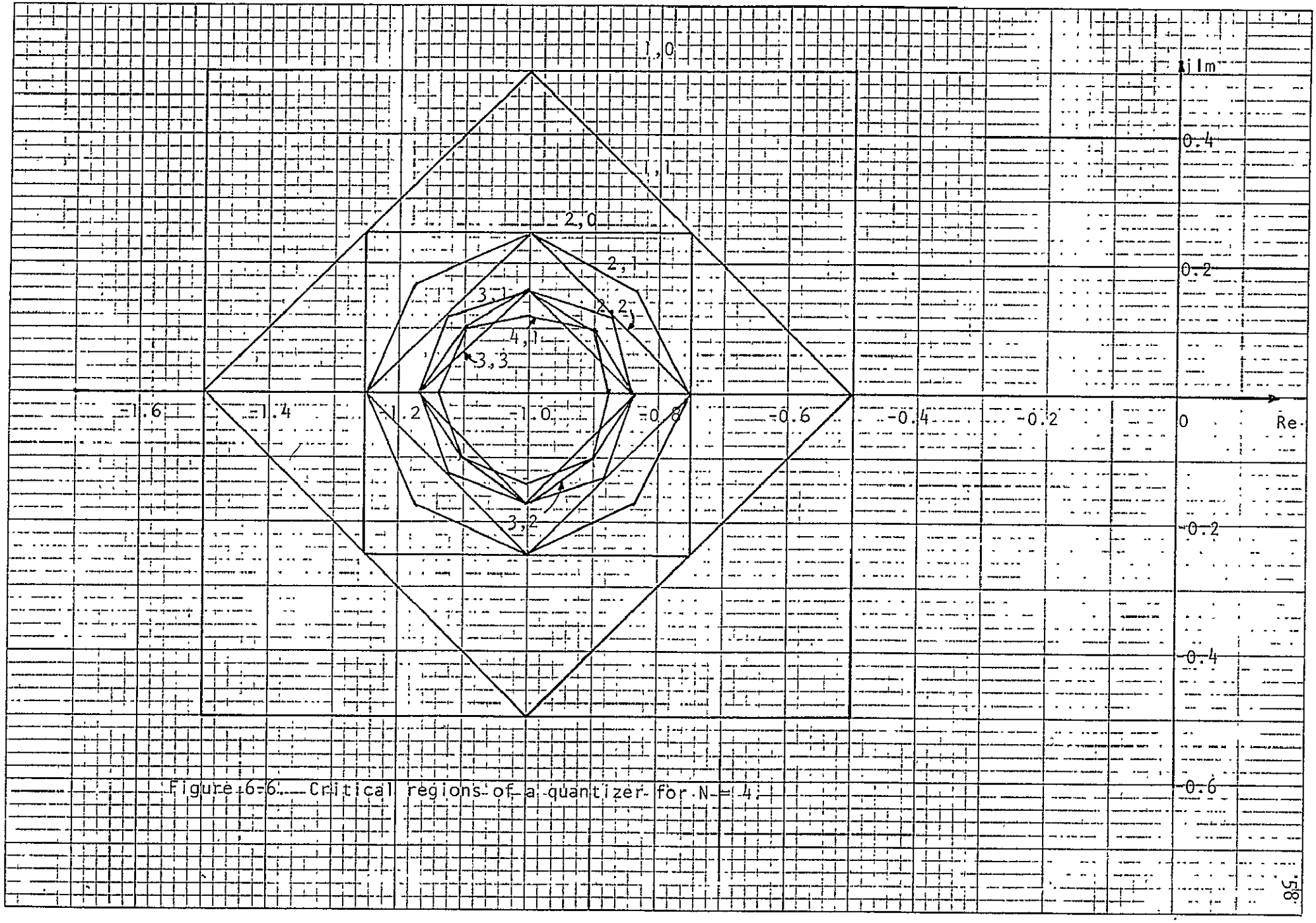

Figure 6-6. Critical regions of a quantizer for N = 4.

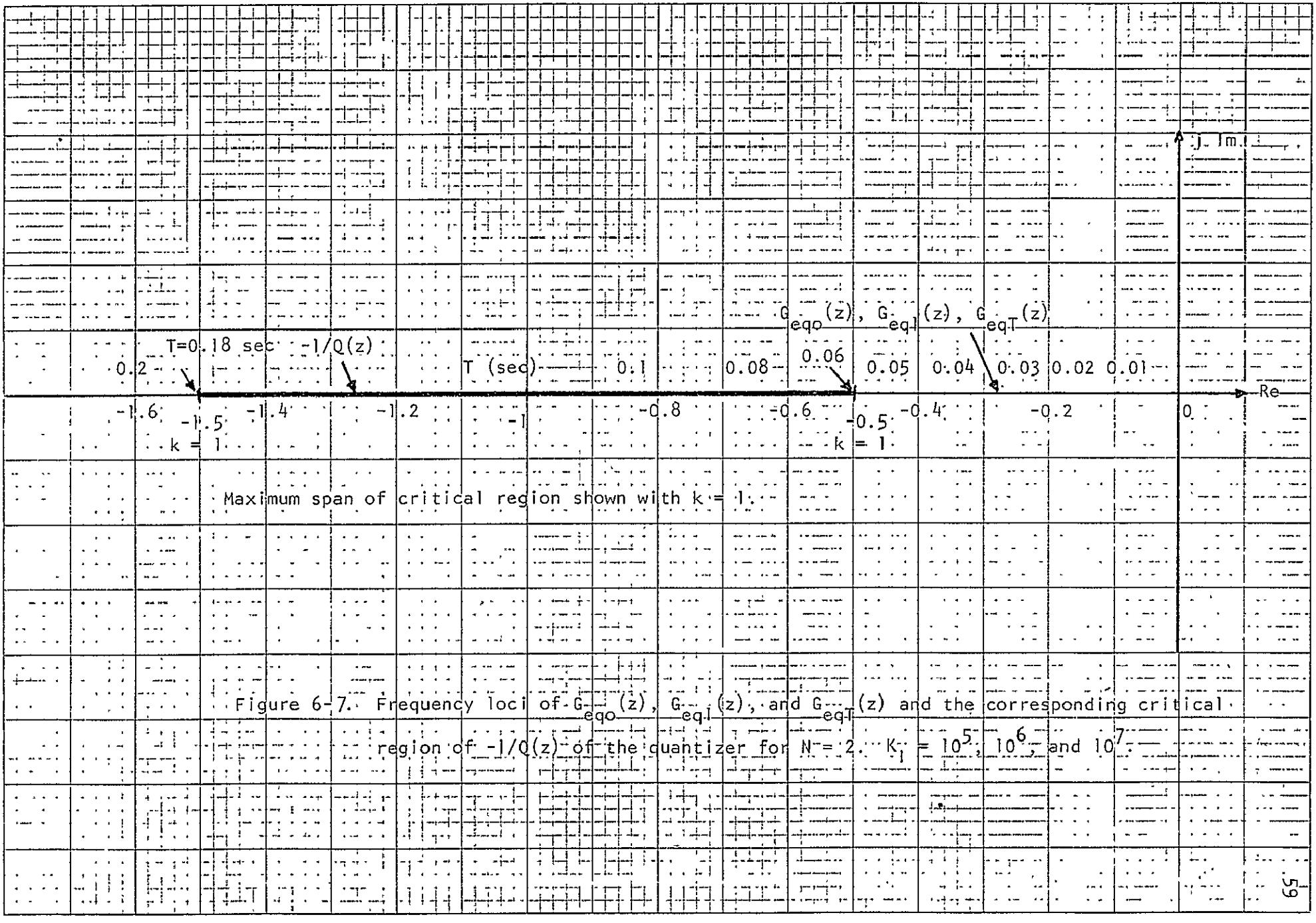

Figure 6-7. Frequency loci of $G_{eqo}(z)$, $G_{eql}(z)$, and $G_{eqT}(z)$ and the corresponding critical region of $-1/Q(z)$ of the quantizer for $N = 2$, $K_1 = 10^5$, 10^6, and 10^7.

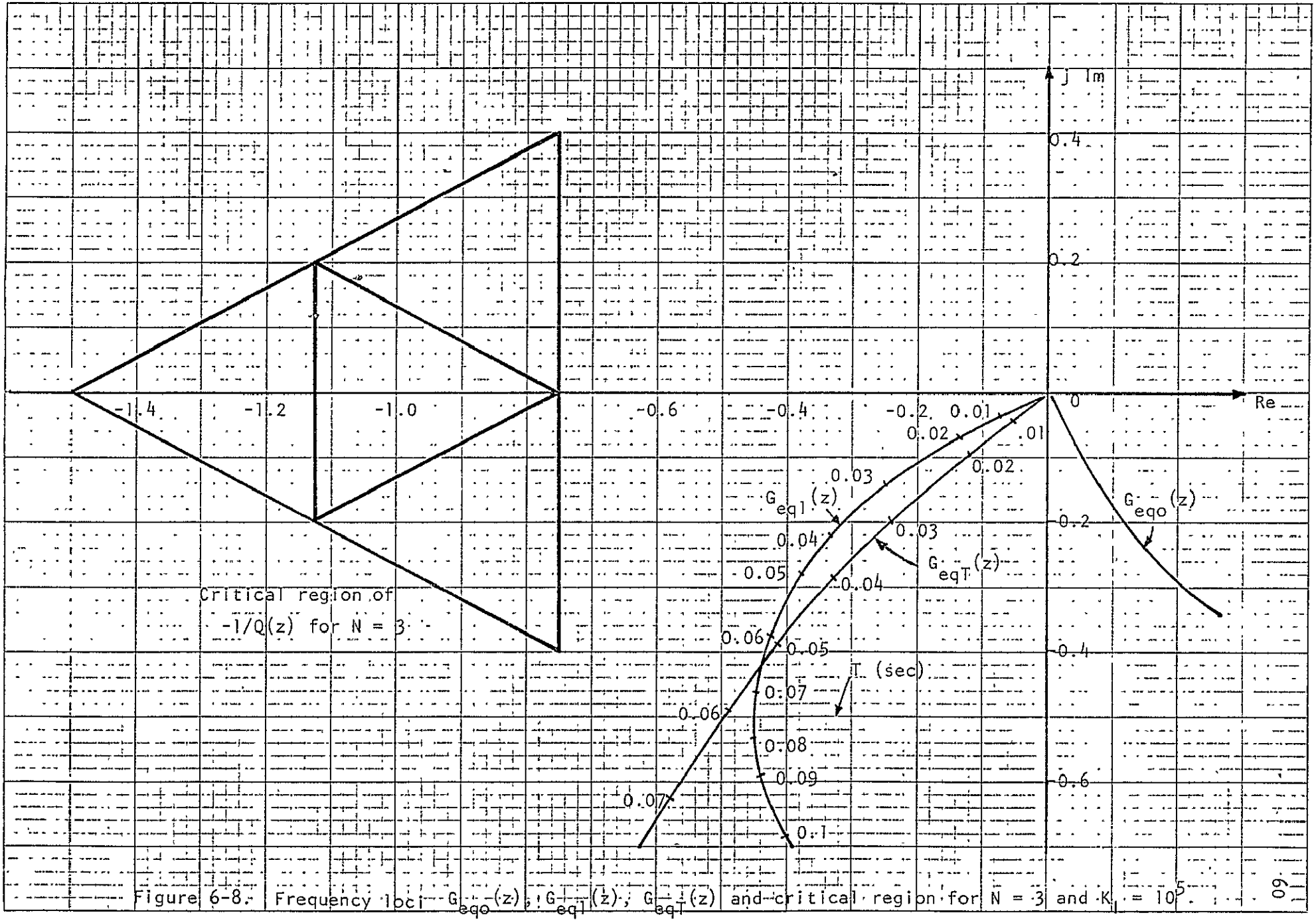

Figure 6-8. Frequency loci $G_{eqo}(z)$, $G_{eq1}(z)$, $G_{eqT}(z)$ and critical region for N = 3 and $K_1 = 10^5$

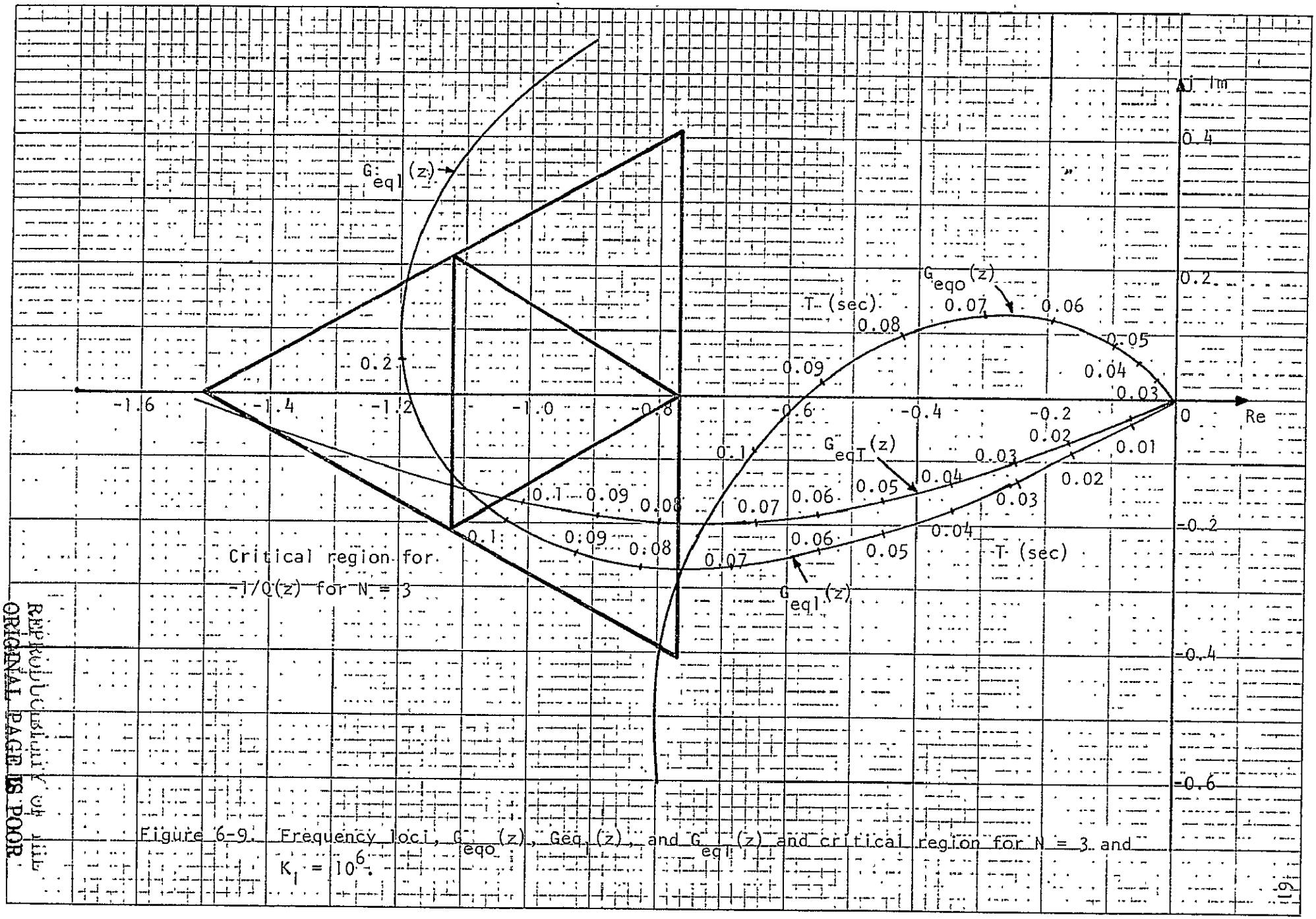

Figure 6-9. Frequency loci, $G_{eqo}(z)$, $G_{eqT}(z)$, and $G_{eq1}(z)$ and critical region for N = 3 and $K_1 = 10^6$.

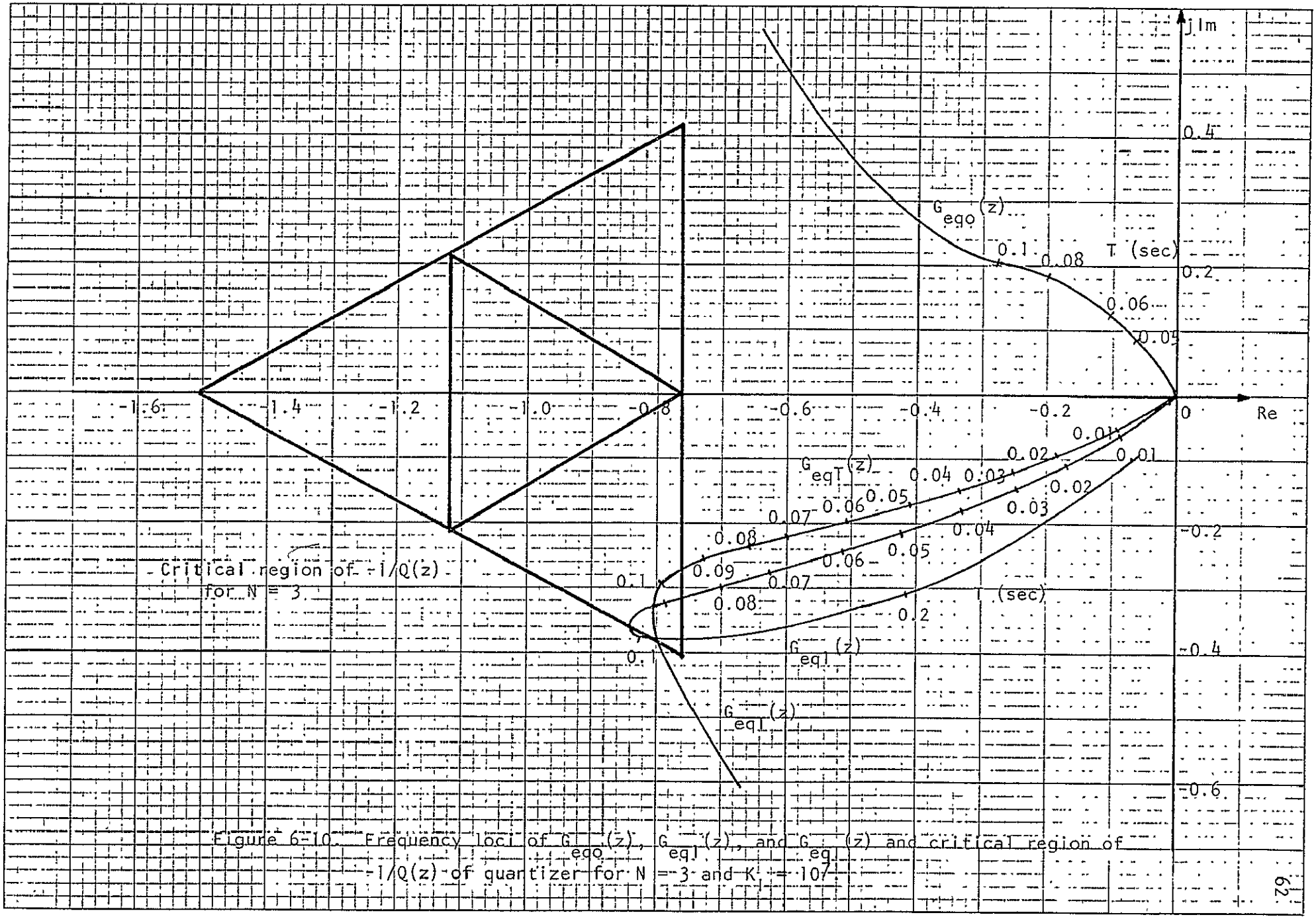

Figure 6-10. Frequency loci of $G_{ego}(z)$, $G_{eqT}(z)$, and $G_{eql}(z)$ and critical region of -1/Q(z) of quantizer for N = 3 and K = 10.

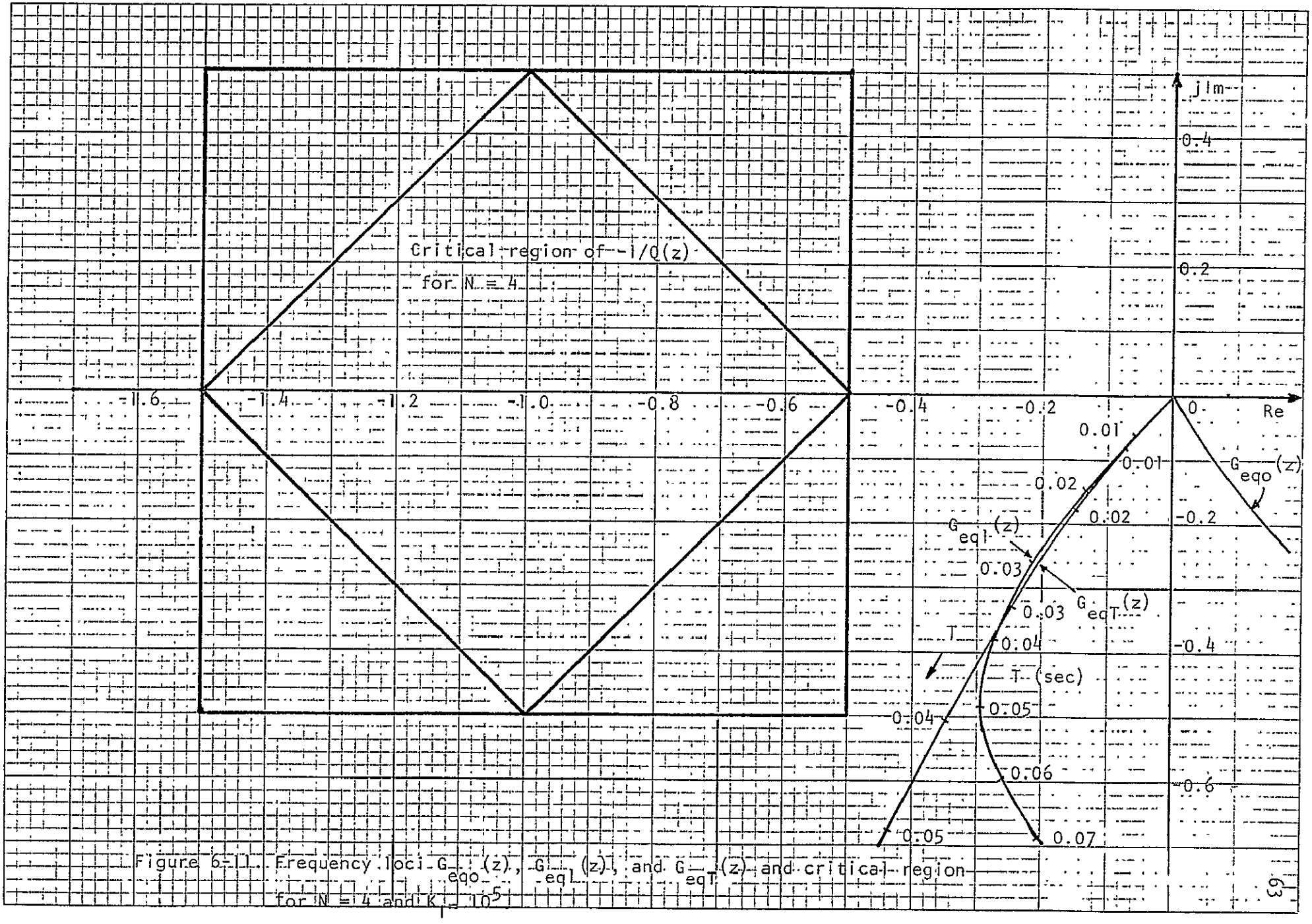

Figure 6-11. Frequency loci $G_{eqo}(z)$, $G_{eq1}(z)$, and $G_{eqT}(z)$ and critical region for $N = 4$ and $K = 10^5$

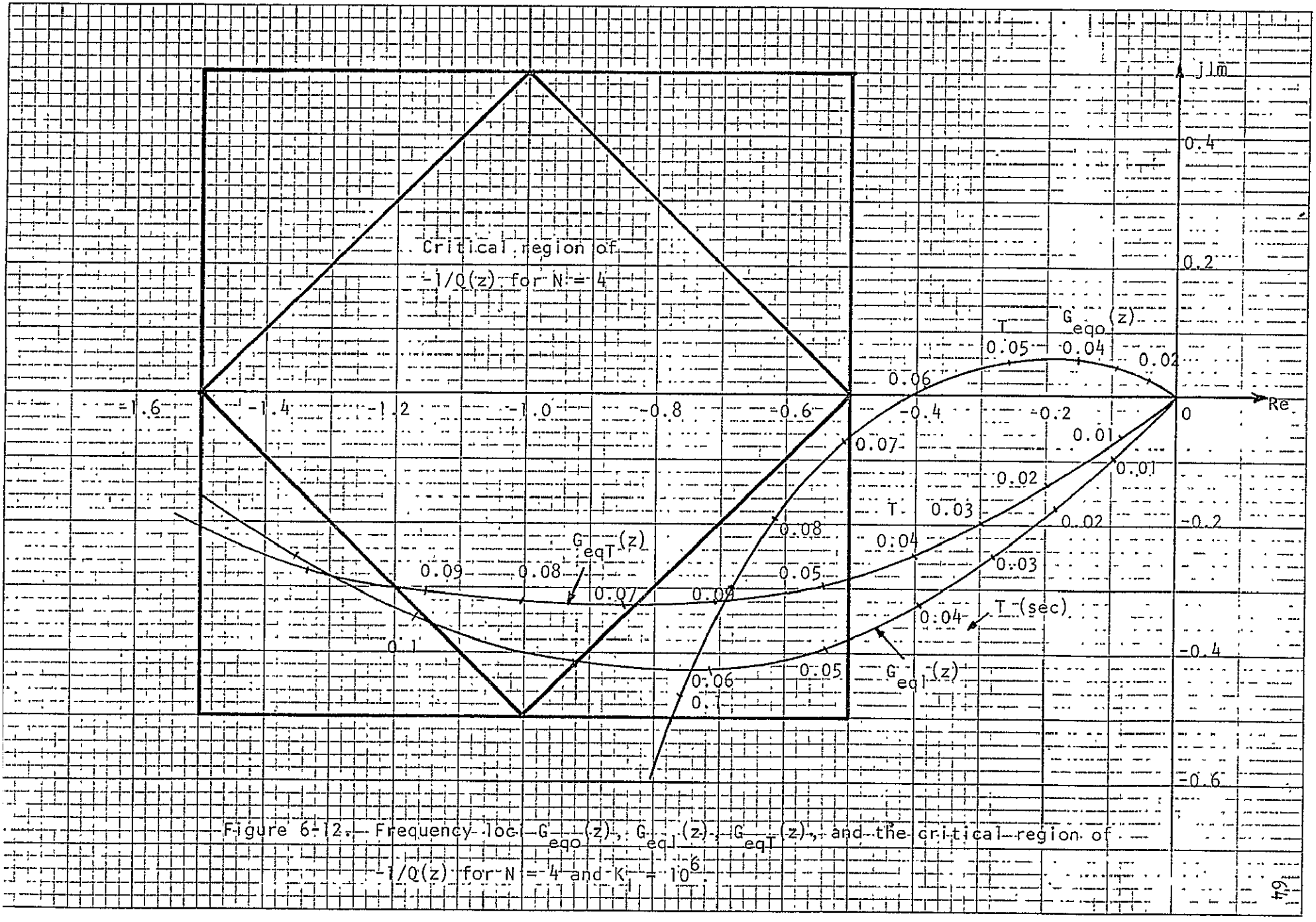

Figure 6-12. Frequency loci $G_{eqo}(z)$, $G_{eq1}(z)$, $G_{eqT}(z)$, and the critical region of $-1/Q(z)$ for $N = 4$ and $K = 10^6$.

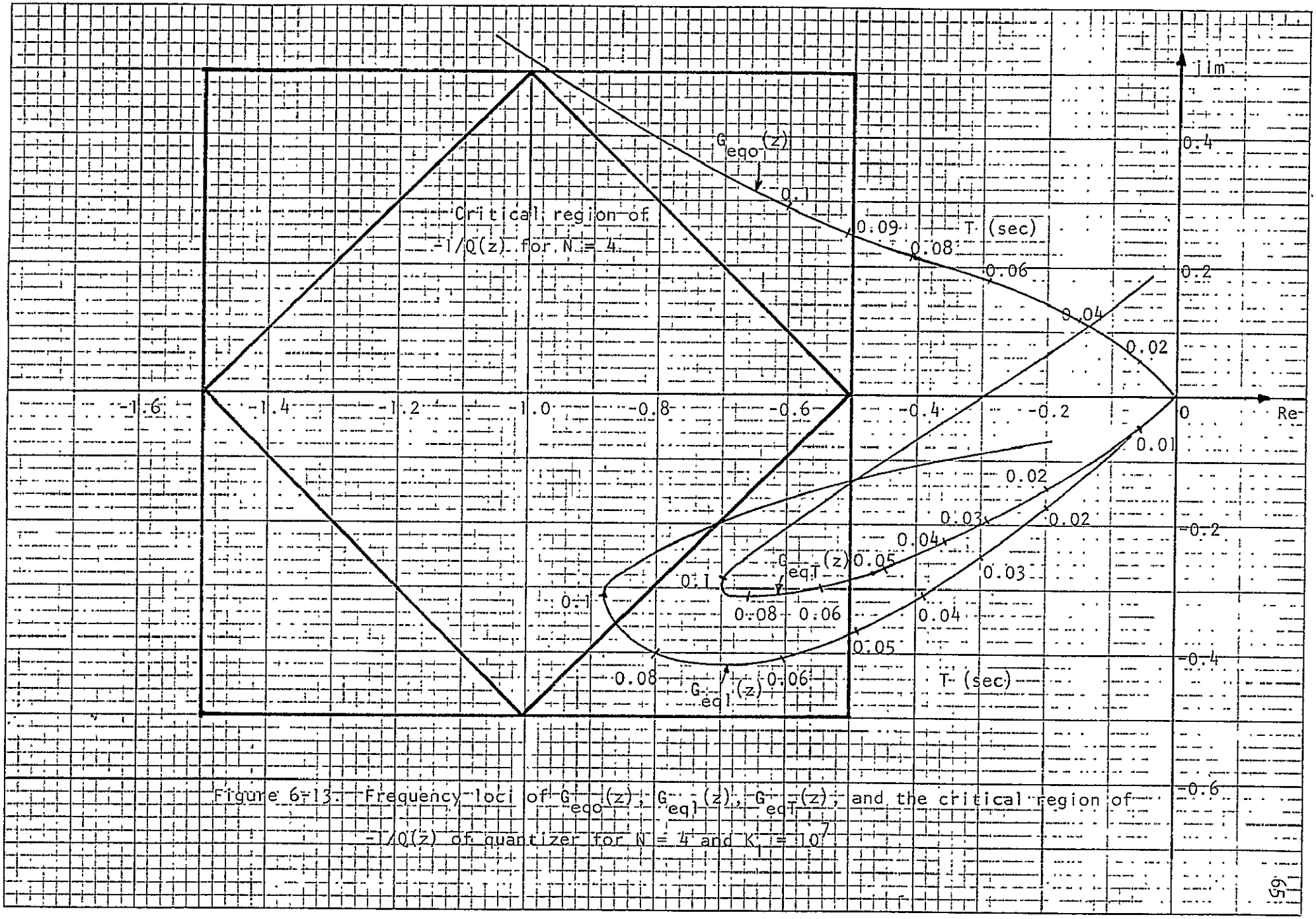

Figure 6-13. Frequency loci of $G_{eqo}(z)$, $G_{eq1}(z)$, $G_{eqT}(z)$, and the critical region of $-1/Q(z)$ of quantizer for N = 4 and $K_1 = 10^7$

7. Digital Computer Simulation of the Digital IPS Control System With Quantization

The digital IPS control system with quantizers has been studied in Chapter 5 and 6 using the gross quantization error and the describing function methods. In this chapter the effect of quantization in the digital IPS is studied through digital computer simulation. The main purpose of the analysis is to support the results obtained in the last two chapters.

The linear IPS control system with quantization is modeled by the block diagram of Figure 5-1, and it is not repeated here. The quantizers are assumed to be located in the T_c, Θ_A, and Ω_A channels. From the gross quantization error analysis it was concluded that the maximum error due to quantization at each of the locations is equal to the quantization level at the point, and it is not affected by the other two quantizers. In Chapter 6 it is found that the quantizer in the T_c channel seems to be the dominant one as far as self-sustained oscillations are concerned. It was also found that the self-sustained oscillations due to quantization may not occur for a sampling period or approximately 0.05 sec or less.

A large number of computer simulation runs were conducted with the quantizer located at the T_c channel. However, it was difficult to induce any periodic oscillation in the system due to quantization alone. It appears that the signal at the output of the quantizer due to an arbitrary initial condition will eventually vary between $h_T/2$ and $-h_T/2$ indefinitely in a random fashion. This points to the fact that the system the quantizer sees is not a low-pass filter so that the describing function method becomes inaccurate. However, the results still substantiates the results obtained in Chapter 5; i.e., the quantization error is $\pm h_T/2$. Figure 7-1 and 7-2 show typical responses of the simulation runs for $K_I = 10^5$ and $T = 0.08$ sec. When $K_I = 10^7$ the system is unstable.

TIME	Y26	I
0.0	8.0000E-01	
4.0000E-02	0.0	
8.0000E-02	-8.0500E-01	
1.2000E-01	0.0	
1.6000E-01	-2.7600E-01	
2.0000E-01	0.0	
2.4000E-01	3.0200E-01	
2.8000E-01	0.0	
3.2000E-01	9.5000E-02	
3.6000E-01	0.0	
4.0000E-01	-1.1300E-01	
4.4000E-01	0.0	
4.8000E-01	-3.2000E-02	
5.2000E-01	0.0	
5.6000E-01	4.3000E-02	
6.0000E-01	0.0	
6.4000E-01	1.0000E-02	
6.8000E-01	0.0	
7.2000E-01	-1.6000E-02	
7.6000E-01	0.0	
8.0000E-01	-2.0000E-03	
8.4000E-01	0.0	
8.8000E-01	5.0000E-03	
9.2000E-01	0.0	
9.6000E-01	1.0000E-03	
1.0000E 00	0.0	
1.0400E 00	-1.0000E-03	
1.0800E 00	0.0	
1.1200E 00	0.0	
1.1600E 00	0.0	
1.2000E 00	0.0	
1.2400E 00	0.0	
1.2800E 00	0.0	
1.3200E 00	0.0	
1.3600E 00	0.0	
1.4000E 00	0.0	
1.4400E 00	1.0000E-03	
1.4800E 00	0.0	
1.5200E 00	-1.0000E-03	
1.5600E 00	0.0	
1.6000E 00	1.0000E-03	
1.6400E 00	0.0	
1.6800E 00	0.0	
1.7200E 00	0.0	
1.7600E 00	0.0	
1.8000E 00	0.0	
1.8400E 00	0.0	
1.8800E 00	0.0	
1.9200E 00	0.0	
1.9600E 00	0.0	
2.0000E 00	0.0	

Figure 7-1. Response of output of quantizer at T_c. $h_T/2=0.001$, $K_I = 10^5$, T = 0.08 sec.

TIME	Y26	I
2.0400E 00	0.0	----------+
2.0800E 00	1.0000E-03	----------+
2.1200E 00	0.0	----------+
2.1600E 00	0.0	----------+
2.2000E 00	0.0	----------+
2.2400E 00	-1.0000E-03	----------+
2.2800E 00	0.0	----------+
2.3200E 00	1.0000E-03	----------+
2.3600E 00	0.0	----------+
2.4000E 00	0.0	----------+
2.4400E 00	0.0	----------+
2.4800E 00	0.0	----------+
2.5200E 00	0.0	----------+
2.5600E 00	0.0	----------+
2.6000E 00	0.0	----------+
2.6400E 00	1.0000E-03	----------+
2.6800E 00	0.0	----------+
2.7200E 00	-1.0000E-03	----------+
2.7600E 00	0.0	----------+
2.8000E 00	0.0	----------+
2.8400E 00	0.0	----------+
2.8800E 00	1.0000E-03	----------+
2.9200E 00	0.0	----------+
2.9600E 00	0.0	----------+
3.0000E 00	0.0	----------+
3.0400E 00	0.0	----------+
3.0800E 00	0.0	----------+
3.1200E 00	0.0	----------+
3.1600E 00	0.0	----------+
3.2000E 00	0.0	----------+

Figure 7-1 (continued).

TIME	Y26	I
0.0	8.0000E-01	----------+----------
4.0000E-02	0.0	----------+
8.0000E-02	-8.0520E-01	+
1.2000E-01	0.0	----------+
1.6000E-01	-2.7570E-01	----------+
2.0000E-01	0.0	----------+
2.4000E-01	3.0210E-01	----------+----------
2.8000E-01	0.0	----------+
3.2000E-01	9.4800E-02	----------+----------
3.6000E-01	0.0	----------+
4.0000E-01	-1.1300E-01	----------+
4.4000E-01	0.0	----------+
4.8000E-01	-3.2000E-02	----------+
5.2000E-01	0.0	----------+
5.6000E-01	4.2300E-02	----------+----------
6.0000E-01	0.0	----------+
6.4000E-01	1.1000E-02	----------+
6.8000E-01	0.0	----------+
7.2000E-01	-1.5500E-02	----------+
7.6000E-01	0.0	----------+
8.0000E-01	-3.6000E-03	----------+
8.4000E-01	0.0	----------+
8.8000E-01	6.0000E-03	----------+
9.2000E-01	0.0	----------+
9.6000E-01	1.3000E-03	----------+
1.0000E 00	0.0	----------+
1.0400E 00	-2.0000E-03	----------+
1.0800E 00	0.0	----------+
1.1200E 00	-2.0000E-04	----------+
1.1600E 00	0.0	----------+
1.2000E 00	8.0000E-04	----------+
1.2400E 00	0.0	----------+
1.2800E 00	4.0000E-04	----------+
1.3200E 00	0.0	----------+
1.3600E 00	-3.0000E-04	----------+
1.4000E 00	0.0	----------+
1.4400E 00	2.0000E-04	----------+
1.4800E 00	0.0	----------+
1.5200E 00	2.0000E-04	----------+
1.5600E 00	0.0	----------+
1.6000E 00	1.0000E-04	----------+
1.6400E 00	0.0	----------+
1.6800E 00	1.0000E-04	----------+
1.7200E 00	0.0	----------+
1.7600E 00	1.0000E-04	----------+

Figure 7-2. Response of output of quantizer at T_c. $h_T/2=0.0001$, $K_I = 10^5$, $T = 0.08$ sec.

```
1.0960E 01     0.0
1.1000E 01     0.0
1.1040E 01     0.0
1.1080E 01     0.0
1.1120E 01     0.0
1.1160E 01     0.0
1.1200E 01     0.0
1.1240E 01     0.0
1.1280E 01     0.0
1.1320E 01     0.0
1.1360E 01     0.0
1.1400E 01     0.0
1.1440E 01    -1.0000E-04
1.1480E 01     0.0
1.1520E 01     1.0000E-04
1.1560E 01     0.0
1.1600E 01     0.0
1.1640E 01     0.0
1.1680E 01    -1.0000E-04
1.1720E 01     0.0
1.1760E 01     0.0
1.1800E 01     0.0
1.1840E 01     1.0000E-04
1.1880E 01     0.0
1.1920E 01    -1.0000E-04
1.1960E 01     0.0
1.2000E 01    -1.0000E-04
1.2040E 01     0.0
1.2080E 01     1.0000E-04
1.2120E 01     0.0
```

Figure 7-2 (continued).

8. Modeling of the Continuous-Data IPS Control System With Wire Cable Torque and Flex Pivot Nonlinearities

In this chapter the mathematical model of the IPS Control System is investigated when the nonlinear characteristics of the torques caused by the wire cables and the friction at the flex pivot of the gimbal are considered. In Chapter 3 the IPS model includes the wire cable disturbance which is modeled as a nonlinear spring (Figure 3-3). The combined effect of the wire cable and flex pivot is also modeled as a nonlinear spring characteristics as shown in Figure 3-4.

In this chapter the Dahl model[4,5] is used to represent the ball bearing friction torque at the flex pivot of the gimbal, together with the nonlinear characteristics of the wire cables.

Figure 8-1 shows the block diagram of the combined flex pivot and wire cables torque characteristics, where it is assumed that the disturbance torque at the flex pivot is described by the Dahl dry friction model. The combined torque is designated T_N.

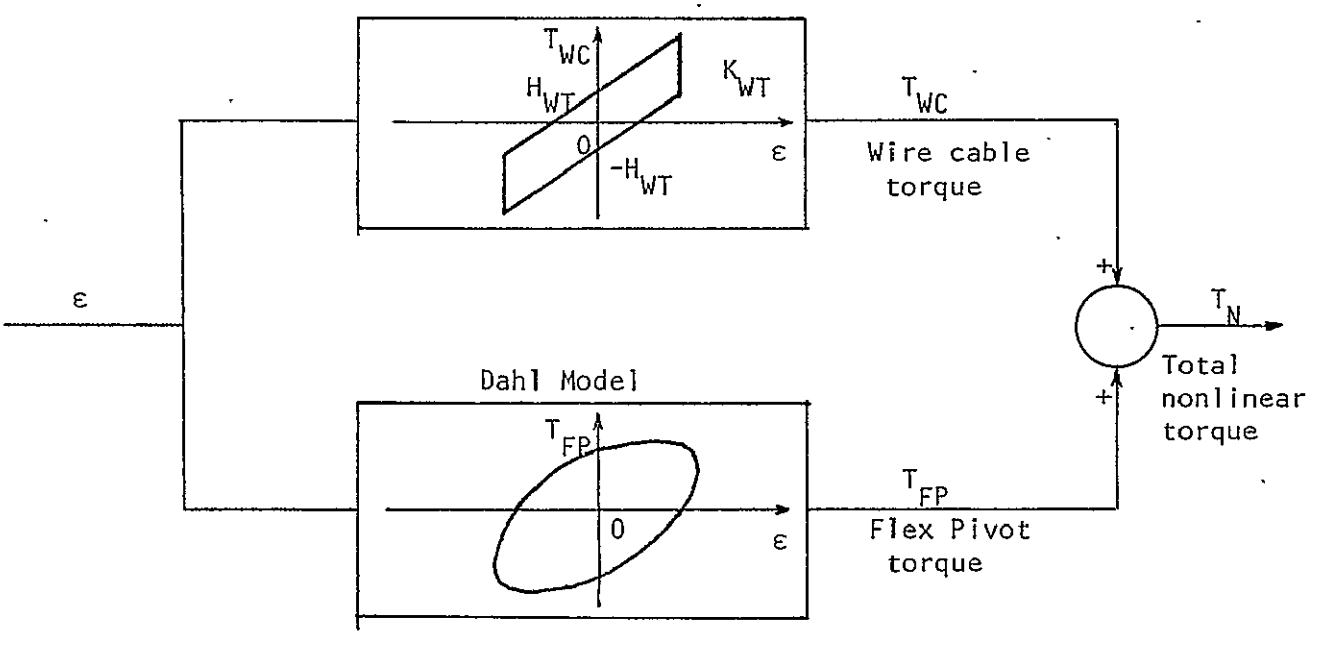

Figure 8-1. Block diagram of combined nonlinear torque characteristics of flex pivot and wire cables of LST.

Figure 8-2 shows the simplified IPS control system with the nonlinear flex pivot and wire cable torque characteristics.

The nonlinear spring torque characteristics of the wire cable are described by the following relations:

$$T_{WC}(\varepsilon) = H_{WT}SGN(\dot{\varepsilon}) + K_{WT}\varepsilon \tag{8-1}$$

where H_{WT} is in N-m, K_{WT} in N-m/rad, ε is in rad, and $T_{WC}(\varepsilon)$ in N-m.

Equation (8-1) is also equivalent to

$$T_{WC}^{+}(\varepsilon) = H_{WT} + K_{WT}\varepsilon \qquad \dot{\varepsilon} \geq 0 \tag{8-2}$$

$$T_{WC}^{-}(\varepsilon) = -H_{WT} + K_{WT}\varepsilon \qquad \dot{\varepsilon} \leq 0 \tag{8-3}$$

It has been established that the solid rolling friction characteristic can be approximated by the nonlinear relation,

$$\frac{dT_{FP}(\varepsilon)}{d\varepsilon} = \gamma(T_{FPI} - T_{FPO})^{i} \tag{8-4}$$

where

i = positive number

γ = positive constant

$T_{FPI} = T_{FP}SGN(\dot{\varepsilon})$

T_{FPO} = saturation level of T_{FP}

For $i = 2$, Equation (8-4) is integrated to give

$$\varepsilon + C_1 = \frac{-1}{\gamma(T_{FP}^{+} - T_{FPO})} \qquad \dot{\varepsilon} \geq 0 \tag{8-5}$$

$$\varepsilon + C_2 = \frac{-1}{\gamma(T_{FP}^{-} + T_{FPO})} \qquad \dot{\varepsilon} \leq 0 \tag{8-6}$$

where C_1 and C_2 are constants of integration, and

$$T_{FP}^{+} = T_{FP} \qquad \dot{\varepsilon} \geq 0 \tag{8-7}$$

$$T_{FP}^{-} = T_{FP} \qquad \dot{\varepsilon} \leq 0 \tag{8-8}$$

The constants of integration are determined at the initial point where

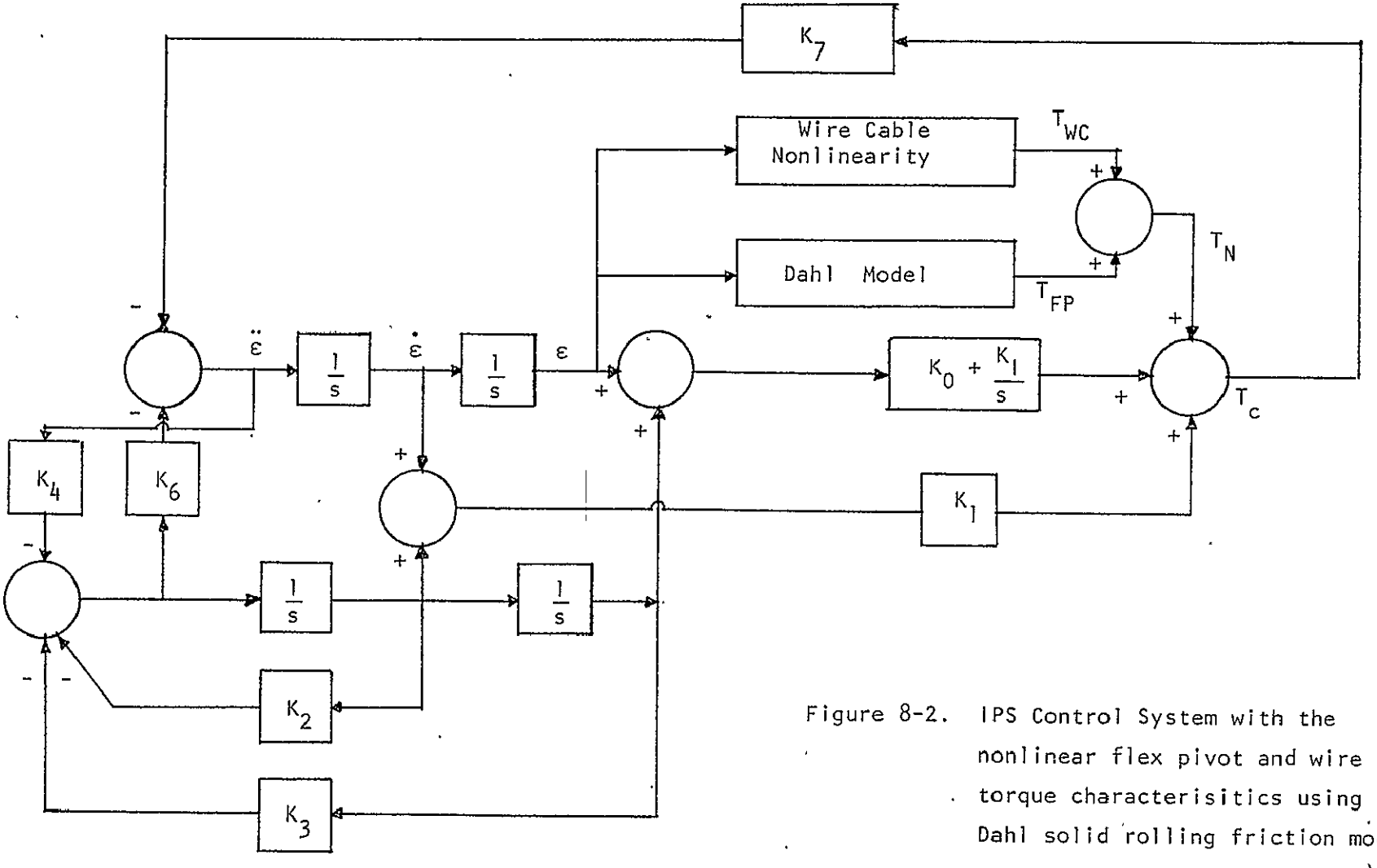

Figure 8-2. IPS Control System with the nonlinear flex pivot and wire cable torque characterisitics using the Dahl solid rolling friction model.

ε_i = initial value of ε

T_{FPi} = initial value of T_{FP}

Then

$$C_1 = -\varepsilon_i - \frac{1}{\gamma(T^+_{FPi} - T_{FP0})} \qquad \dot{\varepsilon} \geq 0 \tag{8-9}$$

$$C_2 = -\varepsilon_i - \frac{1}{\gamma(T^-_{FPi} + T_{FP0})} \qquad \dot{\varepsilon} \leq 0 \tag{8-10}$$

The main objective is to investigate the behavior of the nonlinear elements under a sinusoidal excitation, so that the describing function analysis can be conducted.

Let $\varepsilon(t)$ be described by a cosinusoidal function,

$$\varepsilon(t) = A\cos\omega t \tag{8-11}$$

Then,

$$\dot{\varepsilon}(t) = -A\omega\sin\omega t \tag{8-12}$$

Thus,

$$\varepsilon_i = -A \qquad \dot{\varepsilon} \geq 0 \tag{8-13}$$

$$\varepsilon_i = A \qquad \dot{\varepsilon} \leq 0 \tag{8-14}$$

The constants of integration in Eqs. (8-9) and (8-10) become

$$C_1 = A - \frac{1}{\gamma(T^+_{FPi} - T_{FP0})} \tag{8-15}$$

$$C_2 = -A - \frac{1}{\gamma(T^+_{FPi} - T_{FP0})} \tag{8-16}$$

Substitution of Eqs. (8-11) and (8-15) in Eq. (8-5) and simplifying, the solution of T^+_{FP} is

$$\frac{T^+_{FP}}{T_{FP0}} = \frac{\frac{R}{R-1} + \frac{a}{2}(1 - \cos\omega t)}{\frac{a}{2}(1 - \cos\omega t) + \frac{1}{R-1}} \tag{8-17}$$

which is valid for $\dot{\varepsilon} \geq 0$ or $(2k+1)\pi \leq \omega t \leq (2k+2)\pi$, $k = 0, 1, 2, \ldots$

$$a = 2\gamma A T_{FP0} \tag{8-18}$$

$$R = -\frac{1}{a} + \sqrt{\frac{a^2 + 1}{a^2}} = \frac{T_{FPi}}{T_{FP0}} \tag{8-19}$$

Similarly, for $\dot{\varepsilon} \leq 0$, using Eqs. (8-11) and (8-16) in Eq. (8-6), we have

$$\frac{T_{FP}^{-}}{T_{FP0}} = \frac{\frac{R}{R+1} - \frac{a}{2}(1 - \cos\omega t)}{\frac{a}{2}(1 - \cos\omega t) + \frac{1}{R+1}} \tag{8-20}$$

which is valid for $2k\pi \leq \omega t \leq (2k+1)\pi$, $k = 0, 1, 2, \ldots$.

The expressions for T_{FP}^{+} and T_{FP}^{-} obtained in Eqs. (8-17) and (8-20) together with those of $T_{WC}(\varepsilon)$ in Eqs. (8-2) and (8-3) are useful for the derivation of the describing function of the combined nonlinearity of the wire cable and the flex pivot characteristics.

The torque disturbance due to the two nonlinearities is modeled by

$$\begin{aligned} T_N^{+} &= T_{WC}^{+} + T_{FP}^{+} \\ &= H_{WT} + K_{WT}A\cos\omega t + T_{FP0}\frac{\frac{R}{R-1} + \frac{a}{2}(1 - \cos\omega t)}{\frac{a}{2}(1 - \cos\omega t) + \frac{1}{R-1}} \end{aligned} \tag{8-21}$$

$(2k+1)\pi \leq \omega t \leq (2k+2)\pi$, $k = 0, 1, 2, \ldots$

$$\begin{aligned} T_N^{-} &= T_{WC}^{-} + T_{FP}^{-} \\ &= -H_{WT} + K_{WT}A\cos\omega t + T_{FP0}\frac{\frac{R}{R+1} - \frac{a}{2}(1 - \cos\omega t)}{\frac{a}{2}(1 - \cos\omega t) + \frac{1}{R+1}} \end{aligned} \tag{8-22}$$

Figure 8-3 shows the T_{FP}/T_{FP0} versus ε/A characteristics for several values of A when the input is the cosinusoidal function of Eq. (8-11). Figure 8-4 shows the normalized $(3T_{FP} + T_{WC})/(3T_{FP0} + K_{WT} + H_{WT})$ versus ε/A for several typical combinations of A, H_{WT}, and K_{WT}.

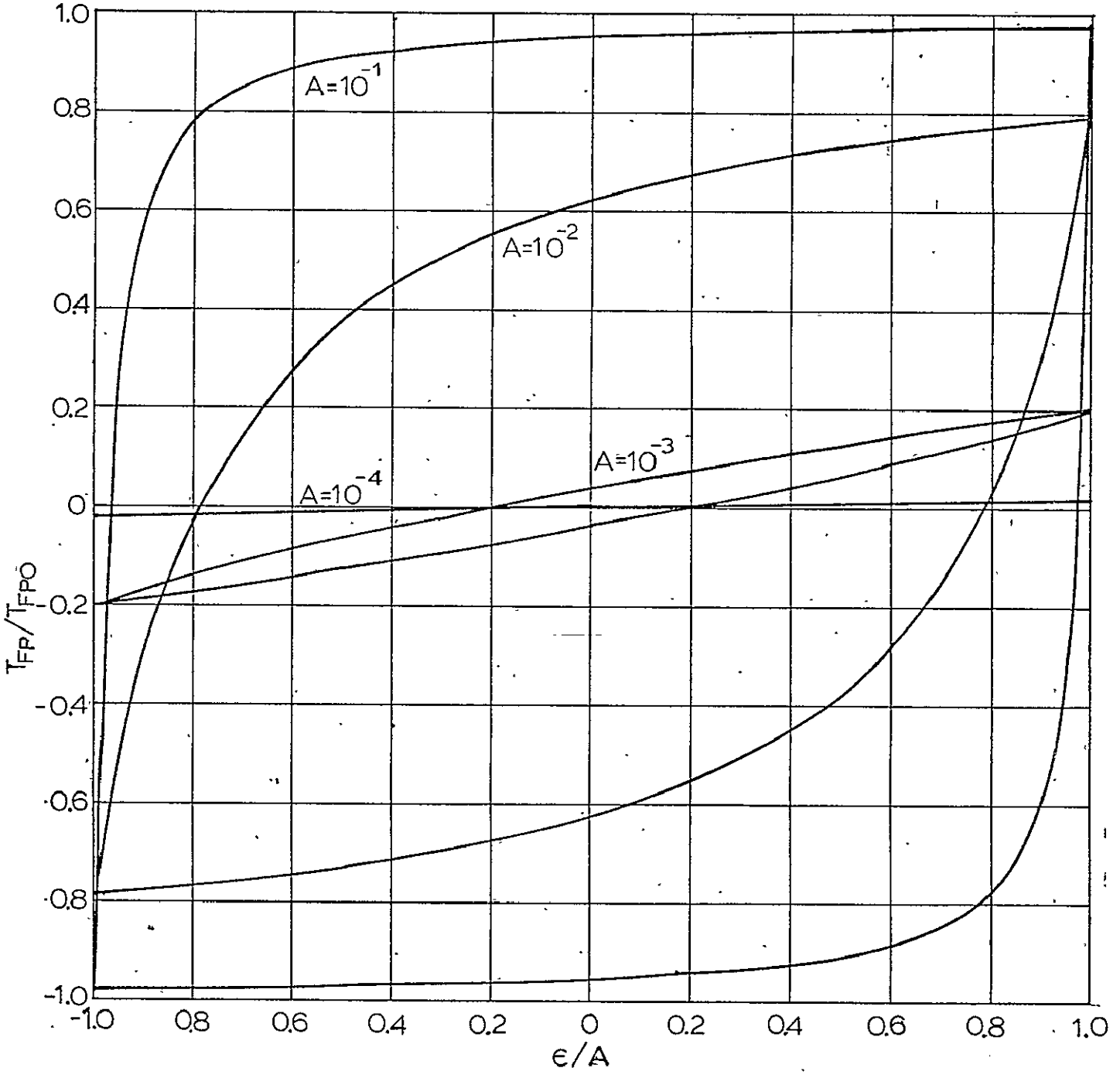

Figure 8-3. Normalized flex pivot torque (Dahl model) versus ϵ/A for IPS with cosine function input.

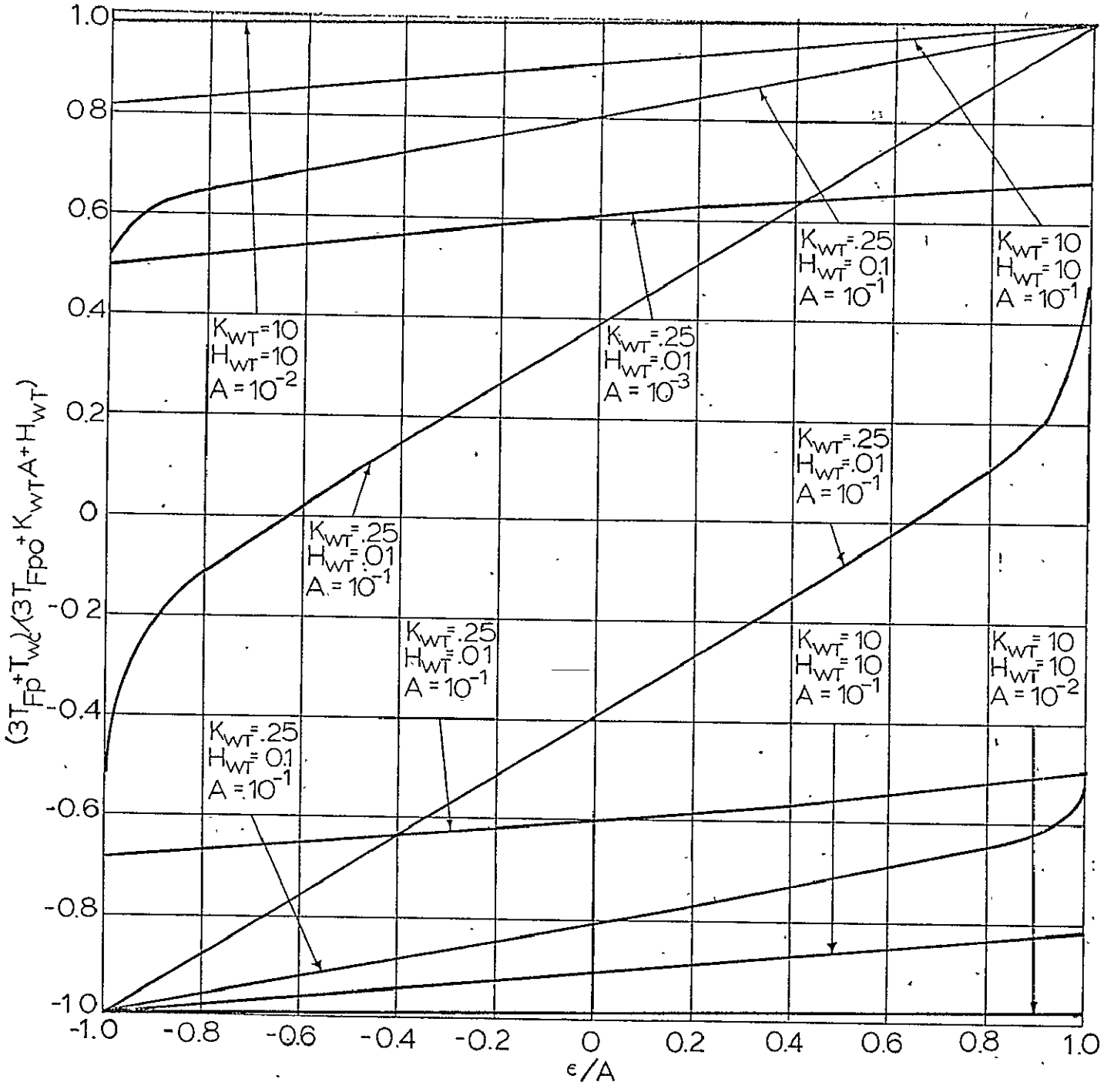

Figure 8-4. Normalized flex pivot plus wire cable torques versus ε/A for IPS with cosine function input.

9. Describing Function of the Combined Wire Cable and Flex Pivot Nonlinearities

Figure 8-1 shows that the disturbance torques due to the wire cable and the gimbal flex pivot are additive. Thus,

$$T_N = T_{WC} + T_{FP} \tag{9-1}$$

For the cosinusoidal input of Eq. (8-11), let the describing function of the wire cable nonlinearity be designated as $N_{WC}(A)$ and that of the flex pivot nonlinearity be $N_{FP}(A)$. Then, in the frequency domain, the total disturbance torque is

$$T_N(\omega) = N_{FP}(A)\varepsilon(\omega) + N_{WC}(A)\varepsilon(\omega) + \left(N_{FP}(A) + N_{WC}(A)\right)\varepsilon(\omega) \tag{9-2}$$

Thus, let N(A) be the describing function of the combined flex pivot and wire cable nonlinear characteristics,

$$N(A) = N_{FP}(A) + N_{WC}(A) \tag{9-3}$$

The describing function of the Dahl solid friction nonlinearity has been derived elsewhere[6] for the cosinusoidal input. The results is

$$N_{FP}(A) = \frac{B_1 - jA_1}{A} \tag{9-4}$$

where

$$A_1 = -\frac{4}{\pi} T_{FP0} + \frac{2}{\pi A\gamma} \ell n\left(\frac{C_1 + A}{C_1 - A}\right) \tag{9-5}$$

$$B_1 = \frac{2}{\gamma A}\left(\frac{C_1}{\sqrt{C_1^2 - A^2}} - 1\right) \tag{9-6}$$

The describing function of the wire cable nonlinearity is derived as follows.

For a cosinusoidal input the input-output waveform relations are shown in Figure 9-1. The wire cable torque due to the cosinusoidal input, over one period, is

$$T_{WC}(t) = K_{WT}A\cos\omega t - H_{WT} \qquad 0 \leq \omega t < \pi$$

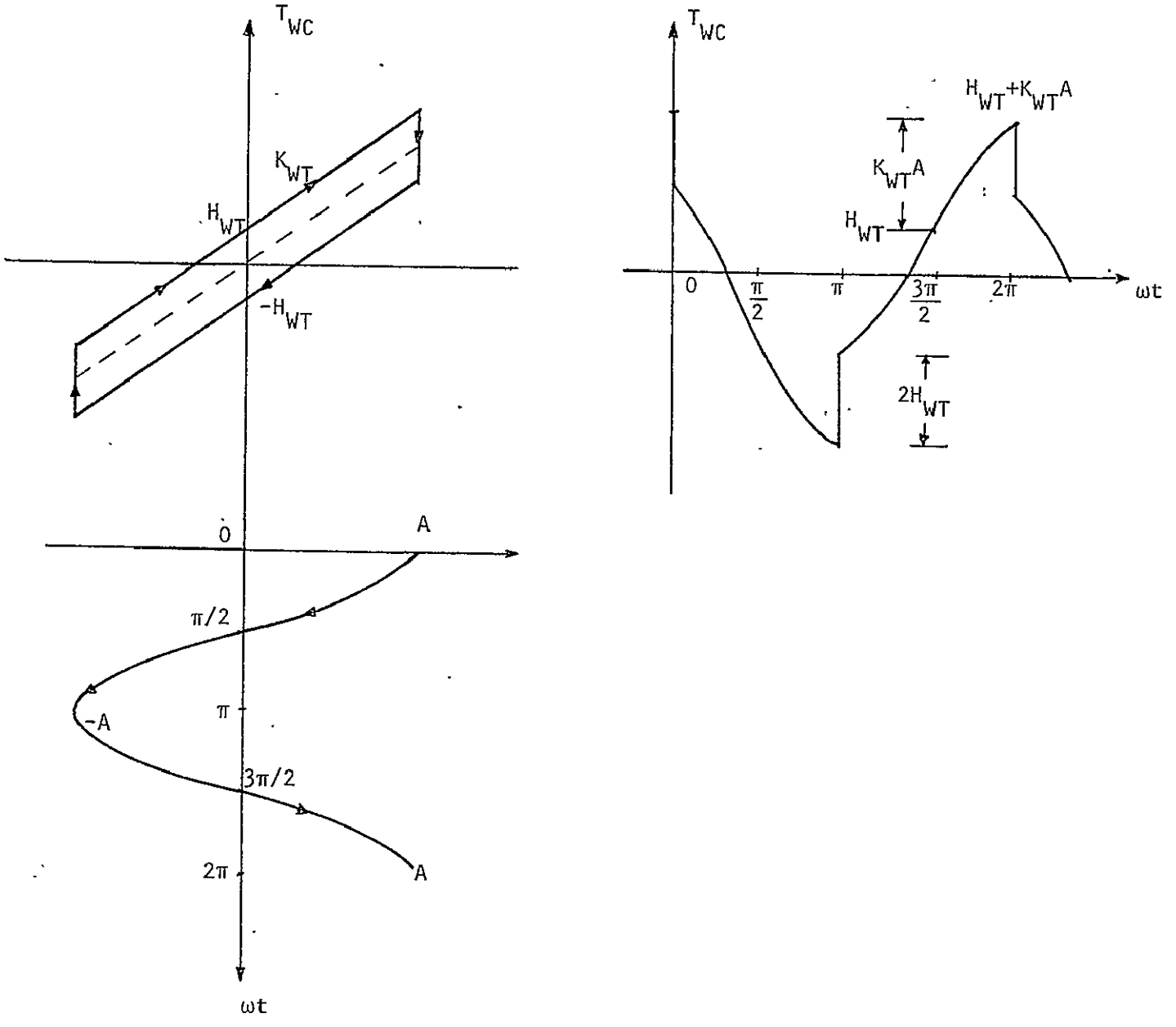

Figure 9-1. Input-output characteristics of wire cable torque nonlinearity.

$$T_{WC}(t) = K_{WT}A\cos\omega t + H_{WT} \qquad \pi \leq \omega t < 2\pi \qquad (9\text{-}7)$$

The fundamental component of the Fourier series representation of $T_{WC}(t)$ is

$$T_{WC}(t) = A_1 \sin\omega t + B_1 \cos\omega t$$

$$= \sqrt{A_1^2 + B_1^2}\,\cos(\omega t - \phi) \qquad (9\text{-}8)$$

$$\phi = \tan^{-1}\frac{A_1}{B_1} \qquad (9\text{-}9)$$

$$A_1 = \frac{1}{\pi}\int_0^{2\pi} T_{WC}(t)\sin\omega t\, d\omega t \qquad (9\text{-}10)$$

$$B_1 = \frac{1}{\pi}\int_0^{2\pi} T_{WC}(t)\cos\omega t\, d\omega t \qquad (9\text{-}11)$$

The coefficients A_1 and B_1 are derived as follows:

$$A_1 = \frac{2}{\pi}\int_0^{\pi} T_{WC}(t)\sin\omega t\, d\omega t$$

$$= \frac{2}{\pi}\int_0^{\pi} (K_{WT}A\cos\omega t - H_{WT})\sin\omega t\, d\omega t$$

$$= -\frac{4H_{WT}}{\pi} \qquad (9\text{-}12)$$

$$B_1 = \frac{2}{\pi}\int_0^{\pi} T_{WC}(t)\cos\omega t\, d\omega t$$

$$= \frac{2}{\pi}\int_0^{\pi} (K_{WT}A\cos\omega t - H_{WT})\cos\omega t\, d\omega t$$

$$= K_{WT}A \qquad (9\text{-}13)$$

Then,

$$\sqrt{A_1^2 + B_1^2} = \sqrt{\left(\frac{4H_{WT}}{\pi}\right)^2 + (K_{WT}A)^2} \qquad (9\text{-}14)$$

$$\phi = \tan^{-1}\left(\frac{-4H_{WT}}{\pi K_{WT}A}\right) \qquad (9\text{-}15)$$

The describing function of the wire cable nonlinearity is written as

$$N_{WT}(A) = \frac{B_1 - jA_1}{A} = \frac{\sqrt{A_1^2 + B_1^2}}{A} \angle\phi$$

$$= \sqrt{\left(\frac{4H_{WT}}{\pi A}\right)^2 + K_{WT}^2} \angle \tan^{-1} \frac{4H_{WT}}{\pi K_{WT} A} \tag{9-16}$$

For the combined nonlinearity, the describing function is the sum of the two describing functions. However, since there are three ball bearings on the flex pivot, the final expression is

$$N(A) = N_{WT}(A) + 3N_{FP}(A) = N_R(A) + jN_I(A) \tag{9-17}$$

where

$$N_R(A) = 3 \frac{2}{\gamma A^2} \left(\frac{C_1}{C_1^2 - A^2} - 1 \right) + K_{WT} \tag{9-18}$$

$$N_I(A) = 3 \left(\frac{4}{\pi A} T_{FPO} - \frac{2}{\pi A^2 \gamma} \ell n \left(\frac{C_1 + A}{C_2 - A} \right) \right) + \frac{4H_{WT}}{\pi A} \tag{9-19}$$

Asymptotic Behavior of $-1/N(A)$ for Very Small Values of A

The asymptotic behavior of $-1/N(A)$ for very small values of A can be derived analytically. It can be shown that

$$\lim_{A \to 0} N_R(A) = \gamma T_{FPO}^2 + K_{WT} \tag{9-20}$$

and

$$\lim_{A \to 0} N_I(A) = \lim_{A \to 0} \frac{4H_{WT}}{\pi A} \tag{9-21}$$

Therefore,

$$\lim_{A \to 0} \frac{-1}{N(A)} = \lim_{A \to 0} \frac{-1}{N_R(A) + jN_I(A)}$$

$$= \frac{-1}{j \lim_{A \to 0} \frac{4H_{WT}}{\pi A}} = 0 \angle -270^\circ \tag{9-22}$$

Asymptotic Behavior of -1/N(A) for Very Large Values of A

For very large values of A it can be shown that

$$\lim_{A\to\infty} N_R(A) = K_{WT} \tag{9-23}$$

and

$$\lim_{A\to\infty} N_I(A) = 0 \tag{9-24}$$

Then,

$$\lim_{A\to\infty} -1/N(A) = \frac{1}{K_{WT}} \angle -180^\circ \tag{9-25}$$

Magnitude Versus Phase Plots of -1/N(A) of the Combined Nonlinearities

A digital computer program for the computation of N(A) and -1/N(A) is listed in Table 9-1. The constant A is designated as E in this program. The parameters of the nonlinearities are:

$$T_{FPO} = 0.00225 \text{ N-m}$$

$$\gamma = 9.2444 \times 10^4 \text{ (N-m-rad)}^{-1}$$

$$K_{WT} = 0.25 \text{ to } 100 \text{ N-m/rad}$$

$$H_{WT} = 0.01 \text{ to } 1 \text{ N-m}$$

Figure 9-2 shows the plots of -1/N(A) for the nonlinearities in magnitude (db) versus phase for varies combinations of K_{WT} and H_{WT}. It is seen that varying the value of H_{WT} between the range of 0.01 to 1 does not affect the curves appreciably.

Prediction of Self-Sustained Oscillations in the IPS System With the Combined Nonlinearity By Means of the Describing Function Method

The characteristic equation of the nonlinear IPS control system with the wire cable Dahl-model nonlinearities is determined from Figure 8-2.

$$1 + N(A)G_{eq}(s) = 0 \tag{9-26}$$

where N(A) is defined in Eq. (9-17), and

TABLE 9-1

IPS CONTINUOUS DESCRIBING FUNCTION OF COMBINED NONLINEARITY

```
      CALCULATION FOR -1/N
      COMPLEX GVV,GN,GV
      REAL*8 P(20),PI,RAD,TO,GAMMA,ESTART,E,AA,R,TGFI,TGFN,
     1TGFP,C1,C2,A1,AI1,B1,BI1
      REAL*8 AI,I
      PI=3.14159D0
      RAD=180.D0/PI
      TO=0.00225D0
      HWT=1.D0
      I=10.D0
      KWT=100.D0
      GAMMA=8*9.2444D3
      ESTART=1.D-10
      NP=5
      ND=12
      WRITE(5,100)
      WRITE(5,101)
      DO 1 J=1,ND
      DO 1 I=1,NP
      E=ESTART*DFLOAT(I)*(10.D0**(J-1))
      AA=2.D0*GAMMA*E*TO
      R=(-1.D0/AA)+DSQRT((AA*AA+1.D0)/(AA*AA))
      TGFI=R*TO
      TGFN=TGFI
      TGFP=-TGFI
      C1=E-1.D0/(GAMMA*(TGFP-TO))
      C2=-E-1.D0/(GAMMA*(TGFN+TO))
      A1=(-4.D0*TO/PI)+(1.D0/(PI*GAMMA*E))*DLOG((1/C1+E)*(C2-E))
     1/((C1-E)*(C2+E)))
      AI=DLOG((1/(C1+E)*(C2-E))/((C1-E)*(C2+E)))
      A1=(-4.D0*TO/PI)+(AI/(PI*GAMMA*E))
      B1=(-1.D0/(GAMMA*E))*(2.D0+C2/DSQRT(C2*C2-E*E)-C1/DSQRT(C1*C1-E
     1*E))
      AI1=-4.D0*HWT/PI
      BI1=E*KWT
      AA1=(3.*A1+AI1)/E
      BB1=(3.*B1+BI1)/E
      GN=CMPLX(BB1,-AA1)
      GV=-1./GN
      G1=REAL(GV)
      G2=AIMAG(GV)
      GMAG=CABS(GV)
      GDB=20.*ALOG10(GMAG)
      GPHASE=RAD*ATAN2(G2,G1)
      IF(GPHASE.GE.0.)GPHASE=GPHASE-360.
      WRITE(5,102)E,TGFI,GPHASE,GDB,GMAG
1     CONTINUE
100   FORMAT('   CONTINUOUS DESCRIBING FUNCTION FOR LST NONLINEARITY
101   FORMAT(/,8X,'E',11X,'TGFI',10X,'PHASE',10X,'DB',9X,'MAGNITUDE'
102   FORMAT(1P5E14.5)
      STOP
      END
```

$$G_{eq}(s) = \frac{0.0013946(s^3 + 0.0012528s^2 + 0.0036846s)}{\Delta(s)} \qquad (9\text{-}27)$$

where $\Delta(s)$ is defined in Eq. (3-4). Notice that $G_{eq}(s)$ in Eq. (9-27) is equal to s^{-1} times the $G_{eq}(s)$ in Eq. (3-3), since in Chapter 3 the input to N is $\dot{\varepsilon}$ whereas now it is ε. The frequency plots of $G_{eq}(s)$ of Eq. (9-27) are plotted in Figure 9-2 for $K_1 = 10^5$ and 10^6. Similar to the curves in Figure 3-6, these frequency loci for $G_{eq}(s)$ have two equilibrium points for each curve, one stable and the other unstable. For instance, for $K_1 = 10^5$, the $G_{eq}(s)$ curve intersects the $-1/N(A)$ loci at $\omega = 0.138$ rad/sec and $\omega = 0.055$ rad/sec. The equilibrium point that corresponds to $\omega = 0.138$ rad/sec is a stable equilibrium point, whereas $\omega = 0.055$ rad/sec represents an unstable equilibrium point. These results are very close to those obtained in Chapter 3 where the flex pivot is presented as a spring. Therefore, the impact of using the Dahl solid friction model is not great although all the loci are substantially different. For $K_1 = 10^6$, the stable equilibrium point is at $\omega = 0.16$ rad/sec, and the unstable equilibrium point is at $\omega = 0.05$ rad/sec.

Figure 9-2 shows that for the system paramters used, the intersections between $G_{eq}(s)$ and $-1/N(A)$ all fall on the portion of the $-1/N(A)$ loci that lie on the -270° axis. This means that as we vary the values of K_{WT} and H_{WT} of the wire cable nonlinearity characteristics within the stipulated ranges, only the amplitude of oscillation, A, will be varied. Equations (9-21) and (9-22) further show that for small values of $-1/N(A)$, which correspond to the range of intersections in the present case, the amplitude of oscillation is not sensitive to the values of γ, T_{FP0}, and K_{WT}. However, the amplitude of oscillation, A, is directly proportional to the value of H_{WT}. Typical results of the stable sustained oscillations are tabulated in Table 9-2.

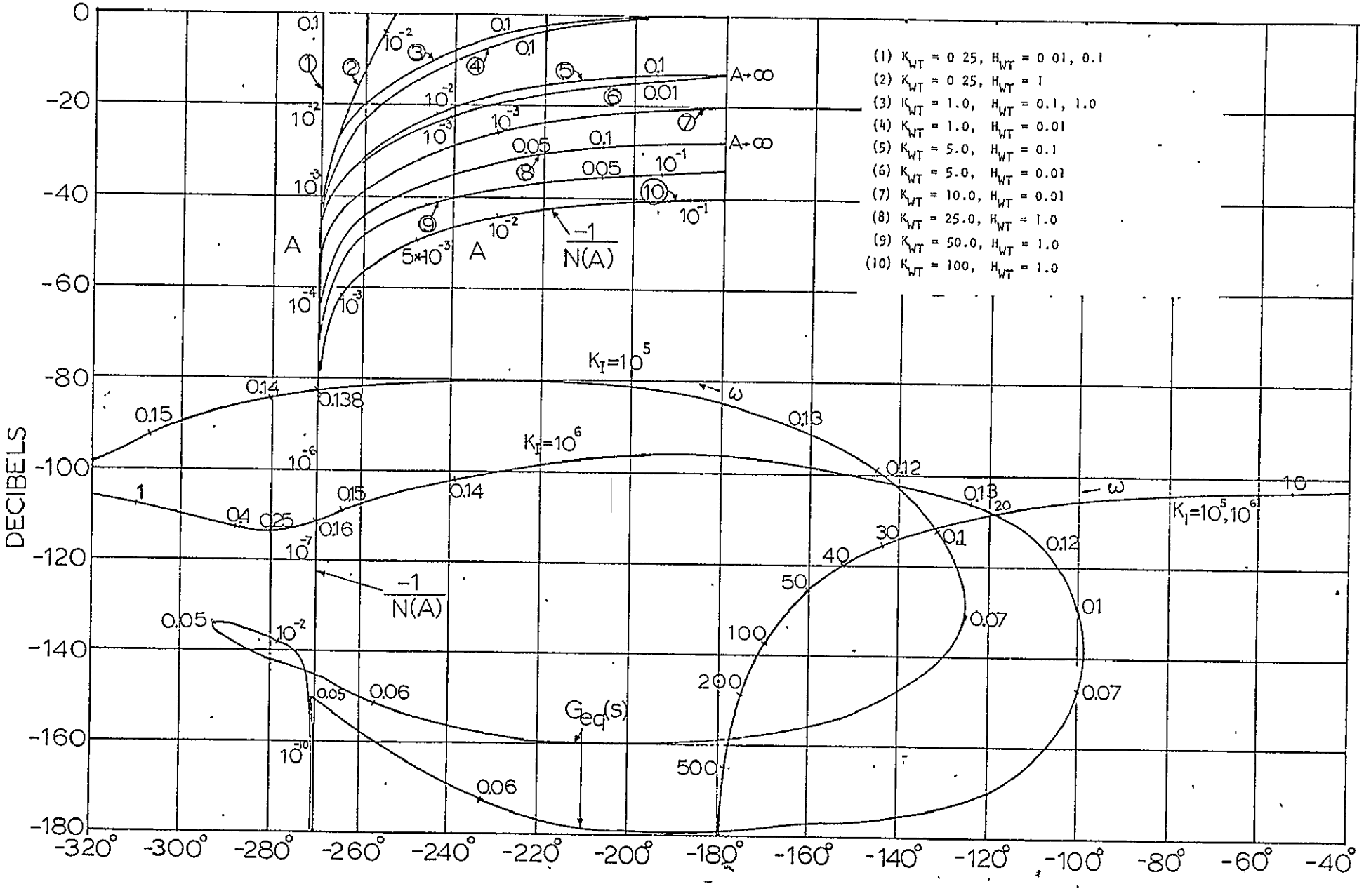

Figure 9-2. Frequency response plots and describing function loci of IPS system with flex pivot and wire cable nonlinearities (Dahl model).

TABLE 9-2

K_I	K_{WT}	H_{WT}	A (rad)	(arc-sec)	ω (rad/sec)
10^5	0.25	0.01	10^{-6}	0.2	0.138
10^5	0.25	0.1	10^{-5}	2.0	0.138
10^5	1.00	0.01	10^{-6}	0.2	0.138
10^5	1.00	1.00	10^{-4}	20.0	0.138
10^5	5.00	0.01	10^{-6}	0.2	0.138
10^5	5.00	1.00	10^{-4}	20.0	0.138
10^5	10.00	0.01	10^{-6}	0.2	0.138
10^5	10.00	1.00	10^{-4}	20.0	0.138
10^5	25.00	1.00	10^{-4}	20.0	0.138
10^5	100.00	1.00	10^{-4}	20.0	0.138
10^6	0.25	0.01	3×10^{-8}	0.006	0.16
10^6	0.25	0.1	3×10^{-7}	0.06	0.16
10^6	1.00	0.01	3×10^{-8}	0.006	0.16
10^6	1.00	1.00	3×10^{-6}	0.6	0.16
10^6	5.00	0.01	3×10^{-8}	0.006	0.16
10^6	5.00	1.00	3×10^{-6}	0.6	0.16
10^6	10.00	0.01	3×10^{-8}	0.006	0.16
10^6	10.00	1.00	3×10^{-6}	0.6	0.16
10^6	25.00	1.00	3×10^{-6}	0.6	0.16
10^6	100.00	1.00	3×10^{-6}	0.6	0.16

It is of interest to compare these results with those obtained in Chapter 3. Using the results tabulated on page 30, the following comparisons are obtained.

$H_{WT} = 1, \quad K_{WT} = \text{arbitrary}$

Results in Chapter 3			Dahl model results	
K_I	A (rad)	ω (rad/sec)	A (rad)	ω (rad/sec)
10^6	3.17×10^{-6}	0.16	3×10^{-6}	0.16
10^5	8.19×10^{-5}	0.14	10^{-4}	0.138

Therefore, we see that for all practical purposes these results are identical

10. Modeling of the Solid Rolling Friction by the First-Order Dahl-Model

It has been established that the solid rolling friction characteristics can be approximated by the nonlinear relation

$$\frac{dT_{FP}(\varepsilon)}{d\varepsilon} = \gamma(T_{FPI} - T_{FP0})^i \tag{10-1}$$

where i = positive number

γ = constant

$T_{FPI} = T_{FP}SGN(\dot{\varepsilon})$

$T_{FP}(\varepsilon)$ = friction torque

T_{FP0} = saturation level of T_{FP}

ε = angular displacement

The describing function of the friction nonlinearity for $n = 2$ has been derived. In this chapter the input-output relationship will be obtained by solving Eq. (10-1) with $i = 1$. The describing function for the $i = 1$ case is derived in the next chapter.

Let the angular displacement ε be a cosinusoidal function,

$$\varepsilon(t) = A \cos \omega t \tag{10-2}$$

Then, we can write

$$\frac{dT_{FP}(\varepsilon)}{dt} = \frac{dT_{FP}(\varepsilon)}{d\varepsilon}\dot{\varepsilon} = -\gamma A\omega \sin \omega t \ (T_{FPI} - T_{FP0}) \tag{10-3}$$

where i has been set to 1.

Since $T_{FPI} = T_{FP}SGN(\dot{\varepsilon})$, Eq.(10-3) is written

$$\begin{aligned}\frac{dT_{FP}(\varepsilon)}{dt} &= -\gamma A\omega \sin \omega t \ (T_{FP} - T_{FP0}) \qquad \dot{\varepsilon} \geq 0 \\ &= \gamma A\omega \sin \omega t \ (T_{FP} + T_{FP0}) \qquad \dot{\varepsilon} \leq 0\end{aligned} \tag{10-4}$$

For $\dot{\varepsilon} \leq 0$, $2\pi k \leq \omega t \leq (2k + 1)\pi$, $k = 0,1,2,\ldots$.

Equation (10-4) is integrated on both sides to give

$$\int_{T_{FP}[\varepsilon(0)]}^{T_{FP}[\varepsilon(t)]} \frac{dT_{FP}(\varepsilon)}{(T_{FP} + T_{FP0})} = \int_0^{\omega t} \gamma A\omega \sin \omega\tau d\tau \qquad (10\text{-}5)$$

Thus,

$$\ell n(T_{FP} + T_{FP0})\Big|_{T_{FP}[\varepsilon(0)]}^{T_{FP}[\varepsilon(t)]} = -\gamma A \cos \omega\tau\Big|_0^{\omega t} \qquad (10\text{-}6)$$

Or,

$$\ell n\left(T_{FP}(\varepsilon) + T_{FP0}\right) - \ell n\left(T_{FP}(0) + T_{FP0}\right) = -\gamma A(\cos \omega t - 1) \qquad (10\text{-}7)$$

$$\ell n\left(\frac{T_{FP}(\varepsilon) + T_{FP0}}{T_{FP}(0) + T_{FP0}}\right) = -\gamma A(\cos \omega t - 1) \qquad (10\text{-}8)$$

Since for the cosinusoidal input $\varepsilon(0) = A$ and $\dot{\varepsilon} \leq 0$ for $2\pi k \leq \omega t \leq (2k + 1)\pi$, $k = 0,1,2,\ldots$, $T_{FP}(0) = T_{FP1} \geq 0$. This is because at $\varepsilon = 0$, ε is decreasing, and T_{FP} acts in the direction opposite to the motion; thus $T_{FP1} \geq 0$. Equation (10-8) is written as

$$\ell n\left(\frac{T_{FP}(\varepsilon) + T_{FP0}}{T_{FP1} + T_{FP0}}\right) = -\gamma A(\cos \omega t - 1) \qquad (10\text{-}9)$$

Or,

$$\frac{T_{FP}(\varepsilon)}{T_{FP0}} = -1 + \left(\frac{T_{FP1}}{T_{FP0}} + 1\right) e^{-\gamma A(\cos\omega t - 1)} \qquad (10\text{-}10)$$

For $\dot{\varepsilon} \geq 0$, $(2k + 1)\pi \leq \omega t \leq (2k + 2)\pi$, $k = 0,1,2,\ldots$.

Equation (10-4) is integrated on both sides to give

$$\int_{T_{FP}[\varepsilon(t)]}^{T_{FP}(2\pi)} \frac{dT_{FP}(\varepsilon)}{(T_{FP} - T_{FP0})} = \int_{\omega t}^{2\pi} -\gamma A \sin \omega\tau \, d\omega\tau \qquad (10\text{-}11)$$

Carrying out the integration, we get

$$\ln\left[\frac{T_{FP}(\varepsilon) - T_{FP0}}{T_{FP}(2\pi) - T_{FP0}}\right] = -\gamma A(1 - \cos \omega t) \tag{10-12}$$

Now at $\omega t = 2\pi$, $T_{FP}(2\pi) = T_{FP1} \geq 0$. Equation (10-12) leads to

$$\frac{T_{FP}(\varepsilon)}{T_{FP0}} = 1 + \left[\frac{T_{FP1}}{T_{FP0}} - 1\right] e^{\gamma A(\cos \omega t - 1)} \tag{10-13}$$

Let

$$R = T_{FP1}/T_{FP0} \tag{10-14}$$

Then, Eqs. (10-10) and (10-13) become

$$\frac{T_{FP}(\varepsilon)}{T_{FP0}} = -1 + (R + 1)e^{-\gamma A(\cos\omega t - 1)} \tag{10-15}$$

$$\frac{T_{FP}(\varepsilon)}{T_{FP0}} = 1 + (R - 1)e^{\gamma A(\cos\omega t - 1)} \tag{10-16}$$

respectively.

In order to evaluate R, we equate the last two equations at $\omega t = \pi$. Then,

$$-1 + (R + 1)e^{2\gamma A} = 1 + (R - 1)e^{-2\gamma A} \tag{10-17}$$

The solution is

$$R = \frac{2}{e^{2\gamma A} - e^{-2\gamma A}} - \frac{e^{2\gamma A} + e^{-2\gamma A}}{e^{2\gamma A} - e^{-2\gamma A}}$$

or

$$R = \operatorname{csch}(2\gamma A) - \coth(2\gamma A) \tag{10-18}$$

Since $\varepsilon = A \cos \omega t$ and $\varepsilon_i = \varepsilon(0) = A$, Eqs. (10-15) and (10-16) are written as

$$\frac{T_{FP}(\varepsilon)}{T_{FP0}} = -1 + (R + 1)e^{-\gamma(\varepsilon - \varepsilon_i)} \qquad \dot{\varepsilon} \leq 0 \tag{10-19}$$

$$\frac{T_{FP}(\varepsilon)}{T_{FP0}} = 1 + (R - 1)e^{\gamma(\varepsilon-\varepsilon_i)} \qquad \dot{\varepsilon} \geq 0 \qquad (10\text{-}20)$$

Figure 10-1 shows the T_{FP}/T_{FP0} versus ε/A characteristics for several values of A when the input is the cosinusoidal function of Eq. (10-2). Figure 10-2 shows the normalized $(3T_{FP} + T_{WC})/(3T_{FP0} + K_{WT} + H_{WT}\dot{})$ versus ε/A for several typical combinations of A, H_{WT}, and K_{WT}.

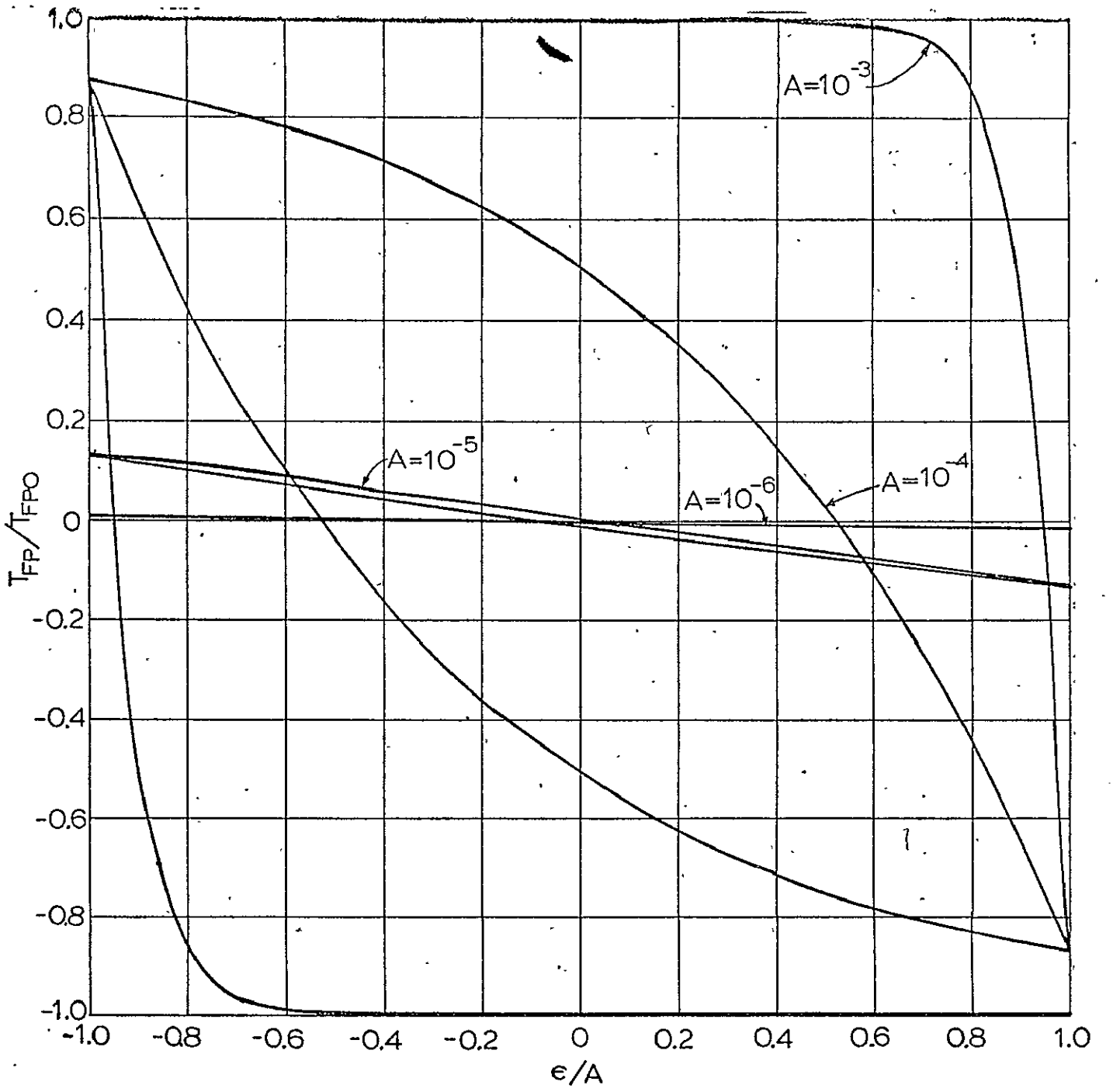

Figure 10-1. Normalized flex pivot torque (Dahl model i = 1) versus ε/A for IPS with cosine function input.

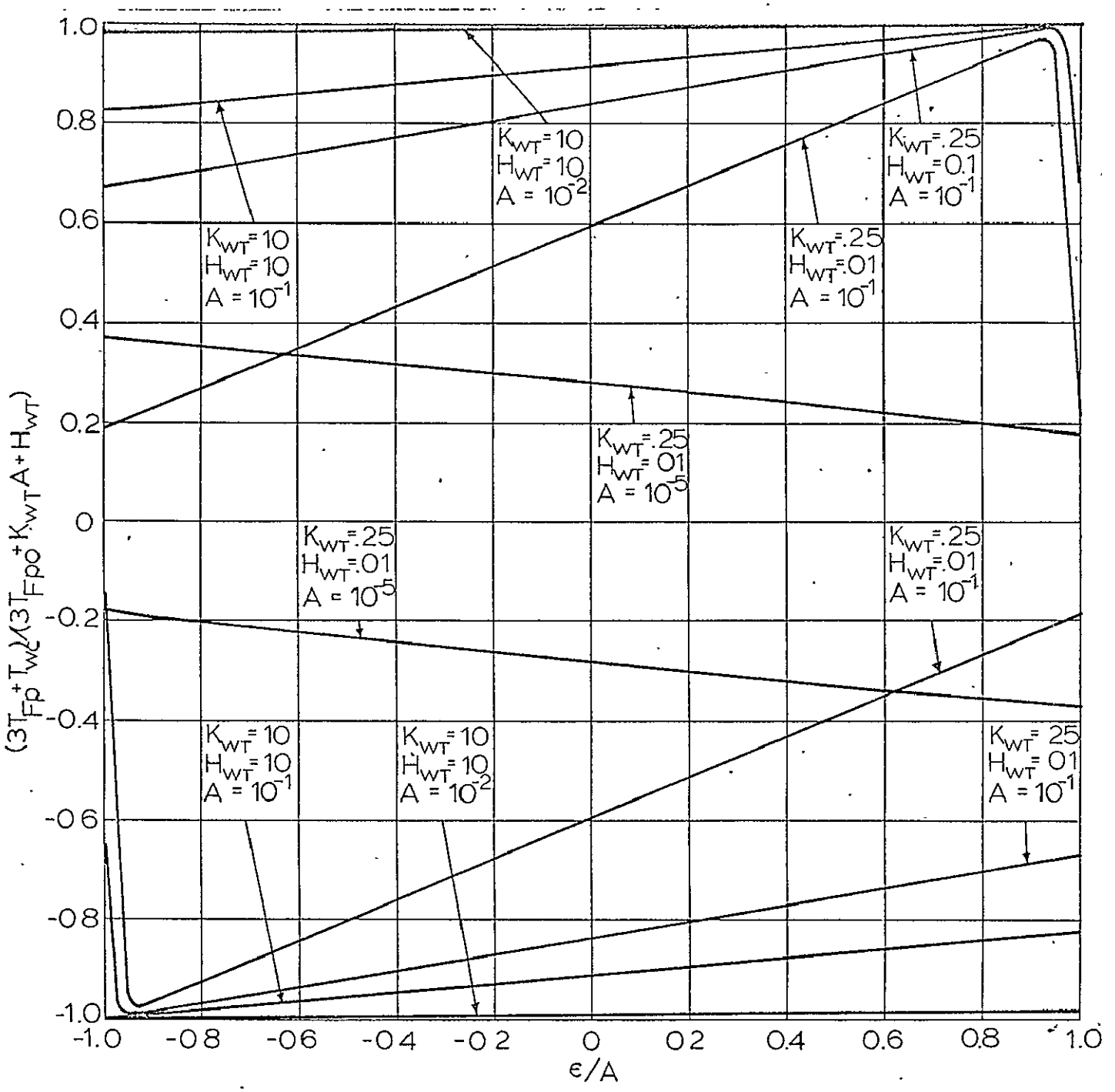

Figure 10-2. Normalized flex pivot plus wire cable torque versus ε/A for IPS with cosine function input.

11. Describing Function of the First-Order Dahl Model Solid Rolling Friction

The mathematical description of the first-order Dahl model of the solid rolling friction is presented in the last chapter. The frictional torques for the two ranges of $\dot{\varepsilon}$ for a cosinusoidal input displacement are given by Eqs. (10-19) and (10-20). These equations are rewritten in the following form:

$$T_{FP}(\varepsilon) = T_{FPI} e^{-\gamma A(\cos\omega t - 1)} + T_{FP0}(e^{-\gamma A(\cos\omega t - 1)} - 1) \qquad (11\text{-}1)$$

$$T_{FP}(\varepsilon) = T_{FPI} e^{\gamma A(\cos\omega t - 1)} - T_{FP0}(e^{\gamma A(\cos\omega t - 1)} - 1) \qquad (11\text{-}2)$$

For the cosinusoidal input, $\varepsilon(t) = A \cos \omega t$, let $T_{FP}(\varepsilon)$ be approximated by the fundamental component of its Fourier series representation, i.e.,

$$T_{FP}(\varepsilon) = A_1 \sin \omega t + B_1 \cos \omega t \qquad (11\text{-}3)$$

The describing function of the friction nonlinearity (i = 1) is defined as

$$N_{FP}(A) = \frac{B_1 - jA_1}{A} \qquad (11\text{-}4)$$

where

$$A_1 = \frac{1}{\pi}\int_0^{2\pi} T_{FP}(\varepsilon) \sin \omega t \, d\omega t$$

$$= \frac{1}{\pi}\int_0^{\pi} \left((T_{FPI} + T_{FP0})e^{-\gamma A(\cos\omega t - 1)} - T_{FP0}\right) \sin \omega t \, d\omega t$$

$$+ \frac{1}{\pi}\int_{\pi}^{2\pi} \left((T_{FPI} - T_{FP0})e^{\gamma A(\cos\omega t - 1)} + T_{FP0}\right) \sin \omega t \, d\omega t \qquad (11\text{-}5)$$

Evaluating the integrals in the last equation, we have

$$A_1 = \frac{-4T_{FP0}}{\pi} + \frac{1}{\pi\gamma A}\left[T_{FPI}(e^{-2\gamma A} + e^{2\gamma A} - 2) + T_{FP0}(e^{2\gamma A} - e^{-2\gamma A})\right] \qquad (11\text{-}6)$$

or

$$A_1 = \frac{-4T_{FP0}}{\pi} + \frac{2}{\pi\gamma A}\left(T_{FP1}(\cosh 2\gamma A - 1) + T_{FP0}(\sinh 2\gamma A)\right) \qquad (11\text{-}7)$$

$$B_1 = \frac{1}{\pi}\int_0^{\pi}\left((T_{FP1} + T_{FP0})e^{-\gamma A(\cos\omega t - 1)} - T_{FP0}\right)\cos\omega t\, d\omega t$$

$$+ \frac{1}{\pi}\int_{\pi}^{2\pi}\left((T_{FP1} - T_{FP0})e^{\gamma A(\cos\omega t - 1)} + T_{FP0}\right)\cos\omega t\, d\omega t \qquad (11\text{-}8)$$

In order to evaluate the integrals of B_1, let us represent $e^{-\gamma A\cos\omega t}$ as a power series:

$$e^{-\gamma A\cos\omega t} = 1 - \gamma A\cos\omega t + \frac{(\gamma A)^2\cos^2\omega t}{2!} - \frac{(\gamma A)^3\cos^3\omega t}{3!} + \cdots \qquad (11\text{-}9)$$

Consider the integral

$$I_{B1} = \int_0^{\pi} e^{-\gamma A\cos\omega t}\cos\omega t\, d\omega t$$

$$= \int_0^{\pi}\left(1 - \gamma A\cos\omega t + \frac{(\gamma A)^2}{2!}\cos^2\omega t - \frac{(\gamma A)^3}{3!}\cos^3\omega t + \cdots\right)\cos\omega t\, d\omega t \qquad (11\text{-}10)$$

Since

$$\int_0^{\pi}\cos^m\omega t\, d\omega t = 0 \quad \text{for} \quad m = \text{odd integers} \qquad (11\text{-}11)$$

Eq. (11-10) becomes

$$I_{B1} = -\sum_{i=0}^{\infty}\frac{(\gamma A)^i}{i!}\int_0^{\pi}\cos^{i+1}\omega t\, d\omega t \qquad i = \text{odd integers} \qquad (11\text{-}12)$$

Evaluating the integral, the result is

$$I_{B1} = \frac{-\pi\gamma A}{2}\left[1 + \frac{(\gamma A)^2}{2!}\left(\frac{1}{4}\right) + \frac{(\gamma A)^4}{4!}\left(\frac{1}{6}\right)\left(\frac{3}{4}\right) + \frac{(\gamma A)^6}{6!}\left(\frac{1\cdot 3\cdot 5}{8\cdot 6\cdot 4}\right)\right.$$

$$\left. + \frac{(\gamma A)^8}{8!}\left(\frac{1\cdot 3\cdot 5\cdot 7}{10\cdot 8\cdot 6\cdot 4}\right) + \cdots\right] \qquad (11\text{-}13)$$

Similarly, the integral

$$I_{B2} = \int_{\pi}^{2\pi} e^{\gamma A \cos\omega t} \cos \omega t \, d\omega t$$

is evaluated, and the result is

$$I_{B2} = -I_{B1} \tag{11-14}$$

Substituting the results of I_{B1} and I_{B2} into Eq. (11-8), we have

$$B_1 = \frac{T_{FP1} + T_{FP0}}{\pi} e^{\gamma A} I_{B1} + \frac{T_{FP1} - T_{FP0}}{\pi} e^{-\gamma A} I_{B2}$$

$$= \frac{I_{B1}}{\pi} \left(T_{FP1} (e^{\gamma A} - e^{-\gamma A}) + T_{FP0} (e^{\gamma A} + e^{-\gamma A}) \right) \tag{11-15}$$

For very small values of γA

$$I_{B1} \cong - \frac{\pi \gamma A}{2} \tag{11-16}$$

Equation (11-15) becomes

$$B_1 \cong - \frac{\gamma A}{2} \left(T_{FP1} (e^{\gamma A} - e^{-\gamma A}) + T_{FP0} (e^{\gamma A} + e^{-\gamma A}) \right) \tag{11-17}$$

or

$$B_1 \cong -\gamma A \left(T_{FP1} \sinh (\gamma A) + T_{FP0} \cosh (\gamma A) \right) \tag{11-18}$$

For large values of γA, I_{B1} becomes very large. However, we shall show that T_{FP1} approaches $-T_{FP0}$ as γA becomes very large, so that B_1 becomes zero.

We shall now investigate the limiting values of A_1/A and B_1/A when A approaches zero and infinity. Since

$$\lim_{A \to 0} T_{FP1} = 0 \, , \tag{11-19}$$

$$\lim_{A \to 0} \frac{A_1}{A} = \lim_{A \to 0} \left(\frac{-4 T_{FP0} \gamma}{2\pi A \gamma} + \frac{4 T_{FP0} \gamma}{2\pi A \gamma} \right) = 0 \tag{11-20}$$

$$\lim_{A\to 0} \frac{B_1}{A} = -\gamma T_{FP0} \tag{11-21}$$

Therefore,

$$\lim_{A\to 0} \left[-1/N_{FP}(A) \right] = \frac{1}{\gamma T_{FP0}} \tag{11-22}$$

When A approaches infinity,

$$\lim_{A\to \infty} T_{FP1} = -T_{FP0} \tag{11-23}$$

$$\lim_{A\to \infty} \frac{B_1}{A} = -\frac{\gamma}{2} \left[-T_{FP0} e^{\gamma A} + T_{FP0} e^{\gamma A} \right] I_{B1}$$

$$= 0 \tag{11-24}$$

The value of A_1/A also approaches zero as A becomes very large; however it decreases at a much slower rate than B_1/A. Thus,

$$\lim_{A\to \infty} \left[-1/N_{FP}(A) \right] = \lim_{A\to \infty} \frac{-1}{jA_1/A} = \infty \angle -270^{\circ}$$

Figure 11-1 shows the plot of $-1/N_{FP}(A)$ in the magnitude (db) versus phase coordinates for

$$\gamma = 13429.75 \text{ (N-m-rad)}^{-1}$$

$$T_{FP0} = 0.0088 \text{ N-m}$$

Magnitude versus Phase Plots of $-1/N_{FP}(A)$ of the Combined Nonlinearities

For the combined nonlinearity of the Dahl friction model (i = 1) and the wire cable, the nonlinear describing function is written as (Eq. (10-17))

$$N(A) = N_{WT}(A) + 3N_{FP}(A) \tag{11-25}$$

where $N_{WT}(A)$ is given in Eq. (9-16).

Figure 11-2 shows the plots of $-1/N(A)$ for the combined nonlinearity in magnitude versus phase for various combinations of K_{WT} and H_{WT}. These

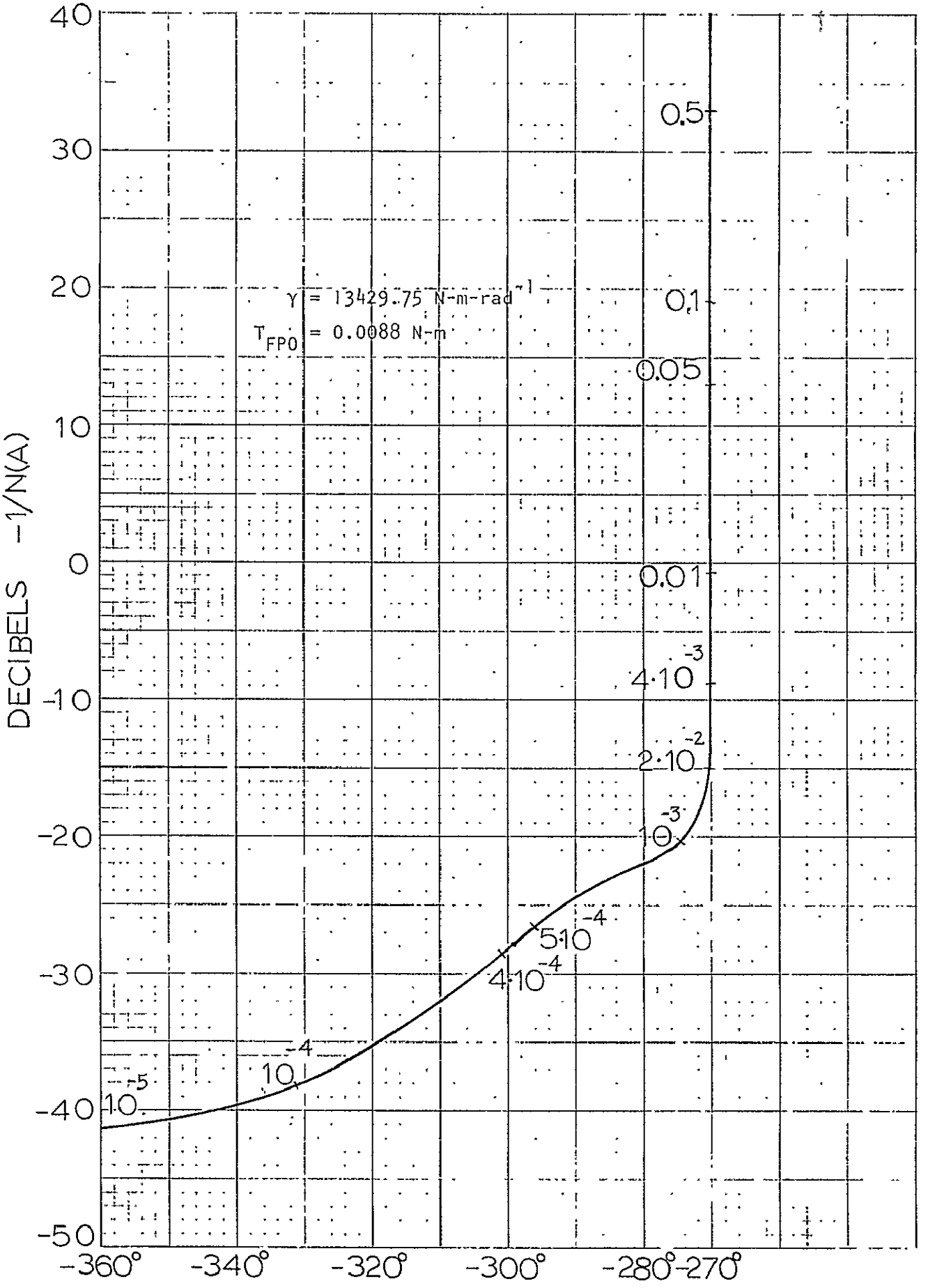

Figure 11-1. Magnitude versus phase plot of $-1/N_{FP}(A)$ of Dahl solid rolling friction model with i = 1.

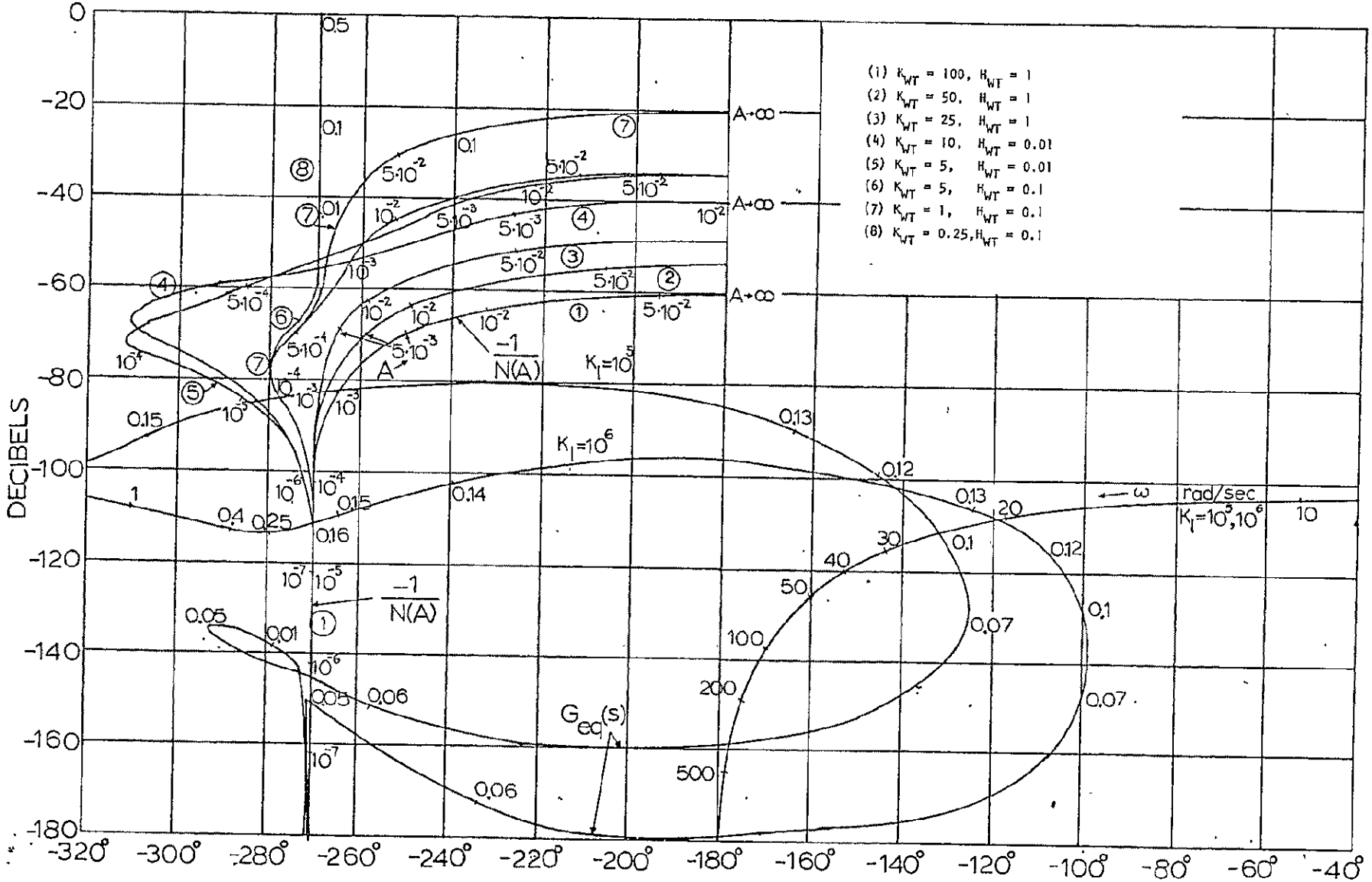

Figure 11-2. Frequency response plots and describing function loci of IPS system with flex pivot and wire cable nonlinearities (Dahl model i = 1).

curves are similar to the plots shown in Fig. 9-2 which are for i = 2 in the Dahl model, especially when the values of A are very small and very large.

The frequency loci of $G_{eq}(s)$ of Eq. (9-27) are plotted in Fig. 11-2 for $K_I = 10^5$ and 10^6. Similar to the cases in Fig. 9-2, these frequency loci have two equilibrium points for each curve, one stable and the other unstable.

For $K_I = 10^6$ the frequency of oscillation at the stable equilibrium is approximately 0.16 rad/sec, and is rather independent on the values of K_{WT} and H_{WT}. This result is identical to that obtained in Chapter 9 when i = 2 is used for the Dahl friction model.

Figure 11-2 shows that for $K_I = 10^5$ the frequency of oscillation at the stable equilibrium varies as a function of the values of K_{WT} and H_{WT}. For the various combinations of K_{WT} and H_{WT} shown in Figure 11-2, the variation of frequency is not large, from 0.138 to 0.14 rad/sec. Of more importance is perhaps the fact that when i = 1, the amplitude of oscillation A is larger as compared with that for i = 2. For example, for $K_{WT} = 100$, $H_{WT} = 1.0$, $K_I = 10^5$, Figure 9-2 shows that the amplitude of A is approximately 10^{-5} for k = 2, whereas for the same set of parameters Figure 11-2 shows that $A = 10^{-3}$ for i = 1.

12. Modeling of the Solid Rolling Friction by the ith-order Dahl Model and The Describing Function

In the previous sections the solid rolling friction was modelled by Eq. (10-1) with i = 1 and 2. In general, the exponent i can be of any other value. In this section we shall derive the mathematical model of the solid rolling friction for $i \neq 1$.

Let the frictional characteristics be approximated by the nonlinear relation

$$\frac{dT_{FP}(\varepsilon)}{d\varepsilon} = \gamma(T_{FPI} - T_{FP0})^i \tag{12-1}$$

where

i = positive number $\neq 1$

γ = constant

$$T_{FPI} = T_{FP}\ SGN(\dot{\varepsilon}) \tag{12-2}$$

$T_{FP}(\varepsilon)$ = friction torque

T_{FP0} = saturation level of T_{FP}

ε = angular displacement

Let the angular displacement ε be a cosinusoidal function,

$$\varepsilon(t) = A \cos \omega t \tag{12-3}$$

Then,

$$\dot{\varepsilon}(t) = -A\omega \sin \omega t \tag{12-4}$$

We can write

$$\frac{dT_{FP}}{dt} = -\gamma A\omega \sin \omega t(T_{FPI} - T_{FP0})^i \tag{12-5}$$

In view of Eq. (12-2), the last equation is written

$$\begin{aligned} \frac{dT_{FP}}{dt} &= -\gamma A\omega \sin \omega t(T_{FP} - T_{FP0})^i \qquad \dot{\varepsilon} \geq 0 \\ &= -\gamma A\omega \sin \omega t(-T_{FP} - T_{FP0})^i \qquad \dot{\varepsilon} \leq 0 \end{aligned} \tag{12-6}$$

If $\dot{\varepsilon} \geq 0$ for $2k\pi \leq \omega t \leq (2k+1)\pi$, $k = 0, 1, 2, \ldots$, Eq. (12-6) is integrated to give

$$\int_{T_{FP}(e(0))}^{T_{FP}(\varepsilon(t))} \frac{dT_{FP}}{(T_{FP} - T_{FP0})^i} = -\gamma A \int_{\omega t = 0}^{\omega t} \sin u\,du = -\gamma A(-\cos u)\Big|_0^{\omega t}$$

$$= -\gamma A(-\cos \omega t + 1) \tag{12-7}$$

The last equation becomes

$$\left[\frac{(T_{FP} - T_{FP0})^{-i+1}}{(-i+1)}\right]_{T_{FPi}}^{T_{FP}} = \frac{(T_{FP} - T_{FP0})^{-(i-1)}}{-(i-1)} - \frac{(T_{FPi} - T_{FP0})^{-(i-1)}}{-(i-1)}$$

$$= \gamma A(\cos \omega t - 1) \tag{12-8}$$

where $T_{FPi} = T_{FP}(\varepsilon(0))$ and $T_{FP} = T_{FP}(\varepsilon(t))$.

Equation (12-8) is further simplified to

$$(T_{FP} - T_{FP0})^{-(i-1)} - (T_{FPi} - T_{FP0})^{-(i-1)} = -(i-1)\gamma A(\cos \omega t - 1) \tag{12-9}$$

Defining

$$R = T_{FPi}/T_{FP0} \tag{12-10}$$

Eq. (12-9) leads to

$$\frac{T_{FP}}{T_{FP0}} = 1 + \frac{R - 1}{\left\{1 - (i-1)\gamma A\left(T_{FP0}R-1\right)\right)^{(i-1)}(\cos \omega t - 1)\}^{1/(i-1)}} \tag{12-11}$$

If $\dot{\varepsilon} \leq 0$, for $(2k+1)\pi \leq \omega t \leq (2k+2)\pi$, $k = 0, 1, 2, \ldots$, Eq. (12-6) is integrated to give

$$\int_{T_{FP}(\varepsilon(\omega t))}^{T_{FP}(\varepsilon(2\pi))} \frac{dT_{FP}}{(-T_{FP} - T_{FP0})^{i}} = -\int_{\omega t}^{2\pi} \gamma A \sin u \, du = A(1 - \cos\omega t) \tag{12-12}$$

Following the same steps as in Eqs. (12-8) through (12-11), we have

$$\frac{T_{FP}}{T_{FP0}} = \frac{R + 1}{\left\{1 + (i-1)\gamma A\left(-T_{FP0}(R+1)\right)^{(i+1)}(\cos \omega t - 1)\right\}^{1/(i-1)}} - 1 \tag{12-13}$$

In order to evaluate R, we equate Eqs. (12-11) and (12-13) at $\omega t = \pi$. After simplification, the result is

$$2 + R\left\{\frac{1}{\left(1 + \hat{a}(R-1)^{(i-1)}\right)^{1/(i-1)}} - \frac{1}{\left\{1 - \hat{a}\left(-(R+1)\right)^{(i-1)}\right\}^{1/(i-1)}}\right\}$$

$$= \left\{\frac{1}{\left(1 + \hat{a}(R-1)^{(i-1)}\right)^{1/(i-1)}} + \frac{1}{\left\{1 - \hat{a}\left(-(R+1)\right)^{(i-1)}\right\}^{1/(i-1)}}\right. \tag{12-14}$$

where

$$\hat{a} = 2(i - 1)\gamma A T_{FP0}^{(i-1)} \tag{12-15}$$

Once the value of i ($i \neq 1$) is specified, R can be solved from Eq. (12-14). We can show that when i = 2,

$$\hat{a} = a = 2\gamma AT_{FP0} \tag{12-16}$$

which is identical to Eq. (8-18), and

$$R = -\frac{1}{a} \pm \sqrt{\frac{a^2 + 1}{a^2}} \tag{12-17}$$

which is the same result as in Eq. (8-19).

Once R is determined from Eq. (12-14), the torque relationships are expressed by Eqs. (12-11) for $\dot{\varepsilon} \geq 0$ and Eq. (12-13) for $\dot{\varepsilon} \leq 0$.

Describing Function For the Dahl Model For $i \neq 1$

Let

$$\beta = \hat{a}/2 = (i - 1)\gamma AT_{FP0}^{(i-1)} \tag{12-18}$$

Equations (12-11) and (12-13) are simplified to

$$\frac{T_{FP}}{T_{FP0}} = \frac{R - 1}{\left(1 - \beta(R - 1)^{(i-1)}(\cos \omega t - 1)\right)^{1/(i-1)}} + 1 \quad (\dot{\varepsilon} \geq 0) \tag{12-19}$$

$$\frac{T_{FP}}{T_{FP0}} = \frac{R + 1}{\left\{1 + \beta\left[-(R + 1)\right)^{(i-1)}(\cos \omega t - 1)\right\}^{1/(i-1)}} - 1 \quad (\dot{\varepsilon} \leq 0) \tag{12-20}$$

For the cosinusoidal input of Eq. (12-3), let the output torque be represented by the fundamental components of its Fourier series; i.e.,

$$T_{FP} = A_1 \sin \omega t + B_1 \cos \omega t \tag{12-21}$$

where

$$A_1 = \frac{1}{\pi}\int_0^{2\pi} T_{FP} \sin \omega t \, d\omega t \tag{12-22}$$

and

$$B_1 = \frac{1}{\pi}\int_0^{2\pi} T_{FP} \cos \omega t \, d\omega t \tag{12-23}$$

Substitution of Eqs. (12-19) and (12-20) into Eq. (12-22), we get

$$A_1 = \frac{T_{FP0}}{\pi}\int_0^{\pi}\left[\frac{R + 1}{\left\{1 + \beta\left[-(R + 1)\right)^{(i-1)}(\cos \omega t - 1)\right\}^{1/(i-1)}} - 1\right]\sin \omega t \, d\omega t$$

$$+ \frac{T_{FPO}}{\pi} \int_{\pi}^{2\pi} \left[\frac{R - 1}{\left(1 - \beta(R - 1)^{(i-1)} (\cos \omega t - 1)\right)^{1/(i-1)}} + 1 \right] \sin \omega t \, d\omega t \quad (12\text{-}23)$$

The last equation is reduced to the following form:

$$A_1 = - \frac{4T_{FPO}}{\pi} + \frac{T_{FPO}(R + 1)}{\pi} \int_0^{\pi} \frac{\sin \omega t \, d\omega t}{\left\{1 + \beta\left(-(R + 1)\right)^{(i-1)} (\cos \omega t - 1)\right\}^{1/(i-1)}}$$

$$+ \frac{T_{FPO}(R - 1)}{\pi} \int_{\pi}^{2\pi} \frac{\sin \omega t \, d\omega t}{\left(1 + (R - 1)^{(i-1)} (\cos \omega t - 1)\right)^{1/(i-1)}} \quad (12\text{-}24)$$

Let

$$x = \beta(R - 1)^{(i-1)} \cos \omega t \quad (12\text{-}25)$$

and

$$y = \beta\left(-(r + 1)\right)^{(i-1)} \cos \omega t \quad (12\text{-}26)$$

Then

$$dx = -\beta(R - 1)^{(i-1)} \sin \omega t \, d\omega t \quad (12\text{-}27)$$

$$dy + \beta(R + 1)^{(i-1)} \sin \omega t \, d\omega t \quad (12\text{-}28)$$

Equation (12-24) is written

$$A_1 = - \frac{4T_{FPO}}{\pi} + \frac{T_{FPO}(R + 1)}{\pi\beta(R + 1)^{(i-1)}} \int_{-\beta(R+1)^{(i-1)}}^{\beta(R+1)^{(i-1)}} \frac{dy}{\left\{1 + \beta\left(-(R+1)\right)^{(i-1)} + y\right\}^{1/(i-1)}}$$

$$- \frac{T_{FPO}(R - 1)}{\pi\beta(R - 1)^{(i-1)}} \int_{-\beta(R-1)^{(i-1)}}^{\beta(R-1)^{(i-1)}} \frac{dx}{\left(1 - \beta(R-1)^{(i-1)} - x\right)^{1/(i-1)}} \quad (12\text{-}29)$$

Let

$$\hat{y} = 1 + \beta\left(-(r + 1)\right)^{(i-1)} + y \quad (12\text{-}30)$$

$$\hat{x} = 1 + \beta(R - 1)^{(i-1)} - \quad (12\text{-}31)$$

Then

$$d\hat{y} = dy \quad (12\text{-}32)$$

$$d\hat{x} = dx \quad (12\text{-}33)$$

Substitution of the last four equations into Eq. (12-29) yields

$$A_1 = - \frac{4T_{FPO}}{\pi} + \frac{T_{FPO}(R + 1)}{\pi\beta\left(-(R+1)\right)^{(i-1)}} \int_1^{1+2\beta(R+1)^{(i-1)}} \frac{d\hat{y}}{(\hat{y})^{1/(i-1)}}$$

$$+ \frac{T_{FPO}(R-1)}{\pi\beta(R-1)^{(i-1)}} \int_1^{1-2\beta(R-1)^{(i-1)}} \frac{d\xi}{(\xi)^{1/(i-1)}} \qquad (12\text{-}34)$$

The integrals on the right-hand side of the last equation are now carried out, and after simplification, the result is

$$A_1 = -\frac{4T_{FPO}}{\pi} + \frac{T_{FPO}(R+1)}{\pi\beta(R+1)^{(i-1)}}\left(\frac{\{1+2\beta(-(R+1))^{(i-1)}\}^{(i-2)/(i-1)} - 1}{(i-2)/(i-1)}\right)$$

$$+ \frac{T_{FPO}(R-1)}{\pi\beta(R-1)^{(i-1)}}\left(\frac{\{1-2((R-1))^{(i-1)}\}^{(i-2)/(i-1)} - 1}{(i-2)/(i-1)}\right) \qquad (12\text{-}35)$$

The Fourier coefficient B_1 is determined as follows:

$$B_1 = \frac{T_{FPO}}{\pi}\int_0^{\pi}\left(\frac{R+1}{\{1+(-\beta(R+1))^{(i-1)}(\cos\omega t - 1)\}^{1/(i-1)}} - 1\right)\cos\omega t\, d\omega t$$

$$+ \frac{T_{FPO}}{\pi}\int_{\pi}^{2\pi}\left(\frac{R-1}{\{1-\beta(R-1)^{(i-1)}(\cos\omega t - 1)\}^{1/(i-1)}} + 1\right)\cos\omega t\, d\omega t \qquad (12\text{-}36)$$

The last equation is simplified to

$$B_1 = \frac{T_{FPO}}{\pi}\left(\frac{(R+1)}{\beta(-(R+1))^{(i-1)}}\int_0^{\pi}\frac{\beta(-(R+1))^{(i-1)}\cos\omega t\, d\omega t}{\{1-\beta(-(R+1))^{(i-1)} + \beta(-(R+1))^{(i-1)}\cos\omega t\}^{1/(i-1)}}\right.$$

$$\left. + \frac{(R-1)}{\beta(R-1)^{(i-1)}}\int_{\pi}^{2\pi}\frac{\beta(R-1)^{(i-1)}\cos\omega t\, d\omega t}{\{1+\beta(R-1)^{(i-1)} - \beta(R-1)^{(i-1)}\cos\omega t\}^{1/(i-1)}}\right) \qquad (12\text{-}37)$$

Letting

$$x = \beta(-(R+1))^{(i-1)}\cos\omega t \qquad (12\text{-}38)$$

$$y = \beta(R-1)^{(i-1)}\cos\omega t \qquad (12\text{-}39)$$

$$dx = -\beta(-(R+1))^{(i-1)}\sin\omega t\, d\omega t \qquad (12\text{-}40)$$

$$dy = -\beta(R-1)^{(i-1)}\sin\omega t\, d\omega t \qquad (12\text{-}41)$$

Eq. (12-37) becomes

$$B_1 = \frac{T_{FPO}}{\pi}\left[\frac{-(R+1)}{\beta\left(-(R+1)\right)^{(i-1)}}\int_{x(0)}^{x(\pi)}\frac{\cot \omega t\, dx}{\left\{1-\beta\left(-(R+1)\right)^{(i-1)}+x\right\}^{1/(i-1)}}\right.$$

$$\left. - \frac{R-1}{\beta(R-1)^{(i-1)}}\int_{y(\pi)}^{y(2\pi)}\frac{\cot \omega t\, dy}{\left(1+\beta(R-1)^{(i-1)}-y\right)^{1/(i-1)}}\right] \qquad (12\text{-}42)$$

For the first integral in the last equation,

$$\cot \omega t = \frac{x}{\sqrt{\beta^2\left(-(R+1)\right)^{2(i-1)}-x^2}} \qquad (12\text{-}43)$$

and for the second integral,

$$\cot \omega t = \frac{y}{\sqrt{\beta^2(R-1)^{2(i-1)}-y^2}} \qquad (12\text{-}44)$$

Therefore,

$$B_1 = \frac{T_{FPO}}{\pi}\left[\frac{-(R+1)}{\beta\left(-(R+1)\right)^{(i-1)}}\int_{x(0)}^{x(\pi)}\frac{x\,dx}{\left\{\beta^2\left(-(R+1)\right)^{2(i-1)}-x^2\right\}^{1/2}\left\{1-\beta\left(-(R+1)\right)^{(i-1)}+x\right\}^{1/(i-1)}}\right.$$

$$\left. - \frac{(R-1)}{\beta(R-1)^{(i-1)}}\int_{y(\pi)}^{y(2\pi)}\frac{y\,dy}{\left(\beta^2(R-1)^{2(i-1)}-y^2\right)^{1/2}\left(1+\beta(R-1)^{(i-1)}-y\right)^{1/(i-1)}}\right] \qquad (12\text{-}45)$$

These integrals can be carried out only if the value of i is given ($i \neq 1$).

13. Digital Computer Simulation of the Continuous-Data Nonlinear IPS Control System With Dahl Model

The IPS control system with the nonlinear flex pivot torque modelled by the Dahl solid friction model is simulated on the digital computer for i = 1 and i = 2. The block diagram of the IPS system is shown in Fig. 8-2, and the nonlinearities are modelled by Fig. 8-1.

The main objective of the computer simulation is to verify the results on the sustained oscillation predicted by the describing function method.

Dahl Model i = 1

The computer program using the IBM 360 CSMP for i = 1 in the Dahl model is given in Table 13-1. The simulation runs were able to predict and verify the results obtained by the describing function methed of Chapter 9. The difficulty with the long response time of the IPS system still exists in this case. Generally, it would be very time consuming and expensive to wait for the transient to settle completely in a digital computer simulation. Figure 13-1 shows the response of $\varepsilon(t)$ over a one-hundred second time interval, with $\varepsilon(0) = 10^{-5}$, $\dot{\varepsilon}(0) = 0$, $K_I = 10^5$, $K_{WT} = 100$, $H_{WT} = 1$. For the Dahl model, i = 1, $T_{FPO} = 0.0088$ N-m, and $\gamma = 13429.75$. The parameters of the linear portion of the system are tabulated on page 4 in Chapterl. Figure 13-1 shows that the response is oscillatory with an increasing amplitude, and the period is 46 sec or 0.136 rad/sec. Since it would take a long time for the amplitude to settle to a final steady-state value, we selected another initial value $\varepsilon(0)$ and repeated the simulation. Figure 13-2 shows the response of $\varepsilon(t)$ with $\varepsilon(0) = 10^{-3}$ which is decreasing in amplitude as time increases. Therefore, the stable operating point should be at an amplitude between 10^{-3} and 10^{-5}, and the frequency of oscillation is 0.136 rad/sec. In general it would be very difficult to find the initial state which corresponds to the steady-state oscillation exactly. The results predicted by Fig. 9-2 are very close for the amplitude

TABLE 13-1

```
LABEL SIMULATION OF NONLINEAR RPS CONTROL SYSTEM
INIT
PARAM    K0=8.75, K1=6.54, K2=0.0012528, K3=0.0036846
PARAM    K4=0.80059, K5=10/98.49, K6=1.1661, K7=0.0000926
PARAM    KL=1.25
PARAM    KWT=100., IWT=1.
PARAM    GAMA=1.3429754, TFP0=0.0000E0
UNLON    E0=1.E-3, EDOT0=0.0
EDIT     II(1)=0
         A=0.70*GAMA*E0
PROCED   KK1=FK(A,EDOT0)
         SGNDOT=1.0
         IF(EDOT0.LT.0.)SGNEDT=-1.0
         KK1=-SGNDOT*(1.E0/SIN(A)-1.E0/TANH(A))
ENDPRO
         K46=K4*K6
         K47=K4*K7
         KLOOP=1.E0-K46
NOSORT
         ELAST(1)=E0
         K(1)=KK1
METHOD   RKSFX
SORT
DYNAM
PROCED   TWC=WIRE(IWT,KWT,E,EDOT)
         SGNEDT=1.D0
         IF(EDOT.LT.0.)SGNEDT=-1.D0
         TWC=SGNEDT*KWT*KWT*E
ENDPRO
PROCED   TFP=DAHL(TFP0,T,EDOT,GAMA,E0)
         IF(.TIME.GT.0.).AND.(.DEP.ER.1))GO TO 1
         GO TO 2
    1    II(1)=1
    2    SGNEDT=1.E0
         IF(EDOT.LT.0.)SGNEDT=-1.E0
         B=GAMA*(E-ELAST(1))*SGNEDT
         TFP=SGNEDT*(1.E0+F(1)-1.E0)*EXP(B))*TFP0
         IF(TFP.GT.TFP0)TFP=TFP0
         IF(TFP.LT.-TFP0)TFP=-TFP0
         IF(II(1).EQ.0)GO TO 3
         F(1)=TFP/TFP0*SGNEDT
         II(1)=0
         CLAST(1)=E
         GO TO 2
    3    TFP=3.E0*TFP
   10    FORMAT(' ',5(1PE13.6),1S)
ENDPRO
         EDOT=-K7*TC-K4*X1
         EDOT=INTGRL(EDOT0,EDOT)
         E=INTGRL(E0,EDOT)
         C1=K47*TC/KLOOP
         C2=K2*X2/KLOOP
         C3=K3*X3/KLOOP
         X1=C1-C2-C3
         X2=INTGRL(0.,X1)
         X3=INTGRL(0.,X2)
         X4=X2+EDOT
         X5=E+X3
         X6=INTGRL(0.,X5)
         TC=K1*X4+K0*X5+K1*X6+TFP+TWC
TERMIN
TIMER    FINTIM=100.,OUTDEL=1.E-3,OUTDEL=2.E0,PRTDEL=2.E0
PRTPLT   E(EDOT,EDOT,TC)
END
STOP
ENDJOB
```

SIMULATION OF NONLINEAR IPS CONTROL SYSTEM PAGE 1

	MINIMUM -5.0883E-05	VERSUS TIME	MAXIMUM 4.7952E-05			
TIME	E	1	1	EVDT	FPDT	IC
0.0	1.0000E-05	----------		0.0	-1.2511E-02	9.0045E-00
2.0000E 00	-3.9811E-05	-----+		-5.3056E-08	1.4059E-03	-1.1497E 00
4.0000E 00	-3.9141E-05	-----+		8.5923E-07	-4.0652E-05	3.0909E-02
6.0000E 00	-3.0808E-05	----------+		4.8671E-06	4.4257E-07	9.9480E-04
8.0000E 00	-2.0304E-05	----------+		5.5698E-06	2.8753E-07	6.1655E-04
1.0000E 01	-8.7507E-06	----------+		5.9142E-06	7.1514E-08	2.3693E-04
1.2000E 01	3.0821E-06	----------+		5.8496E-06	-1.3658E-07	-1.5440E-04
1.4000E 01	1.4376E-05	----------+		5.3797E-06	-3.3111E-07	-5.2929E-04
1.6000E 01	2.4338E-05	----------+		4.5396E-06	-5.3630E-07	-8.2779E-04
1.8000E 01	3.2299E-05	----------+		3.3920E-06	-6.6219E-07	-1.0862E-03
2.0000E 01	3.7725E-05	----------+		2.0195E-06	-7.3159E-07	-1.2646E-03
2.2000E 01	4.0270E-05	----------+		5.2732E-07	-7.6676E-07	-1.3323E-03
2.4000E 01	4.1091E-05	----------+		4.1408E-07	-3.3392E-04	2.3766E-01
2.6000E 01	4.1582E-05	----------+		-6.9258E-07	1.3065E-03	-9.3914E-01
2.8000E 01	3.9177E-05	----------+		-3.1176E-06	7.4651E-07	-2.1915E-03
3.0000E 01	2.7935E-05	----------+		-6.0190E-06	-3.4878E-07	-8.8793E-04
3.2000E 01	1.5340E-05	----------+		-6.4625E-06	1.2093E-07	-6.4743E-04
3.4000E 01	2.2232E-06	----------+		-6.5498E-06	8.3265E-08	-2.1338E-05
3.6000E 01	-1.0563E-05	----------+		-6.1653E-06	2.9663E-07	4.0436E-04
3.8000E 01	-2.2149E-05	----------+		-5.3693E-06	5.4208E-07	7.4673E-04
4.0000E 01	-3.1771E-05	----------+		-4.2156E-06	6.4674E-07	1.0948E-03
4.2000E 01	-3.8799E-05	----------+		-2.7901E-06	7.2140E-07	1.3409E-03
4.4000E 01	-4.2785E-05	----------+		-1.1932E-06	8.2608E-07	1.4210E-03
4.6000E 01	-4.3892E-05	----------+		-2.0433E-07	1.0068E-04	-7.0190E-02
4.8000E 01	-4.4638E-05	----------+		-8.1891E-07	9.8206E-04	-7.0250E-01
5.0000E 01	-4.4335E-05	----------+		2.7074E-07	-1.2983E-04	9.5101E-02
5.2000E 01	-3.4090E-05	----------+		6.0980E-06	4.6409E-07	1.0860E-03
5.4000E 01	-2.1126E-05	----------+		6.7824E-06	2.4197E-07	6.4778E-04
5.6000E 01	-7.2465E-06	----------+		7.0196E-06	-5.3465E-09	1.8895E-04
5.8000E 01	6.6376E-06	----------+		6.7863E-06	-2.3424E-07	-2.7847E-04
6.0000E 01	1.9583E-05	----------+		6.0954E-06	-4.5246E-07	-7.0477E-04
6.2000E 01	3.0721E-05	----------+		4.9949E-06	-6.5986E-07	-1.0500E-03
6.4000E 01	3.9313E-05	----------+		3.5646E-06	-7.7145E-07	-1.3418E-03
6.6000E 01	4.4800E-05	----------+		1.9101E-06	-8.2747E-07	-1.5268E-03
6.8000E 01	4.6849E-05	----------+		1.4790E-07	-9.0037E-07	-1.5392E-03
7.0000E 01	4.7672E-05	----------+		9.4910E-07	-6.0734E-04	4.3351E-01
7.2000E 01	4.7780E-05	----------+		-2.1533E-07	6.8983E-04	-4.9704E-01
7.4000E 01	4.0515E-05	----------+		-6.0526E-06	-5.5524E-07	-1.3139E-03
7.6000E 01	2.7427E-05	----------+		-6.9511E-06	-3.1833E-07	-8.7845E-04
7.8000E 01	1.2997E-05	----------+		-7.3944E-06	-8.6691E-08	-3.8052E-04
8.0000E 01	-1.8151E-06	----------+		-7.3355E-06	1.4275E-07	1.3161E-04
8.2000E 01	-1.6011E-05	----------+		-6.7699E-06	2.4974E-07	6.9714E-04
8.4000E 01	-2.8621E-05	----------+		-5.7709E-06	6.2073E-07	9.9448E-04
8.6000E 01	-3.8807E-05	----------+		-4.3731E-06	7.7556E-07	1.3294E-03
8.8000E 01	-4.5895E-05	----------+		-2.6917E-06	9.3149E-07	1.5163E-03
9.0000E 01	-4.9437E-05	----------+		-8.4867E-07	9.3800E-07	1.6441E-03
9.2000E 01	-5.0341E-05	----------+		-4.9937E-07	2.8640E-04	-2.0314E-01
9.4000E 01	-5.0866E-05	----------+		-1.0628E-07	1.4818E-03	-1.0608E 00
9.6000E 01	-4.6986E-05	----------+		5.8678E-06	9.1792E-07	1.3506E-03
9.8000E 01	-3.4042E-05	----------+		6.9901E-06	4.5654E-07	1.0808E-03
1.0000E 02	-1.9308E-05	----------+		7.6476E-06	2.1592E-07	5.7286E-04

*** CSMP/360 SIMULATION DATA ***

STOP

Figure 13-1. Time response of $\varepsilon(t)$ for $K_I = 10^5$, $K_{WT} = 100$, $H_{WT} = 1$, $\varepsilon(0) = 10^{-5}$, $i = 1$, $T_{FPO} = 0.0088$ N-m, $\gamma = 13429.75$.

SIMULATION OF NONLINEAR ITS CONTROL SYSTEM PAGE

MINIMUM -4.4622E-03 VERSUS TIME MAXIMUM 5.7457E-03

TIME	E		EDOT	EDOT	TC
0.0	1.0000E-03	----------+----------	0.0	-3.1147E 00	8.0113E-02
2.0000E 00	-3.8624E-03	----+	1.7167E-04	7.9631E-05	1.1324E-01
4.0000E 00	-3.3900E-03	-------+	3.0174E-04	6.0263E-05	1.0507E-01
6.0000E 00	-2.6750E-03	---------+	4.0864E-04	4.6701E-05	8.3946E-02
8.0000E 00	-1.7764E-03	------------+	4.8454E-04	2.9574E-05	5.3384E-02
1.0000E 01	-7.6091E-04	----------+	5.2444E-04	9.8418E-06	1.9824E-02
1.2000E 01	2.9584E-04	----------+	5.2580E-04	-9.1835E-06	-1.5555E-02
1.4000E 01	1.3163E-03	----------+	4.8883E-04	-2.7594E-05	-4.9094E-02
1.6000E 01	2.2271E-03	----------+	4.1671E-04	-4.3577E-05	-7.8718E-02
1.8000E 01	2.9631E-03	----------+	3.1517E-04	-5.6449E-05	-1.0203E-01
2.0000E 01	3.4739E-03	----------+	1.9206E-04	-6.5405E-05	-1.1731E-01
2.2000E 01	3.7226E-03	----------+	5.6585E-05	-6.9405E-05	-1.2387E-01
2.4000E 01	3.7089E-03	----------+	-8.2861E-05	-7.0723E-05	-1.1998E-01
2.6000E 01	3.4106E-03	----------+	-2.1305E-04	-6.1490E-05	-1.1072E-01
2.8000E 01	2.8678E-03	----------+	-3.2593E-04	-5.0967E-05	-9.1311E-02
3.0000E 01	2.1234E-03	----------+	-4.1357E-04	-3.6136E-05	-6.6030E-02
3.2000E 01	1.2340E-03	----------+	-4.6994E-04	-1.9643E-05	-3.5713E-02
3.4000E 01	2.6662E-04	----------+	-4.9120E-04	-2.0981E-06	-3.0797E-03
3.6000E 01	-7.0708E-04	----------+	-4.7660E-04	1.6082E-05	2.8825E-02
3.8000E 01	-1.6164E-03	----------+	-4.2738E-04	3.2732E-05	5.8291E-02
4.0000E 01	-2.3950E-03	----------+	-3.4741E-04	4.6067E-05	8.3615E-02
4.2000E 01	-2.9895E-03	----------+	-2.4335E-04	5.6491E-05	1.0203E-01
4.4000E 01	-3.3577E-03	----------+	-1.2303E-04	6.2726E-05	1.1276E-01
4.6000E 01	-3.4765E-03	----------+	-2.5560E-07	1.9646E-04	2.0366E-02
4.8000E 01	-3.3498E-03	----------+	1.3225E-04	6.0850E-05	1.0961E-01
5.0000E 01	-2.9679E-03	----------+	2.4690E-04	5.2867E-05	9.5820E-02
5.2000E 01	-2.3749E-03	----------+	3.4199E-04	4.1822E-05	7.4742E-02
5.4000E 01	-1.6169E-03	----------+	4.1098E-04	2.7155E-05	4.9012E-02
5.6000E 01	-7.5124E-04	----------+	4.4912E-04	1.1569E-05	1.9428E-02
5.8000E 01	1.5759E-04	----------+	4.5410E-04	-5.8268E-06	-1.0334E-02
6.0000E 01	1.0427E-03	----------+	4.2587E-04	-2.2154E-05	-3.9244E-02
6.2000E 01	1.8400E-03	----------+	3.6694E-04	-3.6295E-05	-6.5162E-02
6.4000E 01	2.4926E-03	----------+	2.8202E-04	-4.8042E-05	-8.5670E-02
6.6000E 01	2.9547E-03	----------+	1.7772E-04	-5.5777E-05	-9.9912E-02
6.8000E 01	3.1953E-03	----------+	6.1869E-05	-5.9586E-05	-1.0651E-01
7.0000E 01	3.2117E-03	----------+	-5.9749E-05	-5.8082E-05	-1.0497E-01
7.2000E 01	2.9792E-03	----------+	-1.7194E-04	-5.3752E-05	-9.6886E-02
7.4000E 01	2.5329E-03	----------+	-2.7110E-04	-4.4150E-05	-8.1323E-02
7.6000E 01	1.9081E-03	----------+	-3.4933E-04	-3.2962E-05	-5.9327E-02
7.8000E 01	1.1528E-03	----------+	-4.0103E-04	-1.8101E-05	-3.4133E-02
8.0000E 01	3.2362E-04	----------+	-4.2279E-04	-3.9973E-06	-5.4374E-03
8.2000E 01	-5.1791E-04	----------+	-4.1361E-04	1.2052E-05	2.1947E-02
8.4000E 01	-1.3104E-03	----------+	-3.7431E-04	2.6490E-05	4.7734E-02
8.6000E 01	-1.9968E-03	----------+	-3.0827E-04	3.9157E-05	6.9454E-02
8.8000E 01	-2.5285E-03	----------+	-2.2062E-04	4.8220E-05	8.6247E-02
9.0000E 01	-2.8689E-03	----------+	-1.1809E-04	5.3356E-05	9.6724E-02
9.2000E 01	-2.9956E-03	----------+	-8.2654E-06	5.5307E-05	9.9468E-02
9.4000E 01	-2.9127E-03	----------+	1.0245E-04	5.2428E-05	9.5836E-02
9.6000E 01	-2.6053E-03	----------+	2.0264E-04	4.6838E-05	8.4017E-02
9.8000E 01	-2.1122E-03	----------+	2.8684E-04	3.7078E-05	6.6827E-02
1.0000E 02	-1.4721E-03	----------+	3.4903E-04	2.5437E-05	4.4501E-02

*** CSMP/360 SIMULATION DATA ***

STOP

Figure 13-2. Time response of $\varepsilon(t)$ for $K_I = 10^5$, $K_{WT} = 100$, $H_{WT} = 1$, $\varepsilon(0) = 10^{-3}$, $i = 1$, $T_{FPO} = 0.0088$ N-m, $\gamma = 13429.75$.

and $\omega = 0.138$ rad/sec.

Dahl Model i = 2

Table 13-2 gives the computer simulation program for the i = 2 case, with $T_{FP0} = 0.00225$ N-m and $\gamma = 92444$. All other system parameters are the same as the i = 1 case. Figure 13-3 shows a stable response when the initial state $\varepsilon(0)$ is small, 10^{-10}. As shown in Fig. 11-2, when the initial state is small the stable equilibrium point is $\varepsilon = 0$. Figure 13-4 shows another stable response which would take longer time to die out, when $\varepsilon(0) = 10^{-8}$. Figures 13-5 and 13-6 show a sustained oscillation solution with aplitude lying between 10^{-7} and 7×10^{-7}, and a period of 44 sec or 14.28 rad/sec. These results are again very close to those predicted in Fig. 11-2. The simulations for the i = 2 case are carried out with $K_{WT} = 0.25$, $H_{WT} = 0.1$, and $K_I = 10^6$.

TABLE 13-2.

```
01100    LABEL  SIMULATION OF NONLINEAR TPS CONTROL SYSTEM
01200    INIT
01300    PARAM    K0=3.E5, K1=6.E4, K2=0.0012578, K3=0.0036846
01400    PARAM    K4=0.80059, K5=10798.49, K6=1.1661, K7=0.0000926
01500    PARAM    K1=1.16
01600    PARAM    KWT=.25, HWT=.1
01700    PARAM    GAMA=9.2444E4, TFP0=0.0022500
01800    INCON    E0=1.E-7, EDOT0=0.0
01900    TABLE    JJ(I)=0
01950             GI=GAMA*TFP0
02000             A=2.E0*GAMA*E0*TFP0
02100    PROCED   RRT=SQRT(A+EDOT0)
02200             JJ(1)=1.E0
02300             IF(EDOT0.LT.0.)SGNEDT=-1.E0
02350             AI=1.E0/A
02400             RRL=-SGNEDT*(-AI+SQRT(AI**2+1.E0))
02500    ENDPRO
02600             K46=K4*K6
02700             K47=K4*K7
02800             HLOOP=1.E0-K46
02900    NOSORT
03000             FLAST(J)=E0
03100             R(J)=RRT
03150             G(J)=GI
03200    METHOD   RKGFX
03300    SORT
03400    DYNAM
03500    PROCED   TWC=WIRE(HWT,KWT,E,EDOT)
03600             SGNEDT=1.E0
03700             IF(EDOT.LT.0.)SGNEDT=-1.E0
03800             TWC=SGNEDT*HWT+KWT*E
03900    ENDPRO
04000    PROCED   TFP=QAHL(TFP0,E,EDOT,GAMA,E0)
04100             IF(TIME.GT.0.).AND.(KFLOP.EQ.1))GO TO 1
04200             GO TO 2
04300         1   JJ(J)=1
04400             SGNEDT=1.E0
04500             IF(EDOT.LT.0.)SGNEDT=-1.E0
04700             RI=R(J)-SGNEDT
04800             TFP=(SGNEDT+R(J)/(1.E0-G(J)*(E-FLAST(J))*RI))*TFP0
04810             IF(TFP.GT.TFP0)TFP=TFP0
04820             IF(TFP.LT.-TFP0)TFP=-TFP0
04900             IF(JJ(J).EQ.0)GO TO 3
05000             R(J)=TFP/TFP0
05100             JJ(J)=0
05200             FLAST(J)=E
05300             GO TO 2
05400         3   WRITE(6,10)TFP
05500    10       FORMAT(' ',5(1PE13.6),15)
05600    ENDPRO
05700             FLOOP=K7*TC-K6*X1
05800             EDOT=INTGRL(EDOT0,FLOOP)
05900             E=INTGRL(0.,EDOT)
06000             FLOOP=K7*TC/HLOOP
06100             X1=FLOOP*X2/HLOOP
06200             X2=FLOOP*X3/HLOOP
06300             X3=C4*C2-C3
06400             X2=INTGRL(0.,X1)
06500             X3=INTGRL(0.,X2)
06600             X4=X2*EDOT
06700             X5=E+X4
06800             X6=INTGRL(0.,X5)
06900             TC=K1*X4+K0*X6+K7*X4+TFP+TWC
07000    TERMIN
07010    TIMER    FINTIM=100.,DELT=1.E-3,OUTDEL=2.E0,PRDEL=2.E0
07100    PRTPLT   E,EDOT,EDDOT,TC)
07110    END
07400    STOP
07500    ENDJOB
07600
*E
```

SIMULATION OF NONLINEAR IFS CONTROL SYSTEM PAGE 1

MINIMUM E VERSUS TIME MAXIMUM
-9.7624E-10 4.2560E-09

TIME	E	1	1	CIN01	CIN01	IC
0.0	1.0000E-10	|+	0.0	0.0	-1.3978E-04	1.0028E-01
2.0000E 00	-7.8951E-10	|	2.3502E-08	-1.3978E-04	1.0028E-01	
4.0000E 00	-8.3114E-11	|	2.3735E-08	-1.3978E-04	1.0028E-01	
6.0000E 00	2.7300E-10	\+	2.3601E-08	-1.3978E-04	1.0028E-01	
8.0000E 00	9.4874E-10	|	2.3806E-08	-1.3978E-04	1.0028E-01	
1.0000E 01	1.7078E-09	|	2.3766E-08	-1.3978E-04	1.0028E-01	
1.2000E 01	2.2638E-09	|	2.3695E-08	-1.3978E-04	1.0028E-01	
1.4000E 01	2.8109E-09	\+	2.3664E-08	-1.3978E-04	1.0028E-01	
1.6000E 01	3.1690E-09	|	2.3544E-08	-1.3978E-04	1.0028E-01	
1.8000E 01	3.4069E-09	|	2.3545E-08	-1.3978E-04	1.0028E-01	
2.0000E 01	3.6626E-09	\+	2.3563E-08	-1.3978E-04	1.0028E-01	
2.2000E 01	3.9457E-09	\+	2.3573E-08	-1.3978E-04	1.0028E-01	
2.4000E 01	4.1811E-09	|	2.3514E-08	-1.3978E-04	1.0028E-01	
2.6000E 01	4.2519E-09	\+	2.3406E-08	-1.3978E-04	1.0028E-01	
2.8000E 01	4.1319E-09	|	2.3343E-08	-1.3978E-04	1.0028E-01	
3.0000E 01	4.0270E-09	\+	2.3386E-08	-1.3978E-04	1.0028E-01	
3.2000E 01	3.9545E-09	|	2.3406E-08	-1.3978E-04	1.0028E-01	
3.4000E 01	3.9269E-09	|	2.3398E-08	-1.3978E-04	1.0028E-01	
3.6000E 01	3.8287E-09	\+	2.3361E-08	-1.3978E-04	1.0028E-01	
3.8000E 01	3.6559E-09	\+	2.3329E-08	-1.3978E-04	1.0028E-01	
4.0000E 01	3.4792E-09	|	2.3346E-08	-1.3978E-04	1.0028E-01	
4.2000E 01	3.3330E-09	\+	2.3385E-08	-1.3978E-04	1.0028E-01	
4.4000E 01	3.1909E-09	\+	2.3395E-08	-1.3978E-04	1.0028E-01	
4.6000E 01	2.9941E-09	|	2.3279E-08	-1.3978E-04	1.0028E-01	
4.8000E 01	2.6581E-09	|	2.3240E-08	-1.3978E-04	1.0028E-01	
5.0000E 01	2.3587E-09	\+	2.3290E-08	-1.3978E-04	1.0028E-01	
5.2000E 01	2.1089E-09	|	2.3307E-08	-1.3978E-04	1.0028E-01	
5.4000E 01	1.9548E-09	\+	2.3431E-08	-1.3978E-04	1.0028E-01	
5.6000E 01	2.1248E-09	|	2.3567E-08	-1.3978E-04	1.0028E-01	
5.8000E 01	2.4753E-09	|	2.3619E-08	-1.3978E-04	1.0028E-01	
6.0000E 01	2.8252E-09	\+	2.3567E-08	-1.3978E-04	1.0028E-01	
6.2000E 01	3.0004E-09	\+	2.3453E-08	-1.3978E-04	1.0028E-01	
6.4000E 01	2.9414E-09	\+	2.3342E-08	-1.3978E-04	1.0028E-01	
6.6000E 01	2.7356E-09	|	2.3327E-08	-1.3978E-04	1.0028E-01	
6.8000E 01	2.5573E-09	|	2.3351E-08	-1.3978E-04	1.0028E-01	
7.0000E 01	2.4438E-09	\+	2.3387E-08	-1.3978E-04	1.0028E-01	
7.2000E 01	2.4009E-09	|	2.3432E-08	-1.3978E-04	1.0028E-01	
7.4000E 01	2.4287E-09	|	2.3457E-08	-1.3978E-04	1.0028E-01	
7.6000E 01	2.5273E-09	\+	2.3493E-08	-1.3978E-04	1.0028E-01	
7.8000E 01	2.6885E-09	\+	2.3501E-08	-1.3978E-04	1.0028E-01	
8.0000E 01	2.7812E-09	|	2.3444E-08	-1.3978E-04	1.0028E-01	
8.2000E 01	2.7737E-09	|	2.3415E-08	-1.3978E-04	1.0028E-01	
8.4000E 01	2.7511E-09	|	2.3415E-08	-1.3978E-04	1.0028E-01	
8.6000E 01	2.7284E-09	|	2.3415E-08	-1.3978E-04	1.0028E-01	
8.8000E 01	2.7098E-09	|	2.3415E-08	-1.3978E-04	1.0028E-01	
9.0000E 01	2.6831E-09	|	2.3415E-08	-1.3978E-04	1.0028E-01	
9.2000E 01	2.6605E-09	|	2.3415E-08	-1.3978E-04	1.0028E-01	
9.4000E 01	2.6379E-09	|	2.3416E-08	-1.3978E-04	1.0028E-01	
9.6000E 01	2.6322E-09	|	2.3430E-08	-1.3978E-04	1.0028E-01	
9.8000E 01	2.6378E-09	|	2.3416E-08	-1.3978E-04	1.0028E-01	
1.0000E 02	2.6326E-09	|	2.3430E-08	-1.3978E-04	1.0028E-01	

*** CSMP/360 SIMULATION DATA ***

STOP

Figure 13-3. Stable time response of $\varepsilon(t)$ for $K_I = 10^6$, $K_{WT} = 0.25$, $H_{WT} = 0.1$, $\varepsilon(0) = 10^{-10}$, $i = 2$.

SIMULATION OF NONLINEAR IPS CONTROL SYSTEM

MINIMUM -7.3586E-08   E VERSUS TIME   MAXIMUM 3.8577E-08

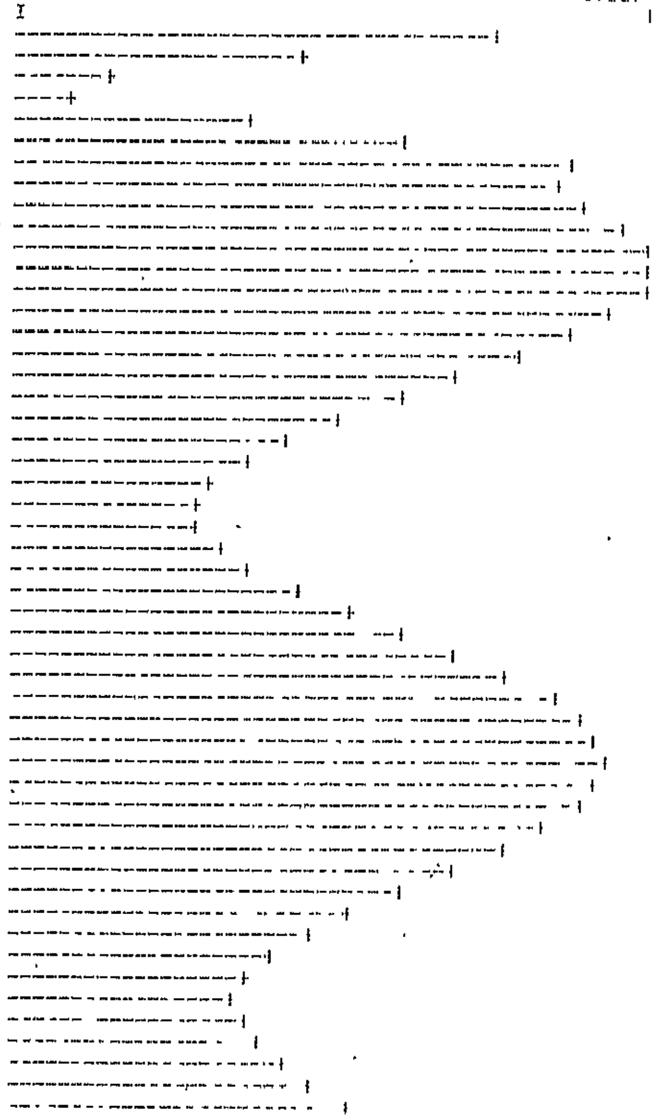

TIME	E	EDOT	EDDOT	TC
0.0	1.0000E-08	0.0	-1.5054E-04	1.0800E-01
2.0000E 00	-2.2653E-08	-8.2574E-09	1.1673E-04	-8.3744E-02
4.0000E 00	-5.6443E-08	-2.5205E-08	1.2598E-04	-9.0379E-02
6.0000E 00	-6.2417E-08	8.1181E-09	-1.3240E-04	9.49[illegible]E-02
8.0000E 00	-3.2854E-08	6.5069E-08	-1.2479E-04	8.9529E-02
1.0000E 01	-5.4728E-09	6.6863E-08	-1.2547E-04	9.0013E-02
1.2000E 01	2.3893E-08	4.9844E-08	-1.3443E-04	9.6442E-02
1.4000E 01	2.1370E-08	-2.4652E-08	1.3979E-04	-1.0029E-01
1.6000E 01	2.6300E-08	-1.9721E-08	1.3978E-04	-1.0028E-01
1.8000E 01	3.3051E-08	-2.0580E-08	1.3978E-04	-1.0028E-01
2.0000E 01	3.7378E-08	-2.2046E-08	1.3978E-04	-1.0028E-01
2.2000E 01	3.8538E-08	-2.3678E-08	1.3978E-04	-1.0028E-01
2.4000E 01	3.6487E-08	-2.5195E-08	1.3978E-04	-1.0028E-01
2.6000E 01	3.1598E-08	-2.6603E-08	1.3978E-04	-1.0028E-01
2.8000E 01	2.4318E-08	-2.7583E-08	1.3978E-04	-1.0028E-01
3.0000E 01	1.5165E-08	-2.8379E-08	1.3978E-04	-1.0028E-01
3.2000E 01	4.7649E-09	-2.8707E-08	1.3978E-04	-1.0028E-01
3.4000E 01	-5.9788E-09	-2.8764E-08	1.3978E-04	-1.0028E-01
3.6000E 01	-1.6321E-08	-2.8373E-08	1.3978E-04	1.0028E-01
3.8000E 01	-2.5585E-08	2.7681E-08	1.3978E-04	-1.0028E-01
4.0000E 01	-3.3067E-08	-2.6612E-08	1.3978E-04	-1.0028E-01
4.2000E 01	-3.8215E-08	-2.5369E-08	1.3978E-04	-1.0028E-01
4.4000E 01	-4.0693E-08	-2.3948E-08	1.3978E-04	-1.0028E-01
4.6000E 01	-4.0272E-08	-2.2504E-08	1.3978E-04	-1.0028E-01
4.8000E 01	-3.7091E-08	-2.1192E-08	1.3978E-04	-1.0028E-01
5.0000E 01	-3.1442E-08	-2.0046E-08	1.3978E-04	-1.0028E-01
5.2000E 01	-2.3830E-08	-1.9246E-08	1.3978E-04	-1.0028E-01
5.4000E 01	-1.4923E-08	-1.8730E-08	1.3978E-04	-1.0028E-01
5.6000E 01	-5.3139E-09	-1.8570E-08	1.3978E-04	-1.0028E-01
5.8000E 01	4.2975E-09	-1.8741E-08	1.3978E-04	-1.0028E-01
6.0000E 01	1.3182E-08	-1.9273E-08	1.3978E-04	-1.0028E-01
6.2000E 01	2.0655E-08	-2.0138E-08	1.3978E-04	-1.0028E-01
6.4000E 01	2.6234E-08	-2.1174E-08	1.3978E-04	-1.0028E-01
6.6000E 01	2.9563E-08	2.2358E-08	1.3978E-04	-1.0028E-01
6.8000E 01	3.0461E-08	-2.3724E-08	1.3978E-04	-1.0028E-01
7.0000E 01	2.8915E-08	-2.4773E-08	1.3978E-04	-1.0028E-01
7.2000E 01	2.5128E-08	-2.5842E-08	1.3978E-04	-1.0028E-01
7.4000E 01	1.9377E-08	-2.6[illegible]E-08	1.3978E-04	-1.0028E-01
7.6000E 01	1.2023E-08	-2.[illegible]E-08	1.3978E-04	-1.0028E-01
7.8000E 01	3.6389E-09	-2.7738E-08	1.3978E-04	-1.0028E-01
8.0000E 01	-4.9831E-09	-2.7714E-08	1.3978E-04	-1.0028E-01
8.2000E 01	-1.3304E-08	-2.7397E-08	1.3978E-04	-1.0028E-01
8.4000E 01	-2.0745E-08	-2.6869E-08	1.3978E-04	-1.0028E-01
8.6000E 01	-2.6868E-08	-2.6070E-08	1.3978E-04	-1.0028E-01
8.8000E 01	-3.1145E-08	-2.5021E-08	1.3978E-04	-1.0028E-01
9.0000E 01	-3.3246E-08	-2.3926E-08	1.3978E-04	-1.0028E-01
9.2000E 01	-3.3069E-08	-2.2770E-08	1.3978E-04	-1.0028E-01
9.4000E 01	-3.0646E-08	-2.1477E-08	1.3978E-04	-1.0028E-01
9.6000E 01	-2.6245E-08	-2.0814E-08	1.3978E-04	-1.0028E-01
9.8000E 01	-2.0389E-08	-2.0263E-08	1.3978E-04	-1.0028E-01
1.0000E 02	-1.3478E-08	-1.9764E-08	1.3978E-04	-1.0028E-01

Figure 13-4. Stable response of $\epsilon(t)$ for $i = 2$. $\epsilon(0) = 10^{-8}$.

MINIMUM E VERSUS TIME MAXIMUM
-6.4579E-07 6.2929E-07

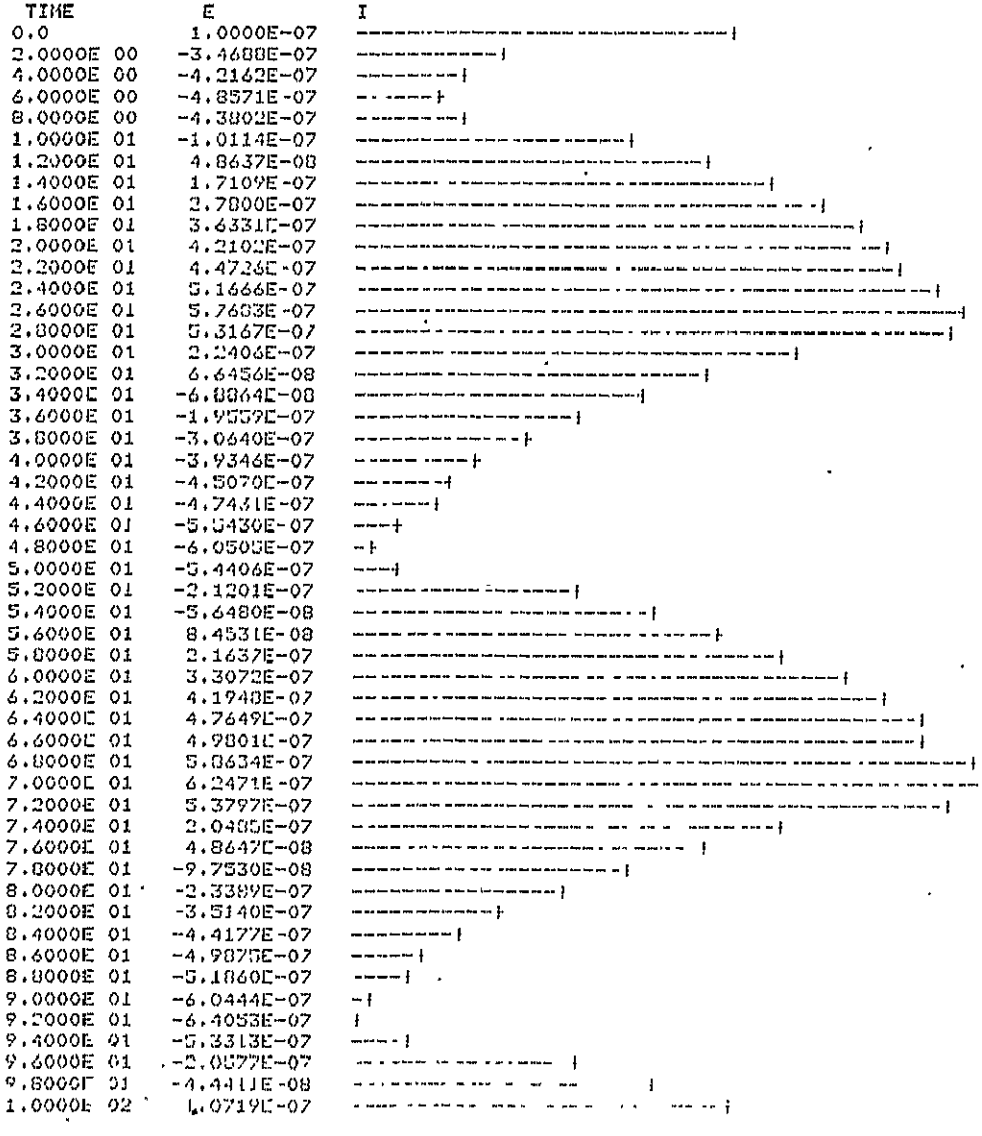

TIME	E	I	EDOT	EDDOT	TC
0.0	1.0000E-07		0.0	-2.5090E-04	1.6000E-01
2.0000E 00	-3.4688E-07		5.3992E-08	9.5392E-08	-5.1260E-05
4.0000E 00	-4.2162E-07		-7.3974E-08	2.5539E-05	-1.8303E-02
6.0000E 00	-4.8571E-07		-1.2232E-08	1.2573E-04	-9.0178E-02
8.0000E 00	-4.3802E-07		1.3923E-03	-1.916?E-05	1.37?6E-02
1.0000E 01	-1.0114E-07		9.7478E-08	4.6322E-08	3.?478E-05
1.2000E 01	4.8637E-08		6.4789E-08	-6.7524E-07	-5.9?05E-07
1.4000E 01	1.7109E-07		5.7641E-08	-3.3634E-09	-6.?37?E-06
1.6000E 01	2.7800E-07		4.8641E-08	-5.4283E-09	-9.7?32E-06
1.8000E 01	3.6331E-07		3.4163E-08	-7.0989E-09	-1.2368E-05
2.0000E 01	4.2102E-07		2.1234E-08	-7.8437E-09	-1.42?6E-05
2.2000E 01	4.4726E-07		1.9291E-09	-8.2681E-09	-1.4901E-05
2.4000E 01	5.1666E-07		2.2465E-08	-6.1985E-05	2.2923E-02
2.6000E 01	5.7603E-07		3.1173E-08	-1.2823E-04	9.1967E-02
2.8000E 01	5.3167E-07		-1.1723E-07	2.9258E-05	-2.1011E-02
3.0000E 01	2.2406E-07		-1.0262E-07	5.1606E-08	-4.?657E-05
3.2000E 01	6.6456E-08		-6.9398E-08	2.1443E-09	-3.5167E-06
3.4000E 01	-6.8864E-08		-6.5876E-08	2.7468E-09	2.2650E-06
3.6000E 01	-1.9559E-07		-6.020?E 08	4.7547E-09	6.61?1E-06
3.8000E 01	-3.0640E-07		-5.0080E-08	6.0500E-09	1.0??9E-05
4.0000E 01	-3.9346E-07		-3.6510E-08	7.4774E-09	1.3471E-05
4.2000E 01	-4.5070E-07		-2.0452E-08	8.4978E-09	1.5140E-05
4.4000E 01	-4.7431E-07		-8.1057 09	8.8147E-09	1.5 3?E-05
4.6000E 01	-5.0439E-07		-4.5453E-08	4.1952E-05	-3.0072E-02
4.8000E 01	-6.0505E-07		3.6446E 08	-1.3419E-04	9.62?8E-02
5.0000E 01	-5.4406E-07		2.3764E 08	-7.?536E-06	5.5854E-03
5.2000E 01	-2.1201E-07		9.2754E 08	-3.2992E-08	3.1948E-05
5.4000E 01	-5.6480E-08		7.1935E-08	-2.2594E-09	3.09?1E-06
5.6000E 01	8.4531E-08		6.8789E-08	-1.9984E-09	-3.5763E-06
5.8000E 01	2.1637E-07		6.2305E-08	-4.3180E-09	-7.9274E-06
6.0000E 01	3.3072E-07		5.1382E-08	-6.3223E-09	-1.1623E-05
6.2000E 01	4.1940E-07		3.6837E-08	-7.9221E-09	-1.43?5E-05
6.4000E 01	4.7649E-07		1.9?9?E-08	-8.8259E-09	-1.6095E-05
6.6000E 01	4.9801E-07		1.6089E 09	-9.2347E-09	-1.6510E-05
6.8000E 01	5.8634E-07		5.3828E-08	-5.1021E-05	3.6577E-02
7.0000E 01	6.2471E-07		-6.?187E-10	1.1860E-04	-8.5?14E-02
7.2000E 01	5.3797E-07		-3.?647E-07	-1.3782E-06	9.7007E-04
7.4000E 01	2.0405E-07		-8.?830E-08	2.1041E-08	-2.3723E-05
7.6000E 01	4.8647E-08		?.4397E-08	1.4875E-09	-2.14?8E-06
7.8000E 01	-9.7530E-08		?.1329E-08	2.2303E-09	4.0531E-06
8.0000E 01	-2.3389E-07		-6.4?5?E-08	4.7462E-09	8.465?E-06
8.2000E 01	-3.5140E-07		5.?718E-08	7.1071E-09	1.2040E-05
8.4000E 01	-4.4177E-07		6.?281E-08	8.?913E-09	1.47?2E-05
8.6000E 01	-4.9875E-07		1.9430E-08	9.2590E-09	1.6807E-05
8.8000E 01	-5.1860E-07		?.911?E-10	9.6258E-09	1.7166E-05
9.0000E 01	-6.0444E-07		-?.8838E-09	5.0834E-05	-3.6442E-02
9.2000E 01	-6.4053E-07		-8.8?4?E 08	1.6222E-04	-1.1?35E-01
9.4000E 01	-5.3313E-07		?.?14E 07	-6.8130E-07	-2.5?08E-04
9.6000E 01	-2.0577E-07		8.9 ?E-08	-2.?241E-08	2.2?90E-05
9.8000E 01	-4.4411E-08		?.?19? 08	6.8950E-10	1.3113E-06
1.0000E 02	4.0719E-07		?.1?3? -08	-2.495?E-09	-4.3511E-06

*** CSMP/360 SIMULATION DATA ***

STOP

Figure 13-5. Time response of $\varepsilon(t)$ for $i = 2$, $\varepsilon(0) = 10^{-7}$.

SIMULATION OF NONLINEAR IPS CONTROL SYSTEM PAGE 1

MINIMUM E VERSUS TIME MAXIMUM
-2.9943E-06 2.7295E-06

TIME	E	J	L	PHOT	EDOT	IC
0.0	7.0001E-07	|		0.0	-9.1997E-04	6.6000E-01
2.0000E 00	-2.9731E-06	+		4.4774E-08	-5.8776E-05	4.2301E-0?
4.0000E 00	-2.3857E-06	-----+		2.0298E-07	-5.2538E-08	1.4359E-04
6.0000E 00	-1.8349E-06	----------+		2.9564E-07	2.6744E-08	6.1095E-05
8.0000E 00	-1.1829E-06	----------+		3.4332E-07	1.9276E-08	3.5644E-05
1.0000E 01	-4.6596E-07	----------+		3.6916E-07	4.4850E-09	1.2577E-05
1.2000E 01	2.7550E-07	----------|		3.6775E-07	-7.7973E-09	-1.2994E-05
1.4000E 01	9.8738E-07	----------|		3.3971E-07	-2.0238E-08	-3.6657E-05
1.6000E 01	1.6174E-06	----------|		2.8729E-07	-3.2165E-08	-5.6505E-05
1.8000E 01	2.1213E-06	----------|		2.1478E-07	-4.1229E-08	-7.2241E-05
2.0000E 01	2.4641E-06	----------|		1.2704E-07	-4.6595E-08	-8.2210E-05
2.2000E 01	2.6226E-06	----------|		3.1480E-08	-4.8680E-08	-8.7261E-05
2.4000E 01	2.6984E-06	----------|		6.9210E-08	-4.3588E-05	3.2581E-02
2.6000E 01	2.7106E-06	----------|		-9.9930E-08	5.1131E-05	-3.6803E-02
2.8000E 01	1.9846E-06	----------|		-3.1399E-07	5.8339E-08	-1.2875E-04
3.0000E 01	1.3819E-06	----------|		-3.0976E-07	-1.7821E-08	-4.4432E-05
3.2000E 01	7.2844E-07	----------|		-2.4903E-07	-1.1356E-08	2.0266E-05
3.4000E 01	3.3217E-08	----------|		-1.5049E-07	-4.8961E-10	1.0958E-06
3.6000E 01	-6.5548E-07	----------|		-6.3463E-07	1.5438E-08	2.4617E-05
3.8000E 01	-1.2871E-06	----------|		-9.9403E-07	2.5328E-08	4.6194E-05
4.0000E 01	-1.8165E-06	----------|		-9.3815E-07	3.4875E-08	6.2227E-05
4.2000E 01	-2.2064E-06	----------|		-1.5558E-07	4.1693E-08	7.4923E-05
4.4000E 01	-2.4304E-06	----------|		-6.7979E-08	4.5364E-08	8.1361E-05
4.6000E 01	-2.5043E-06	----------|		-5.6698E-08	4.5926E-08	8.2615E-05
4.8000E 01	-2.5751E-06	----------|		-4.7209E-08	1.2841E-04	-9.2008E-02
5.0000E 01	-2.1787E-06	----------|		4.4975E-07	-2.4233E-07	2.6710E-04
5.2000E 01	-1.5410E-06	----------|		2.8178E-07	-1.5935E-08	6.8009E-05
5.4000E 01	-9.4821E-07	----------|		3.1147E-07	1.7166E-08	2.4762E-05
5.6000E 01	-3.0338E-07	----------|		3.2957E-07	2.5664E-09	7.0734E-06
5.8000E 01	3.5476E-07	----------|		3.2457E-07	-8.7294E-09	-1.5318E-05
6.0000E 01	9.7860E-07	----------|		2.9559E-07	-2.0113E-08	-3.5644E-05
6.2000E 01	1.5223E-04	----------|		2.4571E-07	-2.6844E-08	-5.0354E-05
6.4000E 01	1.9479E-06	----------|		1.7841E-07	-3.1810E-08	-6.1602E-05
6.6000E 01	2.2259E-06	----------|		9.8969E-08	-3.4711E-08	-7.0381E-05
6.8000E 01	2.3379E-06	----------|		1.3375E-08	4.3248E-08	-7.7665E-05
7.0000E 01	2.4155E-06	----------|		5.0225E-08	-6.1613E-05	4.4098E-02
7.2000E 01	2.4106E-06	----------|		1.8304E-08	2.2882E-05	-1.6417E-02
7.4000E 01	1.6769E-06	----------|		-1.8534E-07	4.0441E-08	-1.0224E-04
7.6000E 01	1.1283E-06	----------|		-1.8229E-07	-9.3500E-09	-4.1909E-05
7.8000E 01	5.3594E-07	----------|		-1.0307E-07	-1.0951E-08	-1.4246E-05
8.0000E 01	-8.5841E-08	----------|		5.1192E-07	2.8444E-08	6.8543E-04
8.2000E 01	-6.9335E-07	----------|		-1.9274E-07	1.0934E-08	2.5332E-05
8.4000E 01	-1.2421E-06	----------|		-1.0431E-07	5.4584E-09	1.4048E-05
8.6000E 01	-1.6928E-06	----------|		-1.6728E-08	5.2185E-09	2.3113E-05
8.8000E 01	-2.0142E-06	----------|		1.3477E-07	3.8655E-08	6.8190E-04
9.0000E 01	-2.1847E-06	----------|		1.0837E-08	4.0484E-08	7.1284E-04
9.2000E 01	-2.2539E-06	----------|		3.3411E-08	1.8655E-08	-1.0098E-02
9.4000E 01	-2.3074E-06	----------|		8.2629E-08	-1.1991E-04	8.8127E-02
9.6000E 01	-1.8305E-06	----------|		-1.5416E-07	-1.9476E-07	2.1851E-04
9.8000E 01	-1.2745E-06	----------|		-1.0737E-07	6.0879E-09	4.9235E-05
1.0000E 02	-7.3302E-07	----------|		-1.0309E-07	1.1845E-08	2.1040E-05

*** DSMP/360 SIMULATION DATA ***

Figure 13-6. Time response of $\varepsilon(t)$ for $i = 2$, $\varepsilon(0) = 7 \times 10^{-7}$.

REFERENCES

1. Waites, H. B., "Planar Equations of Motion of the Spacelab Using Inside-Out Gimbal (IOG) for the Pointing Base," Memorandum EDI-2-75-12 February 27, 1975.

2. Meadows, J. F., "Spacelab Pointing And Stabilization Analysis," Northrop Services, Inc., Huntsville, Alabama, August 1975.

3. Kuo, B. C., and G. Singh, "Stability Analysis of the Low-Cost Large Space Telescope," Final Report, Systems Research Laboratory, Champaign, Illinois, June 30, 1975.

4. Dahl, P. R., "A Solid Friction Model," Report No. TOR-0158(3107-18)-1, Aerospace Corporation, El Segundo, California, May, 1968.

5. Dahl, P. R., "Solid Friction Damping of Spacecraft Oscillations," Report SAMSO-TR-75-285, The Aerospace Corporation, El Segundo, California, September 1, 1975.